WELL-TESTING METHODOLOGIES FOR CHARACTERIZING HETEROGENEITIES IN ALLUVIAL-AQUIFER SYSTEMS: SECOND YEAR (8/1/92 - 7/31/93) REPORT

A research project of the
Water Resources Research Program
United States Department of the Interior
Geological Survey

by

James J. Butler, Jr. and Carl D. McElwee
Kansas Geological Survey
The University of Kansas

with

Geoffrey C. Bohling, Zafar Hyder, Christine M. Mennicke,
Michael D. Orcutt, and Matthias Zenner
Kansas Geological Survey
The University of Kansas

June, 1994

Research supported by the U.S. Geological Survey (USGS), Department of the Interior, under USGS award number 14-08-0001-G2093. The views and conclusions contained in this document are those of the authors and should not be interpreted as necessarily representing the official policies, either expressed or implied, of the U.S. Government.

KGS OFR 94-27

ABSTRACT

A considerable amount of research on the mechanisms of large-scale solute transport has identified the spatial distribution of hydraulic conductivity as a significant factor in determining how a plume of a conservative constituent will move in the subsurface. This report summarizes the work of the second year of a three-year research project whose objective is to assess the potential of well-testing technology for providing accurate estimates of spatial variations in hydraulic conductivity. The research of the second year of this investigation of well tests in heterogeneous formations had both theoretical and field components. The theoretical components of this effort included an evaluation of the viability of multilevel slug tests in layered aquifers, an investigation of hydraulic tomography in a planar steady-state flow field, and an assessment of the Nguyen and Pinder method for slug test analysis. The field components of this work emphasized slug tests. A program of multiwell slug tests (slug tests with observation wells) was initiated and a general unified model for the analysis of anomalous slug-test response data was developed. Additional work performed in year two included further drilling and sampling activities, and laboratory analysis of sampled cores.

TABLE OF CONTENTS

I. INTRODUCTION

A. RESEARCH OBJECTIVES

Over the last decade, a considerable amount of theoretical, laboratory, and field research on the mechanisms of large-scale solute transport has identified the spatial distribution of hydraulic conductivity as a significant factor in determining how a plume of a conservative tracer will move in the subsurface (e.g., Freyberg, 1986; Gelhar, 1986; Dagan, 1986; Moltyaner and Killey, 1988). Many researchers now recognize (e.g., Molz et al., 1989a) that if we are to improve our predictive capabilities for subsurface transport, we must first improve our capabilities for measuring and describing conditions in the subsurface. The estimation of hydraulic conductivity in the subsurface on a scale of relevance for contaminant transport investigations, however, has proven to be a rather difficult task. Recent work at the Kansas Geological Survey and elsewhere (e.g., Streltsova, 1988; Butler and Liu, 1993) has shown that conventional pumping tests provide large-scale volumetric averages of hydraulic conductivity that may be of rather limited use in transport investigations. Although multiwell tracer tests can provide information on the average interwell conductivity, these tests are rather expensive in terms of time, money, and effort. Other techniques are needed if information on conductivity variations is to be used by practicing hydrogeologists outside of the research community. The specific objective of the research described in this report is to assess the potential of well-testing technology for providing more accurate estimates of spatial variations in the physical properties that control contaminant plume movement in saturated porous media. Although effective porosity is clearly an important consideration, the major emphasis of this work is on characterizing spatial variations (heterogeneities) in hydraulic conductivity.

Ideally, heterogeneities in hydraulic conductivity must be studied and characterized at several different scales in order to understand their influence on the movement of a contaminant plume. Although theoretical modeling work is an important element of any study of the influence of spatial variations in hydraulic conductivity on contaminant movement, a rigorous study of this subject must have a major field component. A field site, the Geohydrologic Experimental and Monitoring Site (GEMS), has been established in order to allow researchers at the University of Kansas to pursue work on characterizing spatial variations in flow and transport properties. GEMS is located in the floodplain of the Kansas River, just north of Lawrence, Kansas on land owned by the University of Kansas Endowment Association. Figure I.1 is a map showing the general location of GEMS and some of the major features at the site. GEMS

overlies approximately 21.3 meters (70 ft) of Kansas River valley alluvium. These recent unconsolidated sediments overlie and are adjacent to materials of Pleistocene and Pennsylvanian age. A cross-sectional view of the subsurface at one of the well nests at GEMS is shown in Figure I.2. The alluvial facies assemblage at this site consists of approximately 10.6 meters (35 ft) of clay and silt overlying 10.6 meters (35 ft) of sand and gravel. The stratigraphy is a complex system of stream-channel sand and overbank deposits. The general nature of the stratigraphy would lead one to expect that a considerable degree of lateral and vertical heterogeneity in hydraulic conductivity would be found in the subsurface at GEMS. Although analyses of sampled cores do indicate considerable variability in hydraulic conductivity within the sand and gravel interval at GEMS, it is unclear how the variability at the small scale of a core translates into variability at larger scales.

In the second year of this research, the focus of the work was on the use of well tests to describe spatial variations in hydraulic conductivity. Theoretical and field investigations of the potential of various types of well tests to provide information about lateral and vertical variations in hydraulic conductivity comprise the majority of the work in this period. A considerable amount of additional work, however, was directed at increasing our knowledge of the subsurface at GEMS. This effort involved continued drilling and sampling of the alluvium, and laboratory analysis of sampled cores. These characterization efforts are directed at providing the detailed information that will allow us to better assess the quality of the estimates provided by the various well-testing approaches evaluated in this work. The ultimate goal of these characterization efforts is to describe the site in so much detail that it effectively becomes an underground laboratory at which new technology can be evaluated.

B. BRIEF OUTLINE OF REPORT

The remainder of this report is divided into four major chapters, each of which is essentially a self-contained unit consisting of one or more sections. Although pages are numbered consecutively throughout the report, figures, tables, and equations are labelled by section for the convenience of the reader.

The first of these chapters describes theoretical work directed at developing a better understanding of the information that can be obtained from well tests performed under non-ideal conditions. In the report of the first year of this research, the preliminary results of a numerical investigation of the use of slug tests to describe vertical variations in hydraulic conductivity were presented. The final results of this investigation, which was completed in the second year of this research, are described in

the first section of this chapter. The original proposal for this research project discussed the possibility of hydraulic tomography, i.e. the utilization of data from multiple well tests in a tomographic inversion procedure. An initial investigation of this topic in a steady-state flow field is presented in the second section of this chapter. Many of the wells at GEMS are screened for only a portion of the sand and gravel interval. When data from slug tests performed in these wells are analyzed, the partially penetrating nature of the wells must be considered. One approach for the analysis of slug-test data from partially penetrating wells is the method of Nguyen and Pinder. In the third section of this chapter, a theoretical examination of this method is described. Note that all three sections of this chapter are essentially the text of articles on these topics that have been submitted for publication.

The second chapter primarily describes field investigations of slug tests at GEMS. The original proposal presented pulse testing as a promising well-testing methodology for use in hydrogeologic investigations. The first section of this chapter deals with the simplest type of pulse test: slug tests with observation wells (multiwell slug tests). The results of a program of field testing at GEMS and a subsequent theoretical analysis motivated by those tests are described. In the report of the first year of this research, an extensive series of field experiments, which was undertaken in order to understand the causes of anomalous behavior observed in slug-test data from wells in the sand and gravel section at GEMS, was described. That report also describes the derivation of new models to account for some of the mechanisms affecting the GEMS slug-test data. Those models, however, only proved to be of limited effectiveness in describing the observed behavior at GEMS. In the second year of this research, a considerable effort was made to better understand the anomalous response data. A new unified model that accounts for the major mechanisms thought to be affecting the GEMS slug-test data was developed. This model and its application to data from slug tests at GEMS is described in the second section of this chapter.

The third chapter primarily describes activities directed at increasing our knowledge of the subsurface at GEMS. Drilling and sampling activities that occurred over the last year at GEM are briefly summarized. The analysis of the core samples obtained during drilling is then described. Modifications to the procedures employed in the KGS core measurement laboratory are discussed and the results of the analyses performed in the second year of this project are reported.

The fourth chapter summarizes the report and briefly outlines the work planned for the third year of this project.

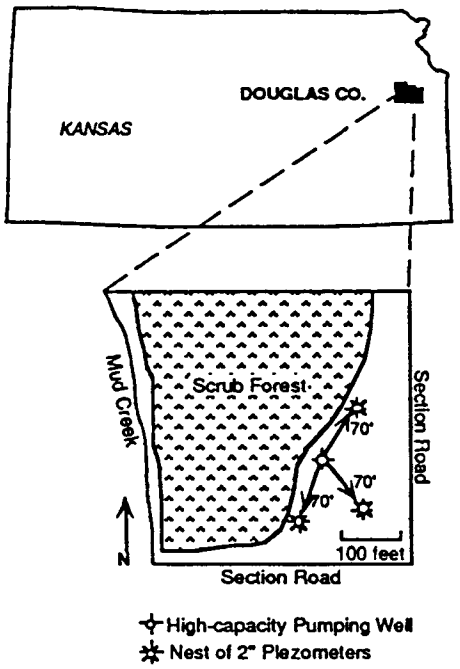

Figure I.1. - Location map for the Geohydrologic Experimental and Monitoring Site (GEMS).

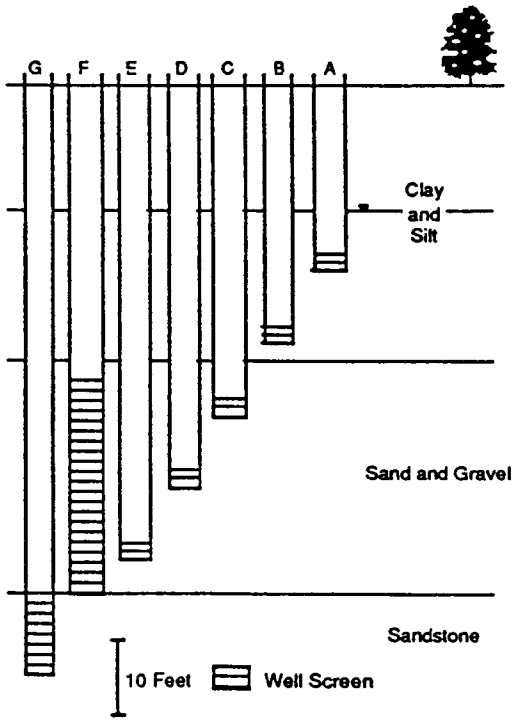

Figure I.2. Cross-sectional view of a well nestt at GEMS. Wells A-E are screened for .8 meters (2.5 ft.), well F is screened for 9.1 meters (30 ft.), and well G is screened for 1.5 meters (5 ft.).

II. THEORETICAL INVESTIGATIONS OF WELL TESTS IN NONIDEAL CONDITIONS

A. THE USE OF SLUG TESTS TO DESCRIBE VERTICAL VARIATIONS IN HYDRAULIC CONDUCTIVITY

Abstract

Multilevel slug tests provide one means of obtaining estimates of hydraulic conductivity on a scale of relevance for contaminant transport investigations. In this section, a numerical model is employed to assess the potential of multilevel slug tests to provide information about vertical variations in hydraulic conductivity under conditions commonly faced in field settings. The results of the numerical simulations raise several important issues concerning the effectiveness of this technique. If the length of the test interval is on the order of the average layer thickness, considerable error may be introduced into the conductivity estimates due to the effects of adjoining layers. The influence of adjoining layers is dependent on the aspect ratio (length of test interval/well radius) of the test interval and the flow properties of the individual layers. If a low permeability skin is present at the well, the measured vertical variations will be much less than the actual due to the influence of the skin conductivity on the parameter estimates. A high permeability skin can also produce apparent vertical variations that are much less than the actual due to water flowing vertically along the conductive skin. In cases where the test interval spans a number of layers, a slug test will yield an approximate thickness-weighted average of the hydraulic conductivities of the intersected layers. In most cases, packer circumvention should not be a major concern when packers of .75 m or longer are employed. Results of this study are substantiated by recently reported field tests that demonstrate the importance of well emplacement and development activities for obtaining meaningful estimates from a program of multilevel slug tests.

Introduction

Over the last decade, a considerable amount of theoretical, laboratory, and field research on the mechanisms of large-scale solute transport has identified the spatial distribution of hydraulic conductivity as a significant factor in determining how a plume of a conservative tracer will move in the subsurface (e.g., Freyberg, 1986; Gelhar, 1986; Dagan, 1986; Moltyaner and Killey, 1988; Hess et al., 1992). The estimation of hydraulic

conductivity in the subsurface on a scale of relevance for contaminant transport investigations, however, has proven to be a rather difficult task. Conventional pumping tests will provide large-scale volumetric averages of hydraulic conductivity, which may be of rather limited use in transport investigations (e.g., Butler and Liu, 1993). Multiwell tracer tests, which can provide information on the average interwell conductivity, are rather expensive in terms of time, money, and effort. Other techniques are needed if information on conductivity variations is to be used by practicing hydrogeologists outside of the research community.

Techniques that have been reported on in the literature include multilevel (straddle-packer) slug tests, borehole flowmeter surveys, laboratory core analyses, correlation with geophysical logs, and a variety of single-well tracer tests. Melville et al. (1991) describe a program of multilevel slug tests at a research site and show that the results compare favorably with the information obtained from a large-scale multiwell tracer test. A number of workers in both the petroleum and groundwater fields (e.g., Hufschmied, 1986; Ehlig-Economides and Joseph, 1987; Morin et al., 1988; Rehfeldt et al., 1989; Molz et al., 1989b; Hess et al., 1992) have shown that borehole flowmeters have the potential to provide detailed information about the vertical variations in hydraulic conductivity at a well. Laboratory analysis of sampled cores is undoubtedly the most common method of assessing vertical variations in hydraulic conductivity. However, the collection of reasonably intact cores in permeable unconsolidated materials, the geologic media in many contaminant transport investigations, can be a rather difficult task (e.g., Zapico et al., 1987; McElwee et al., 1991). In addition, the time and expense of performing permeameter analyses on a complete set of cores can be considerable. Taylor et al. (1990) describe several recently developed techniques for characterizing vertical variations in hydraulic conductivity. One particularly interesting approach is the single-well electrical tracer test (Taylor and Molz, 1990), which involves using a focussed induction downhole probe to measure changes in electrical conductivity as an electrically conductive tracer moves away from the borehole.

The focus of this section is on an evaluation of multilevel slug tests to provide information about vertical variations in the radial component of hydraulic conductivity. Slug tests have both economic and logistical advantages over the other techniques described in the previous paragraph. A logistical advantage that cannot be overemphasized for waste-site investigations is that a slug test can be configured so that water is neither added nor removed from the test well. Such a slug test can be initiated by introducing/removing an object of known volume to/from the water column or by pneumatic means (e.g., Orient et al., 1987; McLane et al., 1990). Problems arising due

to the injection of waters of different compositions or the disposal of potentially contaminated waters can thus be avoided.

A number of authors have examined multilevel slug tests or the related multilevel constant-head injection test using both analytical and numerical approaches. In terms of analytical approaches, Dagan (1978) employed Green's functions and a steady-state approximation to simulate tests in partially penetrating wells in unconfined flow systems. Dougherty and Babu (1984) present a fully transient analytical solution for slug tests performed in partially penetrating wells in isotropic confined systems. Hayashi et al. (1987) develop an analytical solution for multilevel slug tests in vertically unbounded, isotropic confined systems that explicitly includes the effects of packers above and below the test zone. Butler et al. (1990) present a solution for slug tests in partially penetrating wells in vertically bounded, anisotropic confined units that includes the effect of a finite-radius well skin. None of the above contributions, however, consider the effects of formation layering due to the difficulty of incorporating a general representation of formation layering into an analytical solution. Karasaki (1986) looked at the effect of layering on a slug test performed in a well that is fully screened across a layered aquifer in which flow is only in the radial direction. An extension to the general case of unrestricted flow in the vertical direction has apparently not been attempted.

In terms of numerical approaches, Braester and Thunvik (1984) present results of a series of transient numerical simulations of multilevel constant-head injection tests. In a somewhat similar study, Bliss and Rushton (1984) used a steady-state model to simulate constant-head injection tests in a fractured aquifer. More recently, Widdowson et al. (1990) used a steady-state numerical model to develop an approach for analyzing multilevel slug tests based on a method similar to that of Dagan (1978). Melville et al. (1991) employ this approach to analyze multilevel slug tests from an experimental field site.

Although several of the articles cited in the previous paragraphs have touched upon important aspects of the issue of the viability of multilevel slug tests, there are still many unanswered questions about the usefulness of the information provided from such tests under conditions commonly faced in the field, where anisotropy, layering, and well skins of either higher or lower permeability than the undamaged formation may be influencing the measured response data. The purpose of this section is to address many of these questions in the context of a theoretical assessment of the potential of multilevel slug tests to provide information about vertical variations in hydraulic conductivity in the vicinity of the well bore. Since no general analytical solution has been developed for the case of slug tests in layered aquifers, this assessment will be performed through

numerical simulation. The major objectives of this work are 1) to assess possible techniques for the analysis of slug tests in layered systems; 2) to evaluate the effects of various geologic features (e.g., density of layering, anisotropy within layers, distance from boundaries, etc.) and well-construction features (e.g., well skins, length of the test interval, etc.) on the parameters estimated from slug-test data; 3) to explore the nature of vertical averaging in slug tests in layered aquifers; 4) to assess the effects of packer length and determine under what conditions packer circumvention may be an important mechanism; and 5) to make recommendations for the performance of multilevel slug tests in layered systems that can be utilized by the field practitioner.

Problem Statement

The problem of interest here is that of the head response, as a function of r, z, and t, produced by the instantaneous introduction of a slug of water into a portion of the screened interval of a well. As shown in Figure II.A.1, the portion of the screened interval into which the slug is introduced is isolated from adjacent screened sections of the well by a pair of inflatable packers (straddle packer). Different intervals of the screen can be tested by moving the string of packers and pipes up and down in the well. A third packer is set above the top of the screen, isolating the well casing from the screened sections of the well outside of the test interval. Note that this configuration is in keeping with that commonly used in the field for multilevel slug tests (e.g., Melville et al., 1991; Butler and McElwee, 1992). In this analysis, flow properties are assumed to be invariant in the angular direction and radial variations are limited to changes between a well skin created during drilling and development and the adjacent formation. Variations in flow properties of any magnitude are allowed between layers in the vertical direction.

The partial differential equation representing the flow of groundwater in response to the instantaneous introduction of a slug of water at a central well is

$$\frac{\partial}{\partial r}\left(K_r \frac{\partial h}{\partial r}\right) + \frac{K_r}{r}\frac{\partial h}{\partial r} + \frac{\partial}{\partial z}\left(K_z \frac{\partial h}{\partial z}\right) = S_s \frac{\partial h}{\partial t} \qquad \text{(II.A.1)}$$

where h is the hydraulic head, [L]; K_r is the component of hydraulic conductivity in the radial direction, [L/T]; K_z is the component of hydraulic conductivity in the vertical direction, [L/T]; S_s is the specific storage, [1/L]; t is the time, [T]; r is the radial direction, [L]; and z is the vertical direction, [L].

The initial conditions can be written as

$$h(r,z,0)=0, r_w<r<\infty, 0\le z\le B \qquad \textbf{(II.A.2)}$$

$$h(r_w,z,0) = \begin{cases} H_0, & a \le z \le a+b \\ 0, & elsewhere \end{cases} \qquad \textbf{(II.A.3)}$$

where r_w is the radius of the screen in the test interval, [L]; B is the thickness of the aquifer, [L]; H_0 is the height of the initial slug, [L]; a is the distance of the bottom of the test interval above the base of the aquifer, [L]; and b is the width of the test interval, [L].

The boundary conditions are the following:

$$h(\infty,z,t) = 0, \quad t > 0, \quad 0 \le z \le B \qquad \textbf{(II.A.4)}$$

$$\frac{\partial h(r,0,t)}{\partial z} = \frac{\partial h(r,B,t)}{\partial z} = 0, \quad r_w < r < \infty, \quad t > 0 \qquad \textbf{(II.A.5)}$$

$$h(r_w,z,t) = H(t), \quad t > 0, \quad a \le z \le a+b \qquad \textbf{(II.A.6)}$$

$$2\pi r_w \int_a^{a+b} K_r \frac{\partial h(r_w,z,t)}{\partial r} dz = \pi r_c^2 \frac{dH(t)}{dt}, \quad t>0 \qquad \textbf{(II.A.7)}$$

$$\frac{\partial h(r_w,z,t)}{\partial r} = 0, \quad t>0, \qquad \textbf{(II.A.8)}$$
$$a-p \le z < a, \quad a+b < z \le a+b+p$$

$$\frac{\partial h(0,z,t)}{\partial r} = 0, t>0, 0 \le z < a-p \qquad \text{(II.A.9)}$$

$$\frac{\partial h(r_p,z,t)}{\partial r} = 0, t>0, a+b+p < z \le B \qquad \text{(II.A.10)}$$

where H(t) is the head within the well in the test interval, [L]; r_c is the radius of the cased portion of the well above the upper packer, [L]; r_p is the radius of the pipe through which the slug has been introduced to the test interval, [L]; and p is the length of the straddle packer, [L]. Note that conditions (II.A.8)-(II.A.10) are a no-flow condition for the portion of the screen sealed by the packers, a symmetry boundary below the packers, and a no-flow condition along the pipe connecting the straddle packers to the upper packer, respectively.

Equations (II.A.1)-(II.A.10) describe the flow conditions of interest here. Given the generality of the property variations allowed in the vertical direction, analytical approaches are not feasible. Thus, for this work, a numerical model was employed in order to obtain approximate solutions to the mathematical model represented by the above equations.

Numerical Model

In this work, a cylindrical-coordinate, three-dimensional, finite-difference model (3DFDTC), developed at the Kansas Geological Survey (Butler and McElwee, 1992), was employed to simulate multilevel slug tests. The model was centered on the well in which the slug tests were being performed. The influence of well bore storage is taken into consideration using an approach based on earlier work of Settari and Aziz (1974), Rushton and Chan (1977), and Butler (1986). As described by Butler (1986), the approach is based on rewriting the classical pipe flow equation (Vennard and Street, 1975) in a Darcy Law like formulation and defining a term (involving the friction factor, the cross-sectional area of the well bore, and distance along the well bore) analogous to hydraulic conductivity. This approach allows flow inside the well bore to be governed by the porous media flow equation (equation (II.A.1)). Note that the implementation of this approach for this study produces an approximation of well-bore behavior that is equivalent to the hydrostatic head assumption employed in most analytical representations of the well bore (e.g., Papadopulos and Cooper, 1967; Cooper et al., 1967).

In order to demonstrate the validity of the well-bore approximation, the model

has been checked against many analytical solutions for both pumping and slug tests. Two examples of such comparisons are presented here. The first example illustrates model performance when the hydraulic conductivity of adjacent grid cells differs by several orders of magnitude. A slug test in a well surrounded by a low permeability well skin of finite radius was simulated. The well was assumed to be screened throughout the aquifer. Figure II.A.2a illustrates a comparison of the heads simulated by 3DFDTC with the results from the analytical solution of Moench and Hsieh (1985) for a slug test in a well with a skin of finite radius. The plots of the results essentially fall on top of one another. The small differences that do exist are attributed mainly to the error caused by the spatial discretization scheme employed in 3DFDTC (20 nodes in radial direction from .1 to 37,364. meters using equal log spacing). Further simulations have shown that by increasing the number of nodes in the radial direction, the difference between the analytical solution and 3DFDTC results will gradually disappear.

The second example is selected to illustrate model performance when there is a strong component of vertical flow, such as might occur in multilevel slug tests. A slug test is simulated in a well that is screened for only a portion of the aquifer thickness. The aquifer is assumed to be homogeneous and isotropic with respect to flow properties. Figure II.A.2b displays a comparison of the heads simulated by 3DFDTC with the results of the analytical solution of Butler et al. (1990) for a slug test in a well partially penetrating a confined aquifer. As with the previous example, 3DFDTC yields results that are essentially indistinguishable from those of the analytical solution. Note that the error introduced by the radial discretization scheme employed in these examples was considered acceptable for the purposes of this work. Further issues concerning the vertical discretization scheme are discussed later.

Techniques for Analysis of Slug Tests in Layered Systems

The approach employed in this research was to simulate a series of multilevel slug tests using the 3DFDTC model and then estimate the hydraulic conductivity of the portion of the formation opposite the screened interval from the simulated results. Several methods were considered for the analysis of the simulated slug-test responses. The most commonly used methods for the analysis of slug-test data in confined aquifers are the approaches of Cooper et al. (1967 - henceforth designated as the CBP model) and Hvorslev (1951). Since the CBP model was developed for slug tests performed in wells fully screened across an aquifer, the method of Hvorslev was the major focus of this work.

Hvorslev (1951) developed a series of models for the analysis of slug tests

performed in confined aquifers. A major assumption of the Hvorslev approach is that the specific storage of the aquifer can be neglected. Since the head response at the test well is relatively insensitive to specific storage (Cooper et al., 1967), this assumption may be acceptable in many cases. Each of the different well-aquifer configurations that Hvorslev considered requires the use of a "shape factor", which is related to the geometry of the well intake region. The shape factor used here is that of Case 8 described in Hvorslev (1951). Case 8 is for a configuration consisting of a well with a screened interval of finite length located in a uniform, vertically unbounded, aquifer with a horizontal to vertical anisotropy in hydraulic conductivity. The Hvorslev model for this case is in the form of a two-parameter (K_r and anisotropy ratio) function:

$$h(t) = H_0 e^{-t/T_0} \qquad \text{(II.A.11)}$$

where $T_0 = (\pi r_c^2)/FK_r$; $F = (2\pi b)/[\ln(mb/2r_w + \sqrt{1+(mb/2r_w)^2})]$;

and $m = \sqrt{K_r/K_z}$. Unfortunately, the two parameters in (II.A.11) are perfectly correlated, so they cannot be estimated independently. Equation (II.A.11) can be rearranged to produce the following expression for the estimated hydraulic conductivity:

$$K_{HV} = \frac{r_c^2 \ln[mb/2r_w + \sqrt{1+(mb/2r_w)^2}]}{2bt_0} \qquad \text{(II.A.12)}$$

where K_{HV} is the hydraulic conductivity estimated using the Hvorslev model and t_0 is the time at which a normalized head of .37 is reached. Clearly, an anisotropy ratio must be assumed in order to estimate K_{HV}.

An initial series of simulations was performed using 3DFDTC in order to assess the viability of the Hvorslev model for the estimation of hydraulic conductivity from multilevel slug-test data. Figure II.A.3 presents the results of a set of simulations in which the effects of the magnitude of the aspect ratio (b/r_w) on conductivity estimates obtained from slug tests in a uniform aquifer are investigated. Aspect ratios extending over two orders of magnitude were employed in order to evaluate parameter estimates over the range of conditions expected in multilevel slug tests. Note that conductivity estimates obtained using both the Hvorslev and CBP models are included on this plot in order to illustrate the dependence of both models on aspect ratio. Figure II.A.3 indicates that the Hvorslev model should provide acceptable parameter estimates (within

20% of the actual conductivity) for aspect ratios between 3 and 300. Note that the CBP model provides better estimates than the Hvorslev model at large aspect ratios (≥ 200) as a result of the slug-test responses becoming increasingly similar to those from a fully screened well at large aspect ratios.

The results presented in Figure II.A.3 are for the case of the test interval being at a large distance from a formation boundary (infinite aquifer case). Figure II.A.4 depicts the results of a further set of simulations in which the effects of an impermeable boundary on parameter estimates are examined. In these simulations, the test interval, which has an aspect ratio of 5, is progressively moved from the center of the aquifer to the upper impermeable boundary. A test interval with a small aspect ratio and an isotropic aquifer were employed in order to emphasize the effects of vertical flow. The boundary effects are straightforward. As the test interval approaches the boundary, the vertical flow out of the interval is constrained, resulting in a decrease in the K_{HV} estimate. Note that the effect of an impermeable horizontal boundary is less dramatic with larger aspect ratios and/or the presence of a pronounced anisotropy ($K_r > K_z$). Thus, Figures II.A.3 and II.A.4 indicate that for the aspect ratios commonly employed in programs of multilevel slug tests, the Hvorslev model should provide acceptable estimates as long as the test interval is several meters below an impermeable boundary.

Although the focus of this discussion has been on the Hvorslev model, several additional models were considered for the analysis of the simulated slug tests. As discussed in the Introduction, Butler et al. (1990) have developed an analytical solution for slug tests in partially penetrating wells with skins, which can be readily configured to analyze data from multilevel slug tests in homogeneous, anisotropic aquifers. Although this solution avoids the simplifying approximations of the Hvorslev approach, the calculated parameters are not significantly different from those of Hvorslev for the range of aspect ratios commonly employed in multilevel slug tests. A major drawback of this model is that it is computationally intensive as a result of the use of both Fourier and Laplace integral transforms to obtain the solution.

Dagan (1978) and Widdowson et al. (1990) have developed techniques for the analysis of multilevel slug tests that are based on a series of graphs/charts developed from simulation of slug tests under conditions similar to those considered by Hvorslev (1951). A major drawback of these techniques is that new simulations are required for each well-aquifer configuration that is examined.

Given the results of the simulations presented in Figures II.A.3 and II.A.4 and its advantages in terms of computational efficiency, the Hvorslev model was considered the most appropriate model for use here. Thus, in the remainder of this section, the

Hvorslev model is employed for the analysis of simulated slug-test responses. The analyses were performed using the implementation of the Hvorslev model found in the SUPRPUMP automated well-test analysis package of the Kansas Geological Survey (Bohling and McElwee, 1992). This use of the Hvorslev model, however, should not be considered a blanket endorsement of the approach as the model must be used with caution when analyzing actual field data due to its neglect of storage effects on slug-test responses (Chirlin, 1989), its poor performance in the presence of a well skin (Butler et al., 1990), and its increasing error in wells with very small aspect ratios (Hvorslev, 1951).

Dependence of Multilevel Slug Test Results on Density of Layering

The simulations discussed in the previous subsection illustrate the performance of multilevel slug tests in ideal homogeneous systems. Many aquifers in nature, however, consist of layers of differing flow properties. In order to address the effects of layering on multilevel slug tests, a hypothetical aquifer, made up of alternating layers of constant thickness consisting of two distinct materials (denoted here as A and B), was constructed. Although layering in natural systems is clearly more complex than this configuration, the use of an alternating two-component system will enable the major effects of layering on a program of multilevel slug tests to be assessed.

The base set of parameters for this layered aquifer model are given in Table II.A.1. A grid of 20 nodes in the radial (same discretization scheme as used in simulations of Figure II.A.2) and 48 to 96 nodes in the vertical directions was employed. The number of nodes in the vertical varied depending on the layering and test interval length used in a particular scenario. In order to assess the error introduced by the various vertical discretization schemes, a number of additional simulations were performed using increasingly finer vertical discretization. In all cases, the discretization schemes used here were found to introduce an error of less than 2% to the calculated parameters. These errors were considered acceptable for the purposes of this work. Note that in simulations using very small test intervals (.156 m), the thickness of the aquifer (B) was decreased from the base case of 30 m to a thickness of 15 m. In all cases, however, the results reported here were for test intervals far enough away from a boundary that boundary effects were negligible.

The results of the simulations of slug tests in layered aquifers are presented using the range of conductivities estimated from a series of slug tests performed as the packer string was moved in small increments up the well bore. Figure II.A.5 displays a plot of hydraulic conductivity values estimated from such a series of multilevel slug-test

simulations in which the packer string is moved in .94 m increments up the well bore. The results are shown for just a portion of the series of alternating high and low conductivity layers in order to clarify the definition of the range as the distance between the peak and trough of the conductivity versus depth plot. The range of estimated conductivities was considered a succinct way to display the manner in which the actual conductivity variations are being distorted in the results of a program of multilevel slug tests. In addition to the range, however, the estimated maximum and minimum conductivity values are also considered so that the degree of over or underestimation of layer conductivities is clear. Note that the slight overestimation of K_A and K_B shown in Figure II.A.5 is in keeping with the results displayed on Figure II.A.3 for a test interval of the same aspect ratio (b/r_w=25.).

The first set of layered-aquifer simulations was designed to investigate the effect of layering density on multilevel slug tests. For these simulations, the test interval length was constrained to be less than or equal to the layer thickness, which was assumed to be constant for any particular simulation. In a later subsection, simulations using test intervals of lengths greater than the layer thickness are described. Figure II.A.6 displays the results of a series of simulations in which the test interval length was assumed to equal layer thickness. In these simulations, the test interval length (and thus the layer thickness) was gradually decreased from 5 meters (aspect ratio = 100) to .156 meters (aspect ratio $\approx$ 3). The results are displayed in the form of a plot of the range of the estimated conductivities versus aspect ratio. Clearly, the range of estimated conductivities decreases significantly with decreases in aspect ratio. Note that the majority of this decrease is a result of the conductivity estimated for layer B becoming increasingly smaller than the actual conductivity due to suppression of vertical flow by the adjoining layers of material A. Hayashi et al. (1987) describe how a decrease in aspect ratio promotes partial penetration effects, i.e. vertical flow out either end of the test interval. Thus, adjoining lower conductivity layers will have a greater impact on slug-test responses as the aspect ratio decreases and the importance of vertical flow increases.

The general result of these simulations is that the effect of adjoining layers on multilevel slug tests becomes increasingly important as the layers decrease in thickness. Figure II.A.6, however, should only be considered as an example of these effects. The exact nature of the influence of adjoining layers will depend on a number of additional factors including the specific storage of the layers and the degree of anisotropy in layer conductivity. The above simulations were performed assuming a specific storage of $1x10^{-5}$ m^{-1}. Additional simulations have shown that use of a smaller specific storage results

in the pressure disturbance induced by the slug test spreading out more rapidly in all directions, causing the effect of adjoining lower-conductivity layers to be accentuated. The increased influence of adjoining lower-conductivity layers produces considerably lower values for the estimated layer B conductivities. Likewise, a specific storage larger than that used in Figure II.A.6 lessens the influence of adjoining layers on conductivity estimates. Thus, the specific storage can have a considerable influence on the estimated conductivity in layered systems. This is in contrast to slug tests in homogeneous systems where specific storage has relatively little influence on conductivity estimates obtained from heads at the test well (Cooper et al., 1967).

The addition of anisotropy ($K_r > K_z$) into the configuration does not produce results significantly different from those displayed in Figure II.A.6. The influence of adjoining layers is clearly diminished by the addition of anisotropy as a result of the suppression of vertical flow. The suppression of vertical flow itself, however, causes a decrease in the estimated conductivities. The net result is a decrease in the conductivities estimated for both layers and estimated conductivity ranges slightly narrower than those displayed in Figure II.A.6. Note that the analyses described in this paragraph were performed with the Hvorslev model assuming an isotropic aquifer. This is a reasonable assumption since one will not normally know what degree of anisotropy is appropriate. As discussed earlier, the anisotropy ratio and the horizontal conductivity are perfectly correlated in the Hvorslev model. Thus, some error will always be introduced into the parameter estimates as a result of the uncertainty concerning anisotropy.

The results displayed in Figure II.A.6 were obtained assuming that the test interval length was equal to layer thickness. If the test interval length is less than the layer thickness, adjoining layers will have less of an impact on the estimated conductivity. Figure II.A.7 displays the results of a series of simulations in which the layer thickness was progressively increased, while the test interval, which was centered within the layer, was not changed (constant aspect ratio of 25.). As expected, increases in the ratio of layer thickness to test interval length decrease the impact of adjoining layers. In Figure II.A.7, the effects of adjoining layers are essentially negligible for ratios of four or greater (overestimation of K_r seen at $L/b=4$ is in keeping with Figure II.A.3). Note that the exact nature of the decrease in the effects of adjacent layers will depend on the aspect ratio (the larger the aspect ratio, the more rapid the decrease). Clearly, however, the use of a test interval length considerably smaller than the average layer thickness will greatly improve the information obtained from a program of multilevel slug tests. When the results of Figures II.A.6 and II.A.7 are considered together, it is also clear that r_w

should be kept as small as practically possible in order to decrease the impact of the effects of small aspect ratios.

Dependence on Well Skins

The results depicted in Figures II.A.6 and II.A.7 were determined for the ideal case in which formation layering extends to the well screen. Often, however, as illustrated in Figure II.A.1, well drilling and development creates a near-well zone (well skin) of properties differing from those of the formation in which the well is screened. An additional series of simulations was performed here to assess the effects of well skins on multilevel slug test results.

Figure II.A.8 depicts the results from a set of simulations in which a low-permeability well skin was employed. The results are displayed in the form of a plot of the range of estimated conductivities versus simulation case. These results show that the addition of a low permeability skin produces a near complete suppression of the vertical variations in conductivity (calculated conductivity ranges are 2.9% and 1.7% of actual for cases A and B, respectively). In addition to the suppression of the conductivity variations, the estimated conductivities are much lower than in the no-skin case as a result of the heavy weighting of the low permeability skin in the parameter estimates. Butler et al. (1990) discuss the nature of the weighting of a low permeability well skin in conductivity estimates obtained using the Hvorslev model. Note that the estimated conductivities are lower in case B as a result of the greater importance of vertical flow with smaller aspect ratios. In this case, the vertical flow is being suppressed by the low permeability well skin, resulting in lower calculated conductivities.

A well skin may be of higher permeability than the formation as a result of voids forming along the well screen during well emplacement activities or a high permeability sand pack. A high conductivity skin can serve as a conduit for additional vertical flow. Figure II.A.9 displays the results of a series of simulations in which a high permeability skin of .11 meters in radius was employed for most cases. Once again, the results are given in the form of a plot of the range of estimated conductivities versus simulation case. Note that, in relatively thick layers, the width of the calculated conductivity range does not change greatly from the no-skin case (cf. C* and C), although the estimated conductivities themselves increase significantly. As the thickness of the layers decreases, the layers become thin enough such that when the test interval is opposite a layer of material A, substantial amounts of water flow vertically along the well skin and into the layers of material B. This results in a great increase in the conductivity estimated for layers of material A and a dramatic decrease in the calculated conductivity range. As

shown by case G, this effect increases with the thickness of the skin. Clearly, a highly conductive skin in an aquifer consisting of thin layers can cause multilevel slug tests to be of rather limited effectiveness for describing vertical variations in hydraulic conductivity.

Given that a highly conductive skin can greatly limit the effectiveness of multilevel slug tests, a series of additional simulations was performed in order to assess if well-construction measures could be taken to reduce the effect of a conductive skin. One possibility suitable for wells where the sand pack is the high conductivity skin would be to place very thin layers (1-2 cm) of low conductivity material (e.g., bentonite pellets) in the sand pack at an interval similar to the length of the planned test interval. These layers would serve to decrease the vertical movement of water in the sand pack but would have very little impact on horizontal flow. This scheme was evaluated here by simulating slug tests in wells with high conductivity skins in which an anisotropy in conductivity was assumed for the skin. Figure II.A.10 presents the results of a series of simulations in which anisotropy ratios (K_r/K_z) of 1, 2, and 10 were employed (K_r remaining constant, K_z decreasing). As shown in the figure, increases in the anisotropy ratio cause the calculated conductivity range to increase and the estimated conductivities to decrease towards the no skin case. These results indicate that if a well is to be used for multilevel slug tests, the emplacement of periodic thin layers of low conductivity material in the sand pack would be useful in partially mitigating the effect of a high conductivity skin. Unfortunately, in cases where the high conductivity skin is not the sand pack (e.g., uncased wells in consolidated rock), such an approach would not be possible, thereby making it difficult to remove the effect of a high conductivity skin in those situations. Note that the successful emplacement of periodic layers of bentonite in the sandpack should produce much greater anisotropy ratios (>1000) than those employed here. However, practically speaking, it will be difficult to ensure that unbroken layers of bentonite have been placed at the desired locations. Lower anisotropy ratios were therefore employed here in order to yield conservative estimates of the expected behavior.

Vertical Averaging in Slug Tests in Layered Aquifers

One issue of considerable interest to hydrogeologists is the way in which flow properties are averaged in various types of hydraulic tests in heterogeneous systems (e.g., Desbarats, 1992a; Harvey, 1992). Since a number of layers may be spanned by the test interval in a multilevel slug test, the issue of the manner in which the properties of those layers are averaged to form the effective parameter estimated from the response data

is of some importance. In this work, the nature of this vertical averaging was explored empirically through numerical simulation.

The initial step of this investigation was to assess the manner in which hydraulic conductivity values that vary in the vertical direction are averaged in a slug test performed over the entire screened interval of a well fully penetrating the aquifer (fully penetrating slug test). A set of four simulations was performed. These simulations consisted of a uniform, anisotropic aquifer case, and three layered-aquifer cases with alternating layers of high and low conductivity. The layering schemes are shown in Figure II.A.11b and the parameter values used in each case are given in Table II.A.2. Note that all three layering schemes have a thickness weighted average K_r of 9.2×10^{-5}, which is the same value for K_r as used in the uniform aquifer case.

Figure II.A.11a displays the results of the simulations for the case of head in the test well. As shown in this figure, the simulated heads at the test well are essentially identical in the uniform and all three layered cases. Clearly, slug tests over the entire screened interval in fully penetrating wells can provide little information about vertical variations in conductivity when the test well is the measurement location. In all cases, the estimated conductivity will be a thickness-weighted arithmetic average of the horizontal conductivities of the individual layers. Note that this result is an extension of the work of Karasaki (1986), who found the same result using an analytical solution for slug tests in layered aquifers in which there is no vertical flow between layers. Thus, the vertical averaging in fully penetrating slug tests appears to be independent of the degree of vertical flow between layers. It is important to stress that there is vertical flow in the layered simulations of Figure II.A.11. These and additional simulations have shown that there will be considerable differences in head in the vertical direction outside of the test well ($r>r_w$) during a fully penetrating slug test in a layered aquifer (Butler and McElwee, 1992). Apparently, the flow between layers is in some sort of hydraulic balance dependent on the thickness of layers, the density of layering, layer flow properties, etc., such that the response at the central test well is independent of the degree of vertical flow.

Since Figure II.A.11a shows that no indication of layering will be evident from the head response at the test well in a fully penetrating slug test, an obvious question of importance for multilevel slug tests is how much will layering be suppressed as the test interval gets larger than the average layer thickness. Additional simulations have shown that the degree of suppression will depend on vertical variations in the arithmetic average of the conductivities of the test interval and the aspect ratio. In all cases, when the aspect ratio is much greater than 200, the estimated conductivity can be assumed to

be a thickness-weighted average of the conductivities of the layers intersected by the test interval. Note that this statement is based on the assumption that the slug-test responses will be analyzed with the model of Cooper et al. (1967) for aspect ratios greater than 200, in keeping with the results displayed on Figure II.A.3.

Effect of Packer Length

All of the multilevel slug test simulations described above were performed assuming that the well was cased everywhere in the aquifer except at the test interval (infinite packer). This was done in order to remove any effects due to the circumvention of the packers from the results. In field applications, however, packer circumvention is a very real concern. Increased vertical flow due to packer circumvention can result in an overestimation of layer conductivities and an underestimation of the degree of vertical variations.

A series of additional simulations was performed in order to assess the effect of packer length on parameters estimated from multilevel slug tests. In the 3DFDTC model, packers are simulated as no-flow boundaries in the well bore, so there is no restriction on the length of the modelled packers. Four configurations were employed in this analysis in order to allow the effects of packer length to be evaluated in homogeneous and layered situations, both with and without a high conductivity skin (see Table II.A.3 for the parameters used in each configuration). Cases 1 and 2 were designed to assess behavior in homogeneous and layered situations, respectively, in the absence of a high conductivity skin, while Cases 3 and 4 were designed to assess behavior in the same systems in the presence of a high conductivity skin.

Figure II.A.12 presents the results of these simulations in the form of a plot of packer length versus the difference between the estimated conductivity using a packer of that length (K_{packer}) and the estimated conductivity using an infinite packer ($K_{\infty packer}$) normalized by the infinite packer estimate. Note that a dramatic decrease in this difference is seen in all cases with an increase in packer length. This plot clearly indicates that a highly conductive skin will exacerbate packer circumvention problems. In all cases, however, these results demonstrate that the relationships derived in this work are essentially the same as would be obtained using packers of .75-1.5 meters in length, which is the length range of many commercially available packers. Given the skin is 50 times more permeable than layer A, these results should be considered conservative, worst-case estimates. Thus, packers greater than .75 meters in length should prevent packer circumvention in the vast majority of field applications. Bliss and Rushton (1984) found similar results for the effect of packer length on constant-head

injection tests. Note that the results reported here are dependent on the thickness of the high conductivity skin. In cases where very thick skins are suspected, longer packers or a number of packers in series should be employed. However, as demonstrated in an earlier subsection, a thick high conductivity skin will hinder the effectiveness of multilevel slug tests even without packer circumvention.

Recent Field Experiences

Recently reported field experiences with multilevel slug tests in unconsolidated aquifers support some of the findings of this study. Melville et al. (1991) report on a program of multilevel slug tests whose results compared favorably with information obtained from tracer tests. Butler and McElwee (1992), on the other hand, describe a program of multilevel slug tests whose results indicated essentially no vertical variations in flow properties, a finding that was not in agreement with existing core data. Although the test procedures followed in both studies were quite similar, the well drilling and emplacement procedures were not. Melville et al. (1991) describe a procedure of well emplacement using mud rotary drilling followed by forcing a slotted pipe of slightly smaller diameter into the drilled hole. The small annular space between the slotted pipe and the drilled hole was filled by collapsing material from the borehole wall. The wells were then extensively developed in order to remove as much of the drilling mud as possible from the formation. Butler and McElwee (1992) describe a procedure of well emplacement using hollow-stem auger drilling followed by placing a slotted pipe down the center of the augers and withdrawing the auger flights from about the pipe. In this case, a much larger annular space was formed, which was then filled by a natural sand pack consisting of material collapsing inward from the borehole wall. Permeameter analyses of cores from this same formation (Jiang, 1991; Butler and McElwee, 1992) have shown that repacked cores have considerably higher conductivities than the original sampled cores, indicating that the collapsed zone would probably form a skin of higher conductivity than the formation as a whole. The poor results of the tests reported by Butler and McElwee (1992) may well be due to preferential water movement along this thick high conductivity skin. The success of the Melville et al. (1991) program appears to be largely due to the thin well skin coupled with unremoved drilling muds that are apparently preferentially impeding vertical flow. Although their approach seems to have met with success, Melville and coworkers could have suffered from the same effects as illustrated in Figure II.A.8 without a very extensive program of well development. Thus, it is clear that well drilling and development procedures cannot be overemphasized in the planning of multilevel slug tests.

An approach for multilevel slug testing in unconsolidated formations that appears to minimize many of the problems arising due to well emplacement is described by Hinsby et al. (1992). This approach is based on progressively driving a well point and short screen into the formation. At any level desired, well driving can be stopped and a slug test performed. Although the results of the slug tests will still be a function of layering density, etc., as outlined here, this approach appears to have less potential for producing a thick high conductivity skin along the driven pipe. Ongoing work at the Kansas Geological Survey and elsewhere is presently evaluating this approach in more detail.

Summary and Conclusions

This section reported the results of a series of numerical experiments designed to assess the viability of slug tests for the purpose of describing vertical variations in the radial component of hydraulic conductivity. Although most natural systems will not consist of the ideal two-component system of repetitive layers considered here, such a conceptual model allows considerable insight to be gained concerning behavior in more complex systems. Five general conclusions, which are independent of the particular parameter values employed here, can be drawn from this work:

1) When the length of the test interval is on the order of the average layer thickness, considerable error can be introduced into the description of vertical variations in hydraulic conductivity as a result of the influence of layers adjoining the test interval. The magnitude of the influence of the adjoining layers will strongly depend on the aspect ratio (test interval length/r_w). The specific storage of the tested interval will also be an important factor;

2) Regardless of layering density, a low conductivity skin will make it difficult to describe vertical variations in hydraulic conductivity because the estimated conductivity will be strongly influenced by the conductivity of the skin;

3) A high conductivity skin will make it difficult to describe vertical variations in hydraulic conductivity when the test interval and the average layer thickness are both small. In this case, a large amount of vertical flow can occur along the skin, making it difficult to detect the existence of layers of low conductivity. Periodic emplacement of thin, low conductivity layers in the sand pack can help decrease vertical flow and allow a more accurate description of the conductivity variations to be obtained;

4) When the aspect ratio is large (>200), a slug test will yield an approximate thickness-weighted average of the hydraulic conductivities of the layers intersecting the test interval if the data are analyzed with the model of Cooper et al. (1967) (exact

average in the case of a fully penetrating slug test). As the aspect ratio decreases, the properties of layers outside of the test interval will influence the calculated conductivity due to the increased vertical flow;

5) Packer circumvention should not be a major problem in most field applications when packers of .75 meters or longer are employed. Packer circumvention is of greatest concern in the case of a thick, high conductivity skin.

In summary, multilevel slug tests can provide considerable information about vertical variations in hydraulic conductivity under the right conditions. The best conditions would be thick layers using test intervals considerably smaller than the average layer thickness. Even under these conditions, however, well skins can dramatically decrease the effectiveness of the approach. Considerable attention must therefore be given to well construction and development in order to minimize the impact of a well skin on test results. Results from recently reported field tests demonstrate the importance of well construction and development procedures.

Note that the findings of this study must be considered in the light of two major assumptions employed in this work. First, the simulated responses from each slug test were analyzed using a homogeneous-aquifer model, an approach in keeping with standard field practices. Analysis of each test in isolation from the others in the same series of multilevel tests, however, led to the strong dependence of test results on layering density and, in many cases, to a significant underestimation of the actual conductivity variations. A more rigorous approach would be to analyze all the test results together using a numerical model coupled to an optimization routine. An initial attempt at such an approach for a series of drill-stem tests is given by Yu and Lloyd (1992). Even if such a technique was used, however, it would not remove the effects of well skins or vertical averaging from test results. Given the nature of current field practices, the approach employed here was considered appropriate.

Second, the findings discussed in this section were based on a series of simulations performed in perfectly stratified aquifers, i.e. layering is continuous throughout the entire model domain. Although many natural systems consist of a series of discontinuous layers, the rate of variation in flow properties in the direction perpendicular to the plane of layering would be expected to be considerably larger than that in the direction parallel to layering (Butler, 1986; Hess et al., 1992). Thus, the results presented here should be applicable to most field situations. Further work, however, is required to fully assess the effect of layer discontinuity on slug tests.

Table II.A.1 - Parameters for layered aquifer model

H_0 = 1.0 m;
r_w = 0.05 m;
K_A = 2.0×10^{-5} m/s;
K_B = 2.0×10^{-4} m/s;
$S_{SA} = S_{SB}$ = 1.0×10^{-5} m^{-1};
B = aquifer thickness = 30. m;
r_{bnd} = radial distance to outer boundary = 37,364. m.

Table II.A.2 - Parameters for analysis of vertical averaging

uniform, anisotropic case

$K_r = 9.2 \times 10^{-5}$ m/s, $K_z = 9.2 \times 10^{-6}$ m/s;

layered cases

low conductivity layer	$K_r = 2.0 \times 10^{-5}$ m/s, $K_z = 2.0 \times 10^{-6}$ m/s;
high conductivity layer	$K_r = 2.0 \times 10^{-4}$ m/s, $K_z = 2.0 \times 10^{-5}$ m/s.

Table II.A.3 - Parameter sets for packer simulations

Case 1

$K_A = K_B = 2x10^{-5}$ m/s;
$S_{SA} = S_{SB} = 1x10^{-5}$ m^{-1};
b = .15 m;

Case 2

$K_A = 2x10^{-5}$ m/s;
$K_B = 2x10^{-4}$ m/s;
$S_{SA} = S_{SB} = 1x10^{-5}$ m^{-1};
b = .15 m;
L = .15 m;

Case 3

$K_A = K_B = 2x10^{-5}$ m/s;
$S_{SA} = S_{SB} = 1x10^{-5}$ m^{-1};
K_{sk} = .001 m/s;
b = .15 m;
r_{sk} = .11 m;

Case 4

$K_A = 2x10^{-5}$ m/s;
$K_B = 2x10^{-4}$ m/s;
$S_{SA} = S_{SB} = 1x10^{-5}$ m^{-1};
K_{sk} = .001 m/s;
b = .15 m;
L = .15 m;
r_{sk} = .11 m.

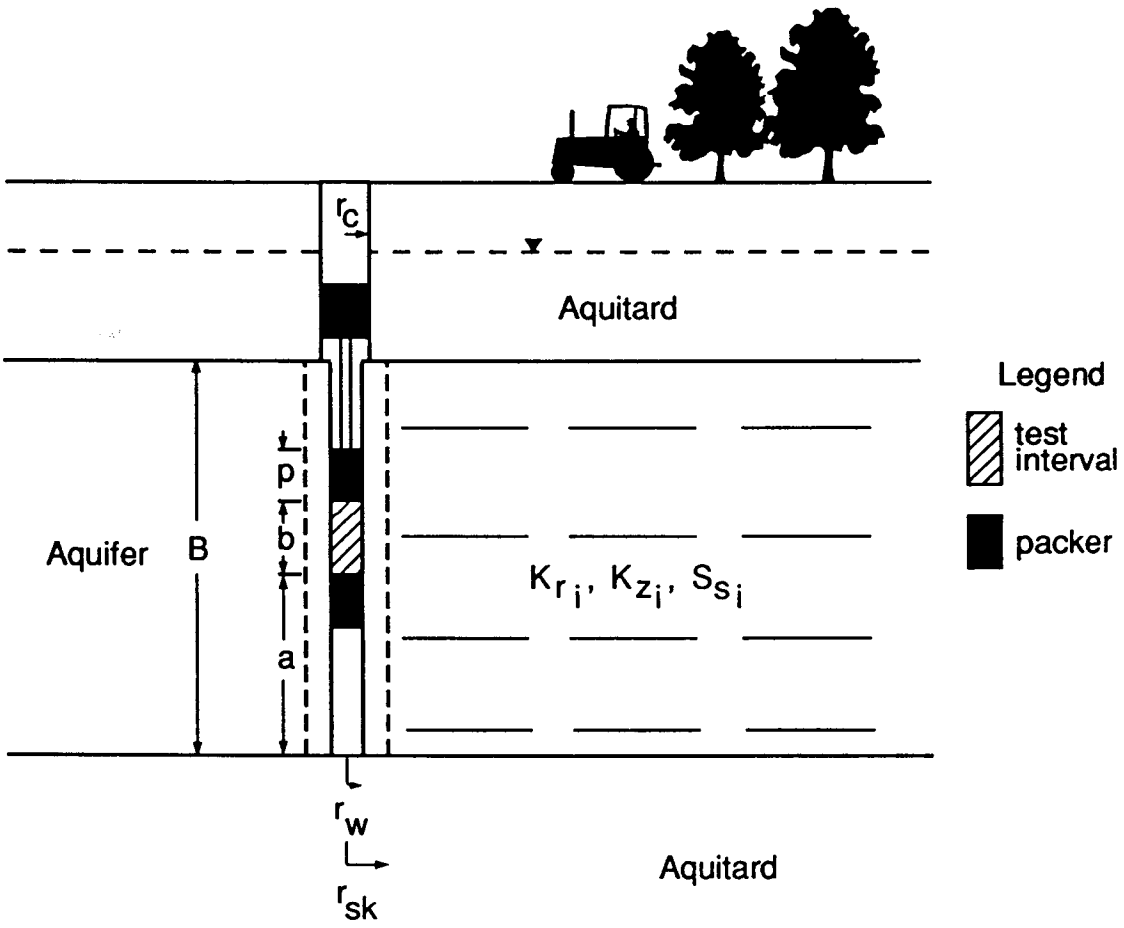

Figure II.A.1 - Cross-sectional view of multilevel slug test configuration (r_w=radius of test interval, r_c=radius of well casing above screen, r_{sk}=radius of skin, B= thickness of aquifer, a=distance of the bottom of the test interval above the base of the aquifer, b=width of the test interval, p=packer length, K_{r_i}, K_{z_i}, S_{s_i} =radial component of conductivity, vertical component of conductivity, and specific storage, respectively, of layer i). Note that layering is assumed to extend throughout the cross section.

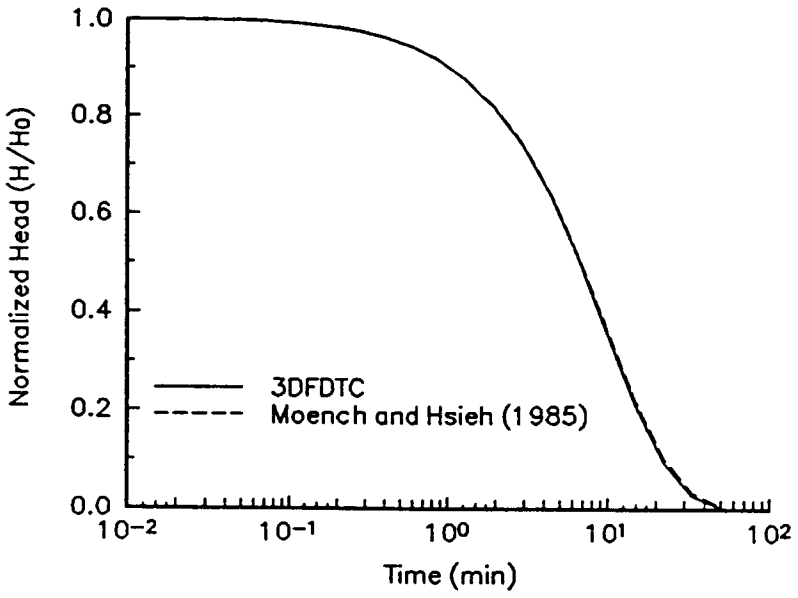

Figure II.A.2 - Normalized head ($H(t)/H_0$) versus time plots comparing analytical solutions to 3DFDTC results: a) Comparison of Moench and Hsieh (1985) solution with 3DFDTC results (r_w=.167 m, r_{sk}=.33 m, T_{sk}=.001 m^2/min, S_{sk}=.001, T_{aq}=1 m^2/min, S_{aq}=.00001);

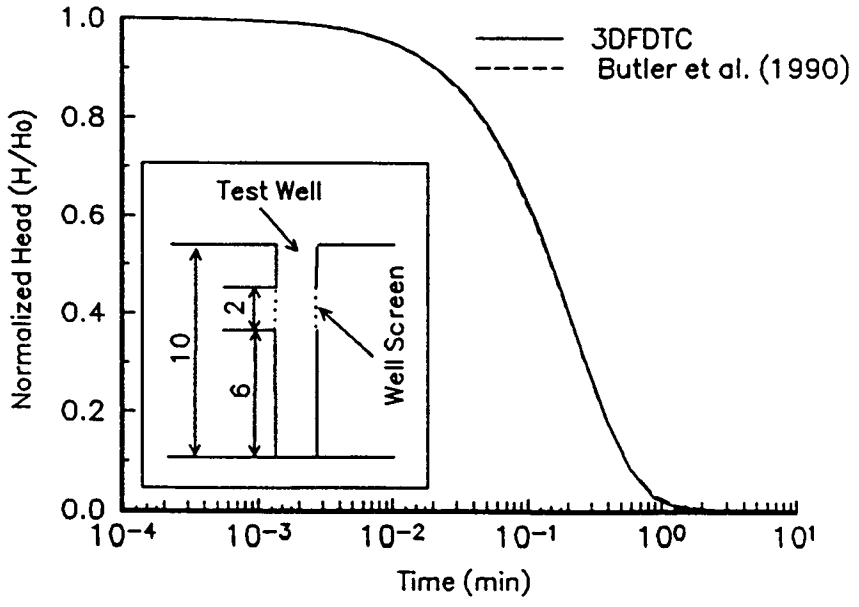

b) Comparison of Butler et al. (1990) solution with 3DFDTC results (r_w=.167 m, K=.1 m/min, S_s=.000001 /m).

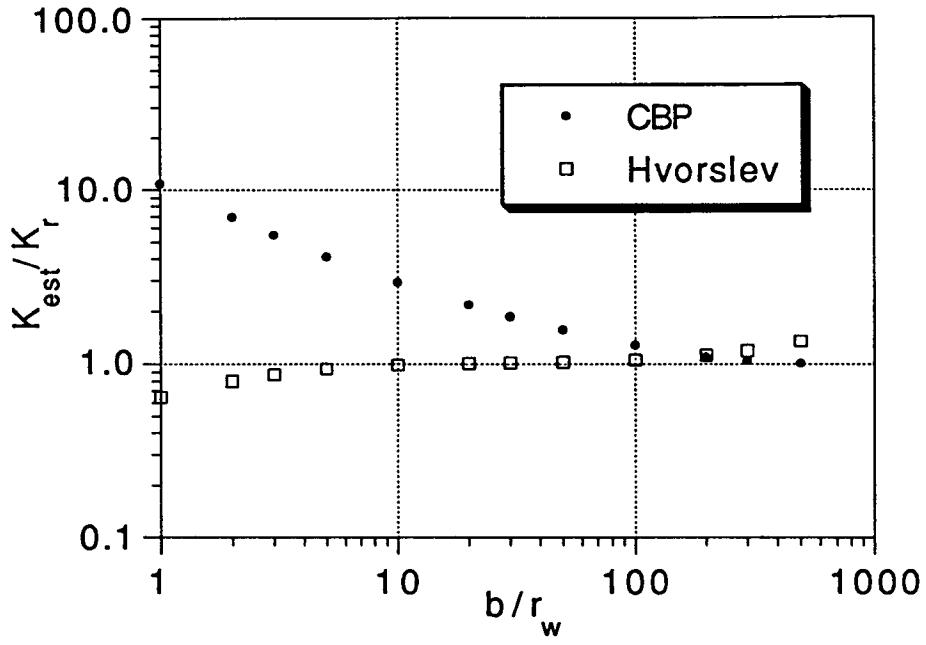

Figure II.A.3 - Aspect ratio (b/r_w) versus conductivity ratio (K_{est}/K_r) plot for the case of boundaries at a large distance from the test interval.

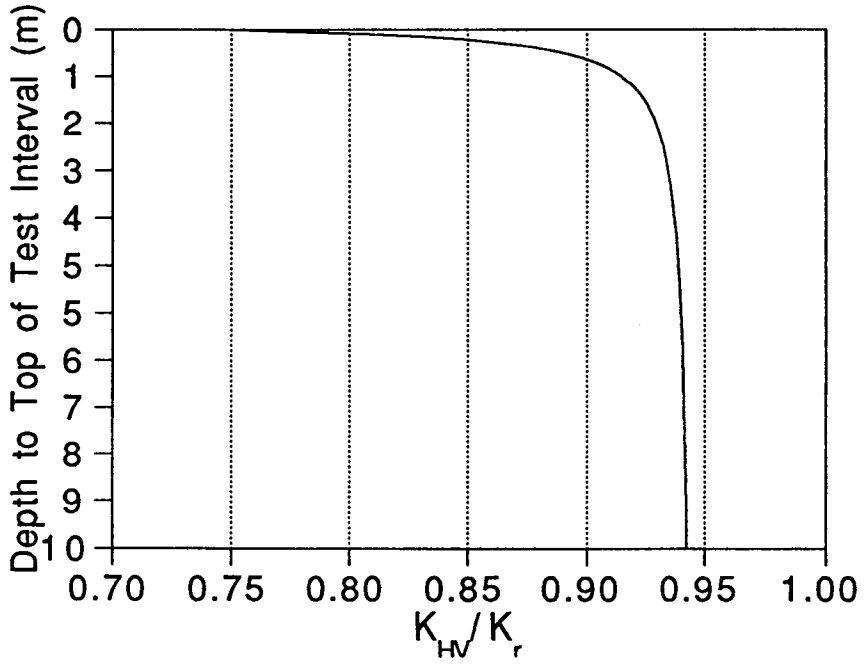

Figure II.A.4 - Plot of conductivity ratio (K_{HV}/K_r) versus depth to top of test interval (aspect ratio (b/r_w) = 5., impermeable boundary assumed at 0.). Note that in Figure 3 (infinite aquifer case) K_{HV}/K_r = .94 for this aspect ratio.

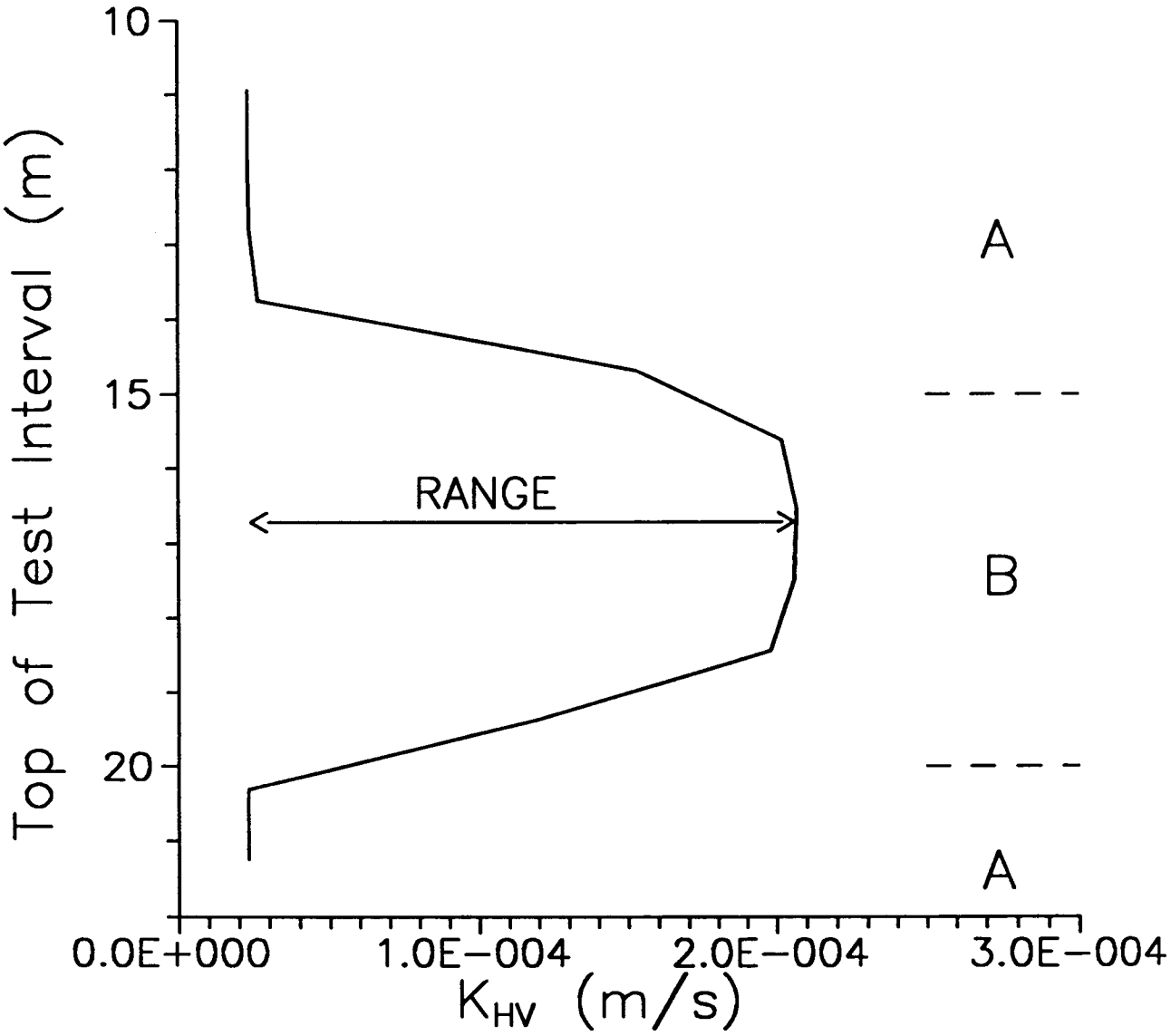

Figure II.A.5 - Estimated conductivity versus depth to top of test interval plot for multilevel slug tests simulated in a layered aquifer consisting of alternating layers of material A and B (see Table II.A.1 - L (layer thickness) = 5 m, b (length of test interval) = 1.25 m). Range is defined as distance between the maximum and minimum estimated conductivity.

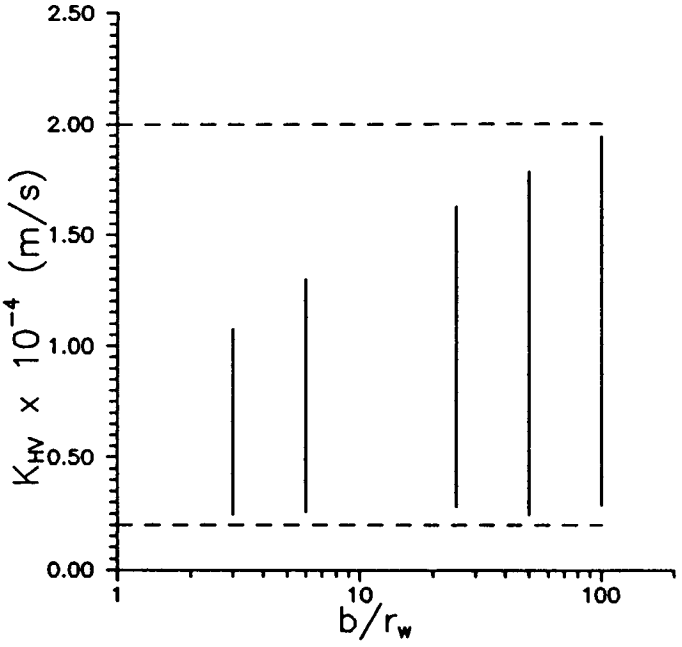

Figure II.A.6 - Range of estimated conductivities versus aspect ratio (b/r_w) plot. Note that layer thickness changes in the same manner as b. Lower and upper dashed lines indicate the conductivities of layers A and B, respectively.

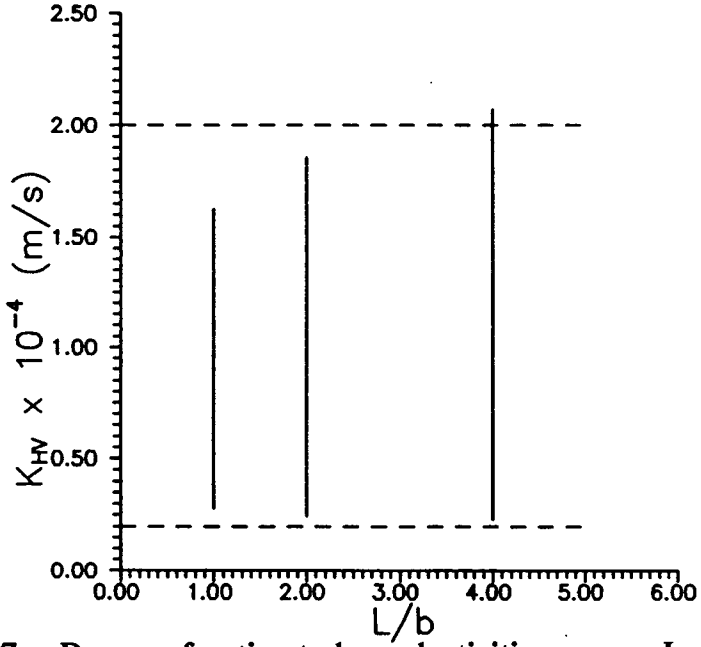

Figure II.A.7 - Range of estimated conductivities versus L (layer thickness) over b (length of test interval) plot. Note that b remains constant (=1.25 m) for the cases displayed on this plot. Lower and upper dashed lines indicate the conductivities of layers A and B, respectively.

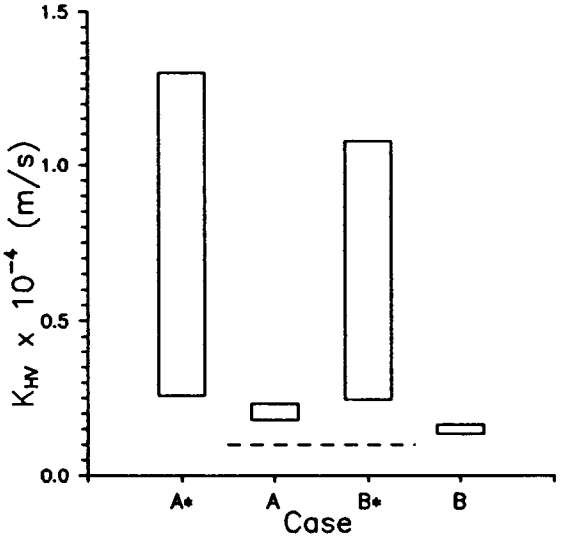

Figure II.A.8 - Range of estimated conductivities versus simulation case plot for the low permeability (K_{sk}=.00001 m/s) skin scenario (Case A* - no skin case, L=b=.312 m; Case A - L=b=.312 m, r_{sk}=.11 m; Case B* - no skin case, L=b=.156 m; Case B - L=b=.156 m, r_{sk}=.11 m). Dashed line indicates the skin conductivity.

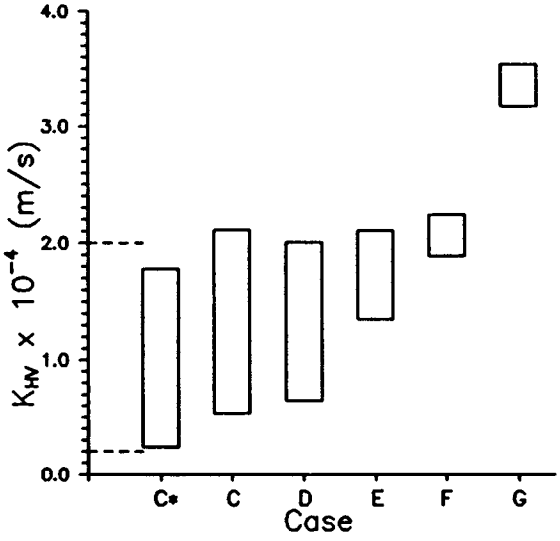

Figure II.A.9 - Range of estimated conductivities versus simulation case plot for the high permeability (K_{sk}=.001 m/s) skin scenario (Case C* - no skin case, L=b=2.5 m; Case C - L=b=2.5 m, r_{sk}=.11 m; Case D - L=b=1.25 m, r_{sk}=.11 m; Case E - L=b=.312 m, r_{sk}=.11 m; Case F - L=b=.156 m, r_{sk}=.11 m; Case G - L=b=.312 m, r_{sk}=.22 m). Lower and upper dashed lines indicate the conductivities of layers A and B, respectively.

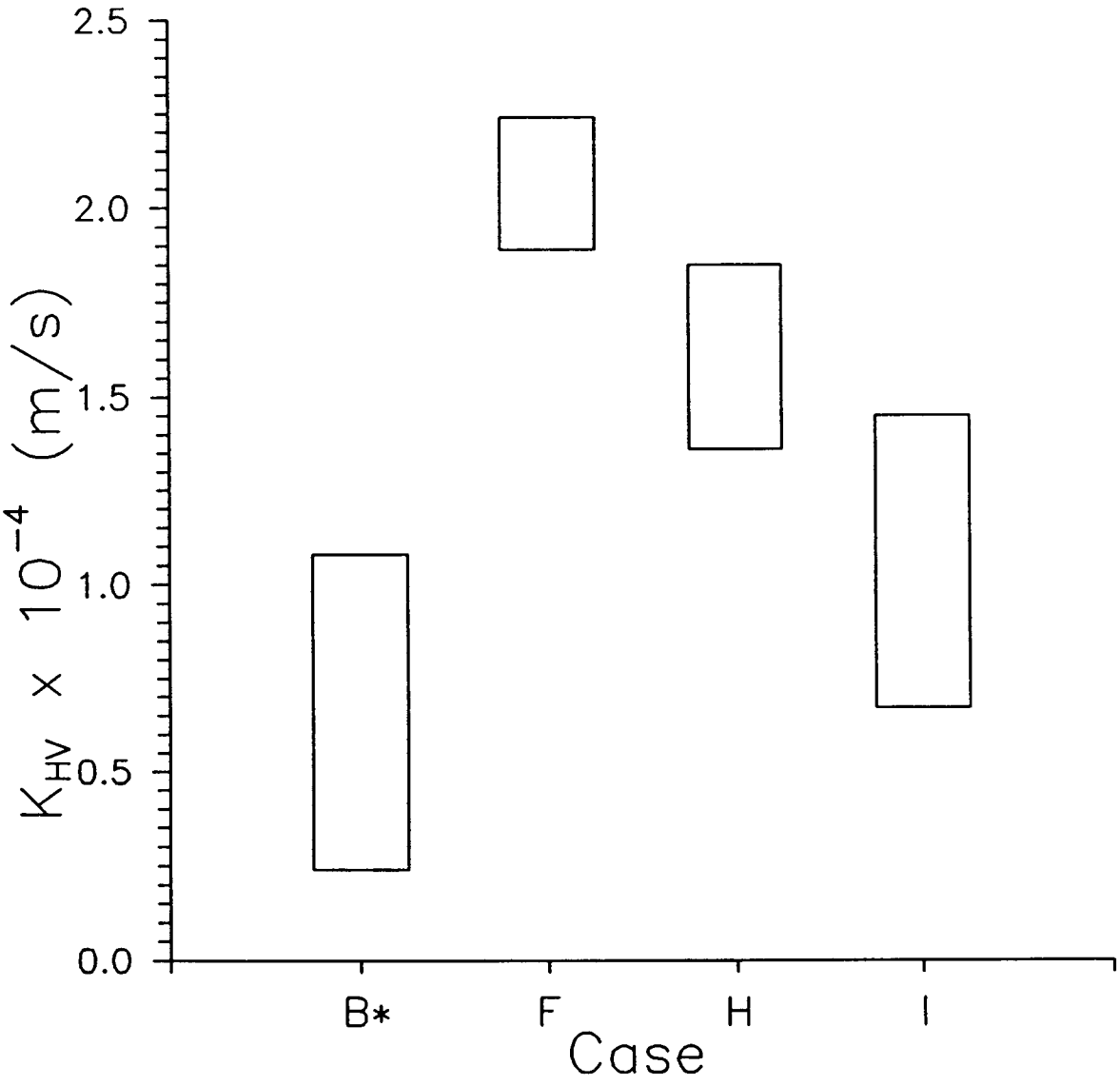

Figure II.A.10 - Range of estimated conductivities versus simulation case plot for the high permeability skin with anisotropy scenario (Case B* - no skin case, L=b=.156 m; Case F - same as in Figure II.A.9; Case H - Case F except $K_{r(skin)}/K_{z(skin)}$ = 2.; Case I - Case F except $K_{r(skin)}/K_{z(skin)}$ = 10.).

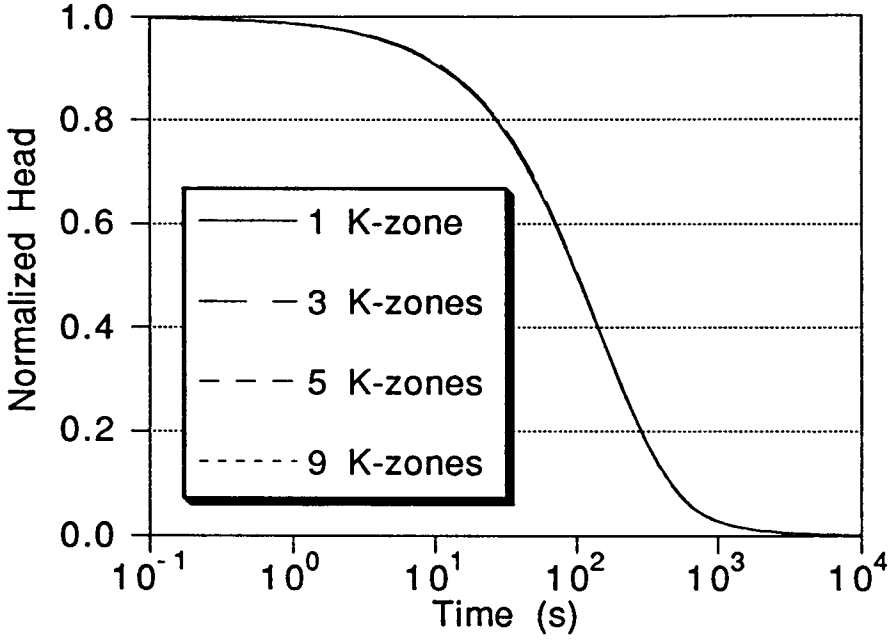

Figure II.A.11 - Effects of variable layering on fully-penetrating slug test results: a) Plot of normalized head ($H(t)/H_0$) at the test well versus time;

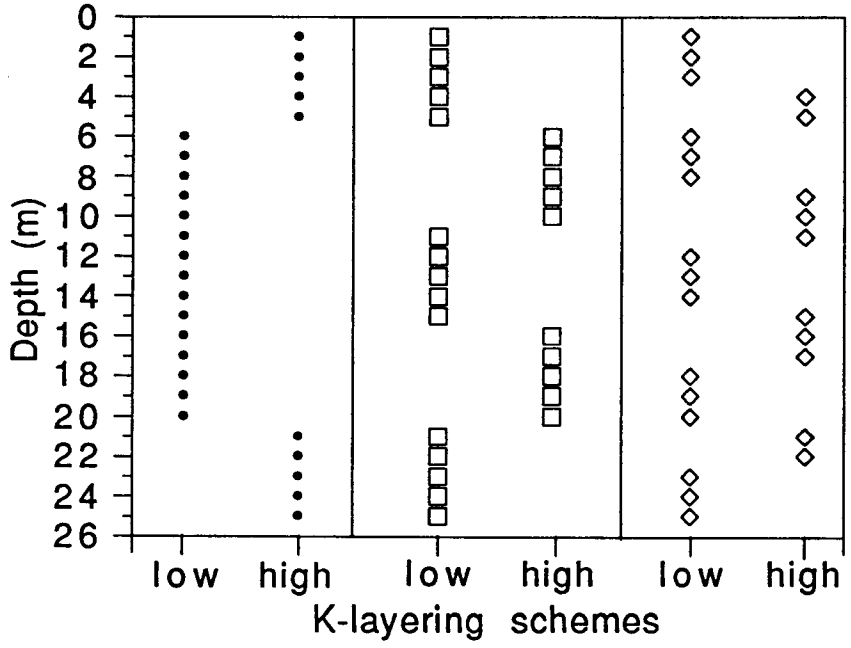

b) Layering schemes employed in the simulations shown in Figure II.A.11a (low and high conductivities defined in Table II.A.2).

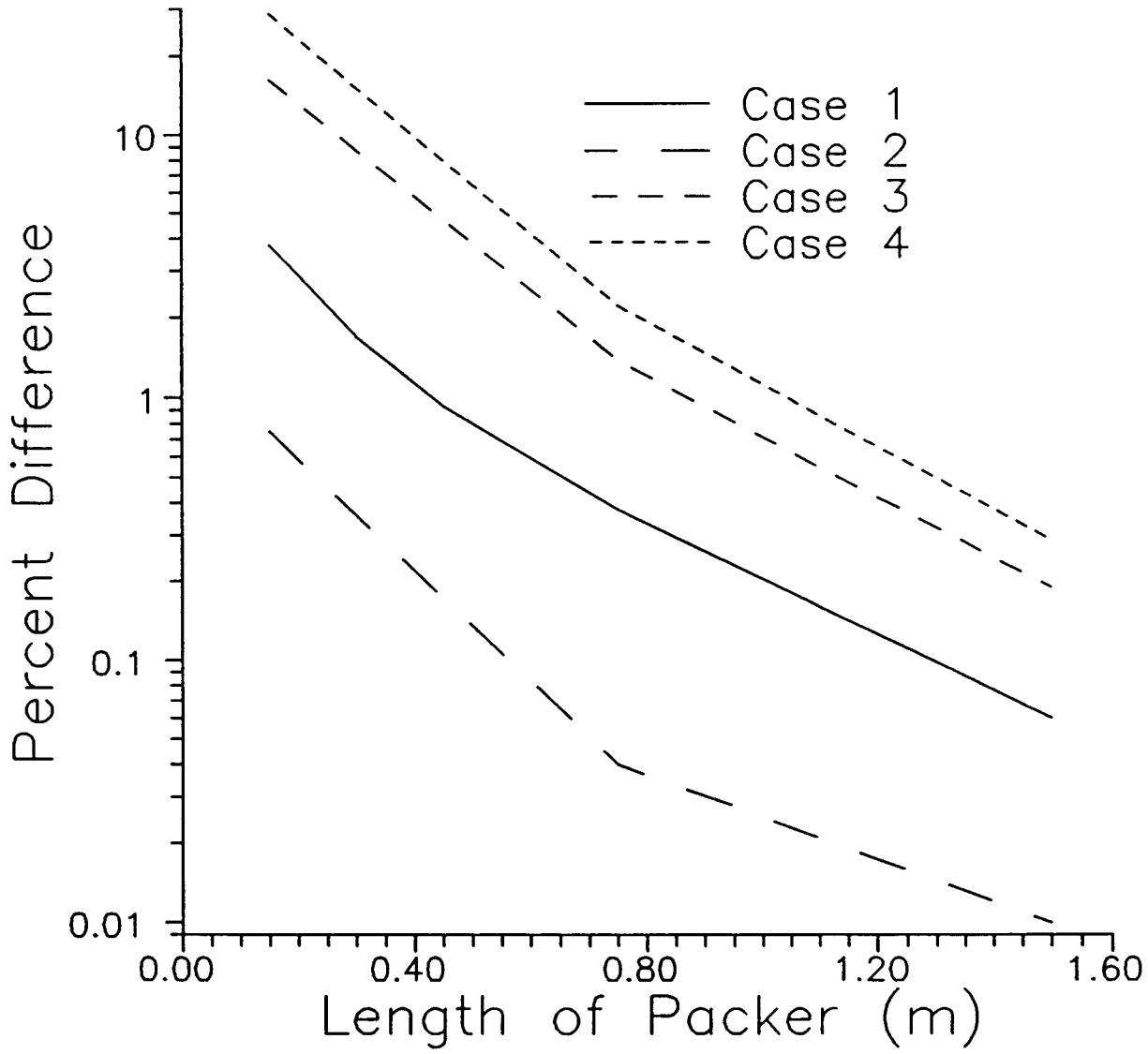

Figure II.A.12 - Packer length versus normalized difference $((K_{packer} - K_{\infty\ packer})/K_{\infty packer}$ x 100.) plot for Cases 1-4 of Table II.A.3. Plotted results are for case of test interval opposite layer A.

B. HYDRAULIC TOMOGRAPHY IN TWO-DIMENSIONAL GROUNDWATER FLOW

Abstract

The head drop between any two points on a streamline is given by a line integral of the flux along the streamline multiplied by the hydraulic resistivity (inverse of hydraulic conductivity). This integral provides the basis for a tomographic method for estimating the distribution of hydraulic resistivities from measured heads in a steady-gradient flow field. Streamline trajectories and flux integrals are computed from a finite difference solution for stream function values based on an estimate of the resistivity distribution. Computing flux integrals along a number of streamlines with known heads at each end results in a system of linear equations which can be solved for an updated set of resistivities. Stream function values and flux integrals are recomputed and the process repeats until the resistivity estimates converge. This section includes numerical examples involving the estimation of the resistivity distribution in a vertical plane.

Introduction

As discussed in *Yeh's* [1986] review of the groundwater inverse problem, most research on aquifer parameter estimation has been cast either in terms of reducing an equation error criterion (direct method) or in terms of reducing an output error criterion (indirect method). In the direct method, the head is assumed to be known and specified exhaustively (typically, at all nodes in a finite difference or finite element grid) and the groundwater flow equation is recast as a first-order partial differential equation in the unknown transmissivity or hydraulic conductivity (assuming all source and sink terms and boundary conditions are known). Head gradient terms, estimated by differences of heads at computational nodes, appear in the left-hand side coefficients in this equation. Examples of application of the direct method include *Frind and Pinder* [1973], *Neuman* [1973], and the important early work by *Nelson* [1960, 1961, 1968].

In the indirect formulation of the inverse problem, the unknown aquifer parameters are iteratively adjusted until model-predicted heads and observed heads are sufficiently close, usually in the least squares sense. In most formulations, the indirect inverse problem depends on the calculation of the Jacobian or sensitivity matrix, where each element (i,j) is given by the partial derivative of a model output value, h_i, to model parameter j. In general, the sensitivity to each unknown parameter is itself a function of time and spatial location.

Sensitivity to the hydraulic conductivity in a certain region of the flow domain obeys an equation of essentially the same form as the equation for the head itself. The inverse problem can be approached by solving a set of 1+M partial differential equations at each iteration, the first describing the head field itself and each of the remaining M equations describing the distribution of the sensitivity to each of the M unknown parameters. As demonstrated in *Yeh* [1986] and *McElwee* [1982], in the sensitivity equation a term involving the head gradient appears in place of the source/sink term in the original equation for head. This head gradient is now evaluated from numerical differentiation of the computed head field, rather than from interpolation between observed head values, as in the direct inverse solution.

Neuman [1980] and *Carrera and Neuman* [1986] present a conjugate gradient minimization approach for solving the indirect inverse problem. The derivative of the objective function (sum squared output error) to each model parameter is derived from an adjoint state function. This method does not require computation of the Jacobian matrix and so does not require solution of the sensitivity equations at each iteration. Evaluation of the head gradient is still required, however, to compute the derivative of the objective function with respect to unknown conductivity values.

Any method for estimating aquifer conductivities (or transmissivities) depends in some way on the evaluation of head gradient terms because of the close relationship between the inverse problem and the Cauchy problem. In an appendix, *Neuman* [1980] discusses the causes for ill-conditioning of the inverse problem in terms of the one-dimensional Cauchy problem. The conductivity at each point in a one-dimensional flow problem is given uniquely by the specific flux at that point divided by the hydraulic gradient. The same condition applies along each flow line in a two- or three-dimensional flow field. If all source terms are known, conductivity can be determined uniquely along each flow line that crosses a surface where Cauchy data (either conductivity or flux) are specified. A specified flux boundary would constitute such a surface.

The relationship between the Cauchy problem and the inverse problem is also discussed in the papers by *Nelson* [1960, 1961, 1968]. *Nelson* [1961] describes a method for solving the direct inverse problem that involves flow net analysis. This is essentially a means of solving the one-dimensional Cauchy problem along each streamtube. A similar method has recently been presented by *Scott* [1992]. *Scott* [1992] derives his streamtube representation from a flow net based on a spline fit to the observed heads in a region, while *Nelson* [1961] uses an orthogonal regression fit. A large amount of head data are required to create an accurate representation of the piezometric surface in either case. Both authors also assume that the distribution of recharge and discharge along each streamtube is known.

Given the transmissivity at any point along the streamtube and the distribution of recharge and discharge, the transmissivity at any other point on the streamtube can be determined uniquely. If the recharge is unknown, only the ratio of transmissivity to recharge can be determined.

The method proposed here shares characteristics both of the indirect solution methods and the direct solution methods based on flow net analysis. A reformulation of the Cauchy problem shows that the head drop between any two points along a streamline is given by the line integral of the specific flux multiplied by the hydraulic resistivity along that streamline. This can also be seen as an integral version of Darcy's law, applied along a streamline. If the model domain is discretized into constant-resistivity zones, then the head drop along each streamline is given by a linear combination of the resistivities encountered along that streamline, with coefficients given by the integral of the specific flux within each constant resistivity zone.

In this study, streamline trajectories and values for specific flux along each streamline are derived from a finite difference solution for the stream function based on the current estimate of the resistivity distribution. Accumulating flux integral information along a number of streamlines connecting points with known heads leads to a system of linear equations yielding a vector of resistivity correction terms. These corrections are used to create an updated set of resistivity values. New stream function values, streamline trajectories, flux integrals, and resistivity corrections are then computed based on the new resistivities. The process continues until resistivity estimates converge. This approach is very similar to that used in seismic tomography [*Peterson et al.*, 1985].

The streamline trajectories and the specific fluxes are derived from the finite difference solution for the stream function using a modified version of a path-tracing algorithm presented by *Pollock* [1988]. *Pollock* [1988] presented a method for tracing advective flow paths based on the heads computed using a block-centered finite difference formulation. His method uses a linear interpolation of each velocity component within a model cell from the velocities computed at the cell faces. In *Pollock* [1988], the cell-face velocities (fluxes scaled by porosity) are derived from the differences of heads computed at the centers of adjacent model cells. In this work, the flux field within each cell is derived from bilinear interpolation of the fluxes at the cell faces, as in *Pollock* [1988]. However, the cell-face fluxes are derived from differences of stream function values at the corners of each cell, using a mesh-centered formulation, rather than from differences of heads in adjacent cells. This study presents the development of a formula for the integral of the flux along a

streamline in each model cell, providing the link between the path-tracing algorithm and the tomographic system of equations.

The original approach in this work was to base the streamline and flux integral calculations on head values computed using a block-centered finite difference formulation, as in *Pollock* [1988]. However, we discovered that there are two important reasons for basing the path-tracing and flux integral computations on a mesh-centered solution for stream functions instead. One reason is that flux values computed from differences of computed stream function values are inherently more accurate than those computed from differences of computed head values, as pointed out by *Frind and Matanga* [1985]. Secondly, the block-centered formulation uses harmonic averages of adjacent cell conductivities to represent cell face conductivities. As pointed out by *Desbarats* [1992a], the resulting distribution of cell-face conductivities tends to underestimate the distribution of cell-by-cell conductivities. As a result, the flux integral calculation, which uses cell-by-cell conductivities, sees a higher overall conductivity than the finite difference model for heads. This inconsistency leads to convergence problems for the inverse technique, since the resistivity corrections derived from the tomographic equations are not necessarily the optimal ones for computing a head field which will result in improved flux integral predictions.

Pollock's method is applicable to general time-varying, three-dimensional problems and can be used to compute particle position along a flow path as a function of time. His presentation is in terms of actual flow velocities, rather than Darcy velocity (specific flux). The two are equivalent, except for a scaling by the value of porosity. For a steady state flow field, a flow path coincides with a streamline. We are only interested in integrals of specific flux along a streamline, so we are interested in time only as a convenient variable of integration. Thus, we can use specific flux in place of flow velocity in Pollock's formulation, recognizing that we are working with a time variable that is scaled by the porosity. This has no effect on the resulting flux integral or on the trajectory of the streamline (assuming a constant porosity). The streamline tracing algorithm is not limited to use with finite difference models. *Cordes and Kinzelbach* [1992] present a modification of Pollock's algorithm applicable to velocity fields computed using finite element techniques. The computation of the flux integral could be added to their algorithm as well.

After the stream function solution is obtained and the streamlines are identified, the flux is integrated along each streamline. Flux integral components in each model cell are added to the appropriate entry in the coefficient matrix for the tomographic system of equations. An arbitrary zonation may be imposed on the model domain to reduce the number

of unknown resistivities. This estimation process is also iterative, since the stream function and streamline distributions depend on the current estimate of the resistivities.

This method (iteratively) identifies the 'characteristics' of the flow system, which coincide with the flow lines in an isotropic system [*Neuman*, 1973]. Since the head drop along any streamline depends only on the resistivities encountered by that streamline, this inverse procedure depends less on the spreading of Cauchy information across the flow field, described as the 'cross-characteristic influence of Cauchy data' by *Neuman* [1973]. This should improve the conditioning of the inverse problem. Another feature of this method is that the head drop along each streamline is a linear function of the sequence of resistivities along the streamline. Given the true model, exact parameter variances and covariances can be computed, since no second order information is being neglected in the forward computation.

The current work is concerned with determining the distribution of hydraulic conductivities (actually resistivities) in a vertical plane, rather than the distribution of transmissivity in a horizontal plane. However, this primarily involves a difference in terminology. The tomographic method could just as easily be applied to determining transmissivity in the horizontal plane.

The current work employs a very simple flow configuration, a vertical rectangular plane between two wells, one extracting water along a limited vertical interval and the other injecting the same amount of water, also along a limited vertical interval. For simplicity, a Cartesian coordinate system is used and local isotropy (within each model cell) is assumed. We are ignoring the fact that the flow to a well is actually radial and the complications caused by anisotropy in the conductivity. However, these simplifications are only for the purpose of demonstrating and testing the method. The theory is applicable to more complex and realistic flow configurations, as long as steady-gradient conditions have been achieved. The method does not require strict steady state conditions, since it depends only on head differences. Heads may be falling or rising at a uniform rate across the flow domain when measurements are taken.

The Finite Difference Model

The differential equation describing the stream function, ψ, in a two-dimensional vertical plane with heterogeneous, isotropic hydraulic resistivity, R, is

$$\frac{\partial}{\partial x}\left(R\frac{\partial \psi}{\partial x}\right)+\frac{\partial}{\partial y}\left(R\frac{\partial \psi}{\partial y}\right)=0 \qquad \text{(II.B.1)}$$

where x is the horizontal coordinate and y is the vertical coordinate (positive upward). As described in *Frind and Matanga* [1985], interior sources and sinks can be included in the stream function formulation by inserting a cut in the model domain connecting the interior source/sink point to the domain boundary, allowing the source/sink term to appear as an external boundary condition. We do not include interior source/sink terms in the current work. They could be incorporated without substantially affecting the hydraulic tomography formulation. However, heads would have to be known at all interior source/sink points, since each such point is the starting or ending point for a certain set of streamlines.

Using the convention adopted by *Frind and Matanga* [1985], the components of specific flux in the x and y directions, q_x and q_y, are related to the stream function by

$$q_x=\frac{\partial \psi}{\partial y} \qquad q_y=-\frac{\partial \psi}{\partial x} \qquad \text{(II.B.2)}$$

(Alternatively, the negative sign may be applied to the y derivative to obtain q_x. The choice is arbitrary.)

In this work, only specified flux boundary conditions are used. These result in first-type (Dirichlet) boundary conditions on the stream function. Following *Frind and Matanga* [1985], if ψ_0 represents the stream function at the point Γ_0 on the boundary, then the stream function along the boundary, Γ, is given by

$$\psi(\Gamma)=\psi_0(\Gamma_0)+\int_{\Gamma_0}^{\Gamma} \mathbf{q}_0\cdot\mathbf{n}\,d\Gamma \qquad \text{(II.B.3)}$$

where $\mathbf{q}_0$ represents the specified boundary flux and $\mathbf{n}$ is the unit normal to the boundary. Thus, stream function values at boundary nodes in a finite difference model are obtained by summing specified boundary fluxes, proceeding around the model boundary in either a clockwise or counterclockwise sense.

Figure II.B.1 is a sketch of a node in a mesh-centered finite difference grid, along with its neighboring nodes and cells. In our formulation, each cell in the model is labeled with the pair of indices identifying the node in its upper right-hand corner. The centered-difference approximation of the derivatives in Equation II.B.1 involves the resistivities at points half-way between nodes, at the midpoints of cell faces. These resistivities are

computed as arithmetic averages of the two adjacent cell resistivities. Thus, the resistivity between node (i,j) and node (i+1,j) is approximated as

$$R_{i+1/2,j} = \frac{R_{i+1,j} + R_{i+1,j+1}}{2} \qquad \text{(II.B.4)}$$

From the perspective of the head field for a linear flow system, hydraulic conductivities in series average harmonically and conductivities in parallel average arithmetically [*McDonald and Harbaugh*, 1984]. Thus, if we were solving for head using the mesh-centered formulation shown in Figure II.B.1, it would be appropriate to use the arithmetic average of the conductivities to represent the conductivity midway between the nodes. Since resistivity plays the same role in the stream function equation as does conductivity in the head equation, the same averaging laws apply to R in the stream function formulation as apply to K in the head formulation.

A mesh-centered finite difference formulation leads to the following equation for each node (i,j):

$$a_{xi,j}\psi_{i-1,j} + a_{yi,j}\psi_{i,j-1} + b_{i,j}\psi_{i,j} + c_{xi,j}\psi_{i+1,j} + c_{yi,j}\psi_{i,j+1} = d_{i,j} \qquad \text{(II.B.5)}$$

where the coefficients for interior nodes are given by

$$a_{xi,j} = \frac{R_{i-1/2,j}}{\Delta x^2} \qquad \text{(II.B.6a)}$$

$$c_{xi,j} = \frac{R_{i+1/2,j}}{\Delta x^2} \qquad \text{(II.B.6b)}$$

$$a_{yi,j} = \frac{R_{i,j-1/2}}{\Delta y^2} \qquad \text{(II.B.6c)}$$

$$c_{yi,j} = \frac{R_{i,j+1/2}}{\Delta y^2} \qquad \text{(II.B.6d)}$$

$$b_{i,j} = -\left(a_{xi,j} + a_{yi,j} + c_{xi,j} + c_{yi,j}\right) \qquad \text{(II.B.6e)}$$

$$d_{i,j} = 0 \qquad \text{(II.B.6f)}$$

Since only Dirichlet boundary conditions are employed, equations for boundary nodes could be eliminated from the system of equations, with equations for adjacent nodes being modified

appropriately. However, for simplicity of coding, the boundary node equations are retained using

$$b_{i,j} = 1 \qquad \text{(II.B.7a)}$$

$$a_{xi,j} = a_{yi,j} = c_{xi,j} = c_{yi,j} = 0 \qquad \text{(II.B.7b)}$$

$$d_{i,j} = \psi_{i,j} \qquad \text{(II.B.7c)}$$

$\psi_{i,j}$ at a boundary node is obtained from summation of the specified boundary flux at each node multiplied by the appropriate cell dimension (Δx for bottom and top nodes, Δy for left and right nodes). A value of zero is assigned for the stream function at the lower left-hand node, (i,j) = (0,0), and the summation proceeds in a counterclockwise fashion.

The program used for this study solves the system of equations using a simple alternating direction implicit technique [*Wang and Anderson,* 1982]. For each direction, the appropriate terms in Equation II.B.5 are moved to the right-hand side, modifying the d vector and resulting in a tridiagonal left-hand coefficient matrix. The method of treating boundary nodes shown in Equation II.B.7 facilitates the production of the tridiagonal coefficient matrix for the entire set of nodes, since boundary nodes need no special treatment aside from the initial computation of their coefficients.

The Streamline-Tracing Algorithm

The streamline-tracing algorithm is derived from that described by *Pollock* [1988], with some minor modifications. The first modification is that the algorithm is recast entirely in terms of specific flux values (Darcy velocities), rather than actual flow velocities. Pollock was interested in tracing the advective transport of particles with time, and so developed his algorithm in terms of flow velocity, v. Flow velocity, v, and specific flux, q, are related by

$$v = \frac{q}{n} \qquad \text{(II.B.8)}$$

where n is the porosity of the medium. We are not interested in the time of travel along a path, but only in the path trajectory and the integral of flux along the path. Thus, the algorithm presented here works directly in terms of specific fluxes using a time given by $t = t_r/n$, where t_r is the real-world travel time. We use this time only as a convenient variable of

integration. However, actual travel time along a path could be derived from it simply by multiplying by the porosity.

The second modification is the use of a slightly different set of coordinates. Pollock works with global coordinates. The streamline-tracing algorithm presented here, however, uses a local coordinate system in each cell, with x ranging from $-\Delta x/2$ to $\Delta x/2$ and y ranging from $-\Delta y/2$ to $\Delta y/2$. Figure II.B.2 is a sketch of a single cell in the finite difference model showing the locations of the cell-face fluxes and one possible flow path through the cell. q_{x1} is the x component of flux at the left face, q_{x2} is the x component of flux at the right face, q_{y1} is the y component of flux at the bottom face, and q_{y2} is the y component of flux at the top face. The flux field is given by

$$q_x(x) = q_{x0} + A_x x \qquad \text{(II.B.9a)}$$

$$q_y(y) = q_{y0} + A_y y \qquad \text{(II.B.9b)}$$

where

$$q_{x0} = \left(q_{x2} + q_{x1}\right)/2 \qquad \text{(II.B.10a)}$$

$$q_{y0} = \left(q_{y2} + q_{y1}\right)/2 \qquad \text{(II.B.10b)}$$

and

$$A_x = \left(q_{x2} - q_{x1}\right)/\Delta x \qquad \text{(II.B.11a)}$$

$$A_y = \left(q_{y2} - q_{y1}\right)/\Delta y \qquad \text{(II.B.11b)}$$

The final, and most important, modification of Pollock's algorithm is that we derive the cell-face fluxes from differences of stream function values computed at nodes located at the corner of each cell, rather than from differences of head values computed at nodes located at the center of adjacent cells (scaled by the cell face conductivity). For example, in *Pollock* [1988] q_{x2} for cell (i,j) is given by

$$q_{x2} = -\frac{K_{i+1/2,j}}{\Delta x}\left(h_{i+1,j} - h_{i,j}\right) \qquad \text{(II.B.12)}$$

where $K_{i+1/2,j}$ is the cell-face conductivity on the right-hand face, $h_{i,j}$ is the head in cell (i,j), and $h_{i+1,j}$ is the head in the cell (i+1,j). In our formulation, however, the right-hand cell-face flux is given by

$$q_{x2} = \frac{(\psi_{i,j} - \psi_{i,j-1})}{\Delta y} \qquad \text{(II.B.13)}$$

where $\psi_{i,j}$ is the stream function value computed at node (i,j), at the upper right-hand corner of cell (i,j), and $\psi_{i,j-1}$ is the stream function value computed at the lower right-hand corner of cell (i,j).

Pollock's development of the equations describing a flow path will be briefly summarized here, being recast in terms of specific flux values and local coordinates. Given the above expressions for the flux components and the entry location of a streamline in local coordinates, the flux components, q_{xp} and q_{yp}, at the entry point, (x_p,y_p), can be obtained from Equation II.B.9. A particle moving through the cell from this entry point will then follow a trajectory determined by the following relationships

$$\frac{dq_x(t)}{dt} = A_x q_x(t) \qquad \text{(II.B.14a)}$$

$$\frac{dq_y(t)}{dt} = A_y q_y(t) \qquad \text{(II.B.14b)}$$

The right-hand sides of Equation II.B.14 are derived from application of the chain rule. A_x is dq_x/dx and $q_x(t)$ is the current value of dx/dt for the particle. Equation II.B.14 can be integrated, to give the following expressions for the flux components as a function of time

$$q_x(t) = q_{xp}\exp(A_x t) \qquad \text{(II.B.15a)}$$

$$q_y(t) = q_{yp}\exp(A_y t) \qquad \text{(II.B.15b)}$$

The trajectory of the streamline is given by integrating equation Equation II.B.15 and requiring that $(x(0),y(0)) = (x_p,y_p)$, yielding

$$x(t) = \frac{1}{A_x}\left(q_{xp}\exp\left(A_x t\right) - q_{x0}\right) \qquad \text{(II.B.16a)}$$

$$y(t) = \frac{1}{A_y}\left(q_{yp}\exp\left(A_y t\right) - q_{y0}\right) \qquad \text{(II.B.16b)}$$

The travel time in the cell is determined by testing the potential travel times to each face of the cell. The minimum positive (physically meaningful) value is the actual travel time, t_c. For example, the potential travel time to the right face is given by

$$t_{x2} = (1/A_x)\ln\left(q_{x2}/q_{xp}\right) \qquad \text{(II.B.17)}$$

if A_x is non-zero or

$$t_{x2} = \left(\frac{\Delta x}{2} - x_p\right)\Big/ q_{x0} \qquad \text{(II.B.18)}$$

if A_x is zero (q_x is constant). It is possible for all the candidate travel times to be non-positive if the cell represents a sink. This possibility is not allowed in the current work, since no sources or sinks are included in the model. A very long (theoretically infinite) travel time would indicate that the cell is located at a stagnation point in the flow field. Pollock points out that another special case can occur when a flow divide passes through the model cell, meaning, for example, that q_{x1} and q_{x2} are of opposite sign.

Once the travel time in the cell is determined, the coordinates of the exit point, (x_e,y_e), can be calculated by plugging the travel time into Equation II.B.16:

$$x_e = \frac{1}{A_x}\left(q_{xp}\exp\left(A_x t_c\right) - q_{x0}\right) \qquad \text{(II.B.19a)}$$

$$y_e = \frac{1}{A_y}\left(q_{yp}\exp\left(A_y t_c\right) - q_{y0}\right) \qquad \text{(II.B.19b)}$$

The particle moves into the appropriate neighboring cell (or in rare cases exits out the corner to a diagonally adjacent cell) and the process continues until the streamline reaches a boundary.

The Tomographic Equations

Assuming isotropy, Darcy's law reduces to a simple one-dimensional relationship along a streamline:

$$q_s(s) = -K(s)\frac{dh}{ds} \qquad \text{(II.B.20)}$$

where $q_s(s)$ is the specific flux (L/T) along the streamline, K(s) is the hydraulic conductivity (L/T) and dh/ds is the directional derivative of head along the streamline (dimensionless). The total head drop, H, along the streamline is given by rearranging Darcy's law and integrating:

$$H = \int_0^{L_s} R(s) q_s(s) ds \qquad \text{(II.B.21)}$$

where L_s is the total length of the streamline and R is hydraulic resistivity (T/L), the inverse of K.

In a finite difference model the resistivity is not a continuous spatial function, but is instead discretized into cell-by-cell values. Assuming that a streamline encounters N different cells, each with a discrete resistivity, R_i, the head drop along the streamline is given by

$$H = \sum_{i=1}^{N} \left(R_i \int_{si} q_s(s) ds \right) \qquad \text{(II.B.22)}$$

where the integral is evaluated separately along the streamline path within each cell, i.

The evaluation of the flux integral within a cell is simplified by recognizing that $q_s(s)ds$ is the same as $q_s^2(t)dt$, since $ds = q_s(t)dt$. Furthermore, $q_s^2(t) = q_x^2(t)+q_y^2(t)$, so that the flux integral within a cell conveniently reduces to the sum of two simple integrals

$$\int_{si} q_s(s) ds = \int_0^{t_c} q_s^2(t) dt = \int_0^{t_c} q_x^2(t) dt + \int_0^{t_c} q_y^2(t) dt \qquad \text{(II.B.23)}$$

Squaring and integrating the expression for $q_x(t)$ in Equation II.B.15 yields

$$\int_0^{t_c} q_x^2(t) dt = \frac{q_{xp}^2}{2A_x} \left(\exp(2A_x t_c) - 1 \right) \qquad \text{(II.B.24)}$$

if A_X is non-zero and

$$\int_0^{t_c} q_x^2(t) dt = q_{x0}^2 t_c \qquad \text{(II.B.25)}$$

if A_x is zero ($q_x(x)$ is constant). The corresponding expressions for the y-component integral are analogous. The addition of Equations II.B.23 -II.B.25 to Pollock's algorithm provides the means for reducing the complex dependence of the head field on the entire field of hydraulic conductivity to a simple set of one-dimensional equations expressing the linear dependence of the head drop between two points on the sequence of resistivities encountered by the streamline between those two points.

To reduce the number of unknown parameters, model cells may be grouped into larger zones of constant resistivity. If M is the number of zones, j is the zone index, and N_j is the number of cells in zone j, then the line integral is given by

$$H = \sum_{j=1}^{M}\left(R_j \sum_{i=1}^{N_j} \int_{si} q_s(s)ds \right) \qquad \text{(II.B.26)}$$

This is the formulation used in the program developed for the present study. The user is allowed to specify an arbitrary zonation of the resistivity field. Each zone may consist of one contiguous region of constant R, or several separate regions, all of the same R. For example, it would be possible to specify a two-zone model with alternating layers of zone-1 resistivity and zone-2 resistivity.

If measured heads are available at both ends of a streamline, these two values can be subtracted to yield an observed head drop. Subtracting the head drop predicted by Equation II.B.26 from the observed head drop yields a head drop residual, here denoted by ΔH. Since the relationship between head drop and resistivity along a streamline is linear, the head drop residual could be accounted for by a series of corrections, ΔR_j, to the zonal resistivities along the flow path. The corrections would need to satisfy

$$\Delta H = \sum_{j=1}^{M}\left(\Delta R_j \sum_{i=1}^{N_j} \int_{si} q_s(s)ds \right) \qquad \text{(II.B.27)}$$

Any set of resistivity corrections that satisfied Equation II.B.27 would allow the predicted head drop along the streamline to exactly match the observed head drop along the streamline, provided that the trajectory of the streamline and the flux integral computed on the basis of the new resistivities were the same as those computed on the basis of the old resistivities. The changes in the streamline trajectory and in the flux integral induced by the change in R values leads to the iterative nature of the parameter estimation process.

If heads have been measured at a number of data points within the model domain, these data points can be used as the beginning points of streamlines. The streamline that passes through a point can be thought of as two streamlines starting from that point, one moving forward, in the positive flux direction, and the other moving backward. In the absence of sources and sinks, each streamline beginning from a point within the model domain is constrained to end on a boundary interval with a non-zero flux, either a specified head boundary or a specified non-zero flux boundary. If heads are also known at all such boundaries, then observed head drops can be computed along each streamline. For each streamline, Equation II.B.26 gives the predicted head drop along that streamline. The head drop residual can then be computed for each streamline. Equation II.B.27 can then be applied, resulting in a set of linear equations

$$\sum_{j=1}^{M} \Delta R_j c_{k,j} = \Delta H_k \qquad k = 1, N_s \tag{II.B.28}$$

where N_s is the number of streamlines and

$$c_{k,j} = \sum_{i=1}^{N_j} \int_{si;k} q_s(s) ds \tag{II.B.29}$$

The integral shown in Equation II.B.29 is evaluated over the path of streamline k in cell i. This result is added into the c_{kj} entry for the zone, j, to which cell i belongs.

Least squares techniques can now be used to solve the set of Equations II.B.28 for the optimal correction values, ΔR_j. These values are then added to the current R estimates and the heads, streamline trajectories, flux integrals and predicted head drops are recomputed. The process continues until the parameter estimates converge or until a specified maximum number of iterations has occurred.

Examples

The initial example simply tests the accuracy of the streamline trajectory and flux integral calculations in a synthetic heterogeneous aquifer. The model domain is nine units on a side, with the upper and lower boundaries representing confining units and the left and right boundaries representing a pair of wells, one injecting water along a limited interval (on the left) and the other extracting the same amount of water along a limited interval (on the right). The spatial distribution of the natural log of the hydraulic resistivity is shown in Figure

II.B.3. This synthetic field was generated using sequential Gaussian simulation [*Deutsch and Journel*, 1992]. The specified variogram was spherical with a sill of 1.0, a range of 1.2 units in the vertical direction, and a range of 24 units in the horizontal direction. Thus, the horizontal range of the log-resistivity field is about 2.7 times the horizontal dimension of the model domain. In contrast, the vertical range is about 13% of the vertical dimension of the model domain. This results in a tendency for the synthetic field to exhibit an imperfectly layered structure similar to that exhibited by natural aquifers. The range of resistivity values corresponding to the log resistivities shown in Figure II.B.3 is 0.04 to 22 (dimensions L/T), or about 2.7 orders of magnitude variation.

Figure II.B.4 displays the head and stream function contours resulting from a single test performed in the synthetic aquifer. In this test water was injected at a rate of 0.5 units (in terms of specific flux, L/T) at each of the six nodes between y=4 and y=5 (inclusive) on the left side and extracted at the same rate along the same vertical interval on the right side. The remaining boundaries are zero-flux boundaries. The two sets of contours are generated from two separate program runs, one for the head solution and one for the stream function solution. The variable resistivity results in a fairly complex flow pattern. The channeling of flow through low-resistivity (high-conductivity) lenses is most evident in the stream function contours, especially near the lower portion of the injection interval on the left-hand side.

The plus signs posted on Figure II.B.4 represent the locations of 27 data points used in this and following program runs. Forward solutions for a set of head fields, using a known resistivity field, are computed for each simulated suite of tests. Head values computed at the posted locations are taken as input data for the subsequent inverse runs. For reasons discussed earlier, the inverse runs base the streamline trajectory and flux integral calculations on stream function solutions, rather than head solutions. At each iteration of an inverse run, streamlines are traced from each data point, at which the head is known, to each non-zero flux boundary. The flux integral along each streamline provides a prediction of the head drop between these two points. These predicted head drops are compared to the observed head drops provided by taking the difference between the observed head at the data point and the observed head at the boundary point where the streamline terminates. In this case the observed heads are provided by the forward solution for the head field. In a real-world application, these values would be provided by measurements in the field.

Figure II.B.5 is a comparison between the head drops computed from the flux integral, using a stream function solution based on the true resistivity field shown in Figure II.B.3, and those calculated from differences of heads computed at the 27 data points and the boundary points intersected by the streamlines. This plot shows that the flux integral results

are consistent with the computed head field, providing some confirmation of the validity of the flux integral formulation.

Before attempting any kind of parameter estimation for groundwater flow systems, a reduction in the dimensionality of the parameter space must be performed. For the purposes of estimating hydraulic conductivity, this reduction is often accomplished by an arbitrary segmentation of the flow domain into a finite number of zones, each characterized by a constant hydraulic conductivity. This discretization of the spatial variability of the conductivity field is one form of model error. Before exploring the effects of this kind of model error on the tomographic method, we will first present results of synthetic tests performed in two simpler aquifers, one consisting of nine constant-resistivity layers and the other consisting of 81 constant-resistivity blocks. The zonations used for parameter estimation will correspond exactly with the geometry of the true conductivity field. This allows us to evaluate the performance of the tomographic method in the absence of model error.

The solid line on Figure II.B.6 represents the true hydraulic resistivity for the simple nine-layer aquifer. This layered resistivity field was created by taking a geometric average of the resistivities of all the cells in sequential five-cell thick layers of the resistivity field shown in Figure II.B.3. Thus, each constant-resistivity layer in the simplified model contains 45 cells in the x direction (the full width of the model domain) and five cells in the vertical direction. The hydraulic tomography program was run in forward mode in order to simulate four different test scenarios in the nine-layer aquifer. The four scenarios examined were a nine-test sequence using nine observation points per test, a nine-test sequence using 27 observation points, a 17-test sequence using nine observation points, and a 17-test sequence using 27 observation points. The forward runs were used to produce head solutions, rather than stream function solutions, in order to provide synthetic head data for the inverse runs. For each test, the heads computed either at all 27 observation points shown in Figure II.B.4 or only those at the nine observation points at x=4.5 were taken as observed heads.

Each test in the suite of nine tests consisted of injecting water at six nodes (bounding a five-cell interval) at the left end of one of the constant-resistivity layers and extracting water at the same rate along the same vertical interval on the right side. The injection rate corresponded to a specific flux rate of 0.5 (L/T) at each node. The fifth test in this sequence, for example, used the same boundary conditions as were used to produce the results shown in Figure II.B.4. The 17-test scenario consisted of the same nine tests with pumping and injection at either end of each layer, plus eight more tests in which the pumping and injection intervals were adjacent to different layers. In the first of these 'crossed' tests, the injection

interval was adjacent to the bottom layer and the pumping interval was adjacent to the top layer. For the next test the injection interval moved up one layer while the pumping interval moved down one layer, and so forth. The middle test of this sequence (with both pumping and injection intervals adjacent to layer five) was included in the original nine tests, and so is skipped in the crossed tests.

The forward runs to produce head data for each test employed specified flux boundary conditions at the pumping and injection intervals. This resulted in the production of a variable head profile over the pumping and injection intervals. These vertically varying heads were averaged over all the nodes in the pumping or injection interval in order to create the boundary heads used as data for the inverse run. In reality, pumping in a well induces a variable flux profile and an essentially constant head along the well intake. Nevertheless, in the absence of data of the sort provided by a flowmeter log, only one flux value and one head value can be assigned to a pumping or injection interval anyway.

Table II.B.1 displays summary statistics for the various tests scenarios in the nine-layer aquifer. The first column displays the correlation between the actual and estimated layer resistivities and the second column displays the root mean squared deviation between these two values. The dashed lines on Figure II.B.6 represent the estimated resistivities for the 9- and 17-test scenarios using nine data points. Figure II.B.7 shows crossplots of true and estimated resistivities for all four test scenarios. Overall, the 17-test scenarios provide a marginally better match to the true resistivity values In the nine tests with the pumping and injection intervals at the same vertical location, flow in the middle of the tested domain is primarily horizontal, with vertical flow restricted to the left and right edges, as shown in Figure II.B.4. The eight additional crossed tests induce more vertical flow in the center of the domain, potentially allowing for better definition of horizontal variation of the resistivity in this region. However, since the properties are assumed to be constant in the horizontal direction, the increased number of more vertical streamlines in the center of the domain contribute little additional information.

Surprisingly, the tests with only nine data points produce somewhat better resistivity estimates (as measured by $\text{cor}(R,\hat{R})$ in Table II.B.1) than those with 27 data points. The streamlines emanating from the 18 data points closer to the left and right edges tend to be more curved than those emanating from the nine data points in the middle of the domain. In addition, those streamlines traveling from each set of 'side' data points to the far well are the longest ones. Increased length and curvature leads to increased potential for inaccuracies in the flux integral calculations. Thus, in this case, it is possible that the additional information

provided by the flux integrals along these streamlines does not offset the deleterious effects of inaccuracies in their calculation.

Figure II.B.8 displays the natural log resistivity field used for the next set of simulated test suites. Each 5X5 block of cells in the 45X45 model grid is represented by a single resistivity value, resulting in a 9X9 array of constant resistivity blocks. The resistivity value assigned to each block is the geometric mean of the cell resistivities for the 25 cells within that block in the fully heterogeneous aquifer shown in Figure II.B.3. The resulting log resistivities for this 81-block aquifer range from -1.90 to 1.97, meaning the actual resistivities range from 0.15 to 7.2. Again, the simulated tests will be analyzed using a zonation corresponding exactly with the true zonation shown in Figure II.B.8 (81 5X5 blocks).

Six different test scenarios were originally used to examine the 81-block aquifer, employing 17, 29 and 45 tests with either nine or 27 data points for each test, as in the nine-layer aquifer tests. The 17-test suite was the same as that described for the nine-layer aquifer. The 29-test suite consisted first of 15 tests, with injection along a four-node (three-cell) vertical interval on the left side and pumping along the same vertical interval on the right side, followed by 14 crossed tests, in a pattern similar to that described for the 17-test scenario. Finally, the 45-test suite employed two-node (one-cell) intervals, with pumping and injection intervals first at the same vertical levels, and then crossed. A greater number of smaller test intervals results in an increased amount of vertical flow. The increased importance of vertical flow should result in a better definition of the horizontal variation in the resistivity. The vertically varying heads along each pumping and injection interval are again averaged before being input as data for the inverse runs.

Analysis of these simulated tests revealed the need for the imposition of bounds on the resistivity estimates. Without bounds, the tomographic inverse algorithm was attempting to drive some resistivity values to zero. Therefore the program was modified so that no resistivity correction would move the corresponding resistivity estimate outside the user-defined upper and lower bounds. This results in a slight alteration of the resistivity correction vector computed using Equation II.B.28. However, the alteration does not appear to adversely affect the overall performance of the algorithm. The upper and lower limits used in the following analyses were 0.1 and 10, respectively. Some experimentation revealed that the value of the imposed lower bound did influence the quality of the estimates somewhat. Therefore, some prior knowledge of a test site would be important in order to define a reasonable lower bound for the resistivities. The upper limit is somewhat less important and can probably be widely overestimated without any harmful results. None of the resistivity

estimates ever started increasing without bound. In fact, the high resistivities were consistently underestimated (meaning low conductivities were overestimated).

Table II.B.2 displays summary statistics for all six simulated test scenarios. The correlation and rms deviation results for the resistivities are displayed in terms of natural log resistivity, since the true resistivities are approximately lognormally distributed in this case. The correlations between true and estimated resistivities increase both with increasing number of tests and increasing number of data points. However, all the correlations are fairly low. The rms deviations decrease with an increasing number of tests, but increase slightly with an increasing number of data points.

The spatial distributions of the estimated resistivities for the test scenarios using 27 observation points are shown in Figures II.B.9A-II.B.9C. Crossplots of the same results are shown in Figures II.B.10A-II.B.10C. The crossplots show clearly that a number of estimated resistivities have been driven to the lower bound of 0.1. Comparison of Figures II.B.8 and II.B.9C shows that the 45-test estimates are indeed beginning to pick up some of the features seen in the true resistivity field. A fairly coarse view of the true resistivity field would split it into five horizontal bands, alternating low-high-low-high-low. This pattern is also beginning to show up in the 45-test results. Note that the definition of the vertical variation is really quite good at the left and right ends of the model domain, immediately adjacent to the wells, while the results are much more ambiguous in the center of the domain.

Due to the fairly disappointing results of the above attempts to identify the spatial variation in the 81-block aquifer, another set of simulations were run to test the influence of the head averaging along the pumping and injection intervals. The data from the test scenarios with 27 observation points were analyzed again, this time using the exact heads computed at the boundary intervals as input data. The summary statistics for these analyses are presented in Table II.B.3. The spatial distribution of the estimates are shown in Figures II.B.9D-II.B.9F and the crossplots of true and estimated resistivity are shown in Figures II.B.10D-II.B.10F. Clearly, the use of the exact head profiles along the pumping and injection intervals leads to a dramatic improvement in the estimates. This is encouraging, since it is possible that the averaging of flux values over a pumping/injection interval that would occur when performing a real test would not have as harmful an effect on the estimates as does the averaging of head values over the interval that occurs when analyzing the synthetic tests.

More surprisingly, the quality of the estimates actually decreases with the increasing number of tests in this case. This implies that the detailed descriptions of a smaller number

of head profiles over longer intervals actually contains more information than detailed descriptions of a larger number of head profiles over shorter intervals. This advantage is lost when only average heads are known over these intervals. Note that the 45-test results do not vary greatly between the analyses using averaged and exact heads. This is not surprising, since heads are averaged over only a two-node interval, so that the averaged heads are not greatly different from the exact heads.

The above sets of experiments show that the experimental configuration described here allows much better definition of vertical variation than it does of horizontal variation. This is a fairly straightforward consequence of the predominantly horizontal nature of the applied stresses and is a well-known characteristic of crosshole seismic tomography [*Peterson et al.*, 1985]. If similar stressed intervals could be placed along the top and bottom boundaries of the aquifer an equally good description of the horizontal variation could be obtained. Fortunately, the most significant variations in hydraulic conductivity occur in the vertical direction at most sites.

The final sequence of simulated tests is carried out in the fully heterogeneous aquifer shown in Figure II.B.3. The same test suite is used for all analyses, the 17-test scenario with 27 data points, described above. Computed heads along the pumping and injection intervals are averaged before being used as input data. Six different zonation schemes are used to analyze the test results, three layered zonations and three zonations using rectangular or square blocks. Figure II.B.11 presents the spatial distributions of the estimated resistivities when the test data are analyzed using the six different zonation schemes. Figure II.B.12 presents the corresponding crossplots of true and estimated resistivities. Since each zone represents a large number of model cells, and therefore a large number of true resistivities, there is no unique value to which to compare each zonal estimate. The 'true' resistivities are represented on Figure II.B.12 by a range of spatial averages of all the resistivities in each zone, with the harmonic average at the left end of each line and the arithmetic average at the right end. The geometric average is represented by the small vertical line in between. These averages are special cases of a general spatial power average [*Desbarats*, 1992b]. Expressed as a discrete average over all N cells in a given zone, the spatially averaged resistivity for each zone is given by

$$R_\omega = \left(\frac{1}{N} \sum_{i=1}^{N} R_i^\omega \right)^{1/\omega}, \quad \omega \neq 0 \qquad \text{(II.B.30)}$$

and

$$R_\omega = \exp\left(\frac{1}{N}\sum_{i=1}^{N}\ln R_i\right), \quad \omega = 0 \qquad \text{(II.B.31)}$$

The harmonic, geometric, and arithmetic averages correspond to ω=-1, ω=0, and ω=1, respectively. One would expect the harmonic and arithmetic averages to provide bounds on the effective resistivities for each zone. From the perspective of the head solution for one-dimensional linear flow, resistivities in series (varying along the direction of flow) would be averaged arithmetically and resistivities in parallel (varying perpendicularly to the direction of flow) would be averaged harmonically. This is the inverse of the averaging rules for conductivities in one-dimensional flow. In addition, *Desbarats* [1991] has demonstrated that the geometric average of point support-scale transmissivities provides a good estimate of effective block-scale transmissivities for various block geometries in two-dimensional linear flow and that the same relationship applies for resistivities. It is impossible to define strictly correct effective resistivities for the simulations performed here, due to the variety of flow configurations experienced by different portions of the model domain during different tests and due to the small dimensions of the zones in comparison to the horizontal and vertical correlation scales of the resistivity field. Nevertheless, it is expected that the range of averages shown approximates the range of 'correct' estimates for the zonal resistivities.

Both the gray-scale (Figure II.B.11) and crossplot (Figure II.B.12) representations show that the layered zonation runs do a good job of reproducing the major features of the true resistivity field. The 9-layer zonation consists of five-cell thick zones and the 15-layer zonation consists of three-cell thick zones. Both produce good estimates overall. The 23-layer zonation consist of 22 two-cell thick layers and one one-cell thick layer (at the top). The results here are still reasonably pleasing, although the correlation with the actual resistivities is beginning to break down.

The three 'block' zonation schemes are derived from the 9-layer zonation, with each layer being successively broken down into three 15X5 blocks (27-block zonation), five 9X5 blocks (45-block zonation), and nine 5X5 blocks (81-block zonation). As expected from the earlier experiments with the 81-block aquifer, the experimental configuration presented here does not allow for reasonable estimation of the horizontal variation of the resistivity and the estimates for all three block zonations are poor. Fortunately, many aquifers do exhibit pronounced stratification in their hydraulic properties and for many purposes can be adequately represented by a layered model.

Concluding Remarks

The synthetic examples described above demonstrate the validity of the proposed inverse method. This method could be applied essentially without modification to planar flow problems, such as horizontal flow in a confined aquifer, provided enough data were available to allow reliable estimates. To be applied to the experimental configuration described here, stressing different isolated intervals of two different wells in order to characterize the hydraulic conductivity distribution between them, the method has to be modified to account for the dual radial flow system involved. This is the subject of ongoing work.

The practicality of the method remains to be tested in the field. One reason for presenting numerical tests based on a two-well (pumping and injection) configuration is that this configuration is expected to produce steady state (actually, steady-gradient) more rapidly than a single-well configuration. Once steady state has been obtained in the field, a fairly large number of head data must be obtained, including measured heads in the pumping and injection wells. These heads must be accurate and all referenced to the same datum, since the parameter estimation process works with differences in measured head. To obtain a reasonable number of streamlines, the testing process needs to be repeated a number of times, using different pumping and injection intervals.

	cor(R,$\hat{R}$)	rmsd(R,$\hat{R}$)	cor(h,$\hat{h}$)	rmsd(h,$\hat{h}$)
9 tests, 9 obs.	0.91	0.83	0.94	0.12
9 tests, 27 obs.	0.89	0.90	0.95	0.13
17 tests, 9 obs.	0.95	0.81	0.96	0.11
17 tests, 27 obs.	0.93	0.80	0.96	0.12

TABLE II.B.1. Correlation (cor) and root mean squared deviation (rmsd) between true and estimated resistivities (R and $\hat{R}$) and between observed and predicted heads (h and $\hat{h}$) for different test scenarios in the simple nine-layer aquifer; 'obs.' is the number of observation points employed in each test.

	cor(lnR,ln$\hat{R}$)	rmsd(lnR,ln$\hat{R}$)	cor(h,$\hat{h}$)	rmsd(h,$\hat{h}$)
17 tests, 9 obs.	0.28	1.14	0.82	0.40
17 tests, 27 obs.	0.38	1.17	0.91	0.19
29 tests, 9 obs.	0.36	1.08	0.86	0.18
29 tests, 27 obs.	0.45	1.09	0.93	0.12
45 tests, 9 obs.	0.52	0.99	0.94	0.08
45 tests, 27 obs.	0.56	0.97	0.96	0.06

TABLE II.B.2. Correlation and root mean squared deviation between natural logs of true and estimated resistivities and between observed and predicted heads for different test scenarios in the 81-block aquifer using averaged heads along pumping and injection intervals.

	cor(lnR,ln$\hat{R}$)	rmsd(lnR,ln$\hat{R}$)	cor(h,$\hat{h}$)	rmsd(h,$\hat{h}$)
17 tests	0.79	0.67	0.96	0.14
29 tests	0.77	0.71	0.98	0.14
45 tests	0.67	0.82	0.97	0.05

TABLE II.B.3. Correlation and root mean squared deviation between natural logs of true and estimated resistivities and between observed and predicted heads for different test scenarios (all using 27 observation points) in the 81-block aquifer using exact heads along pumping and injection intervals.

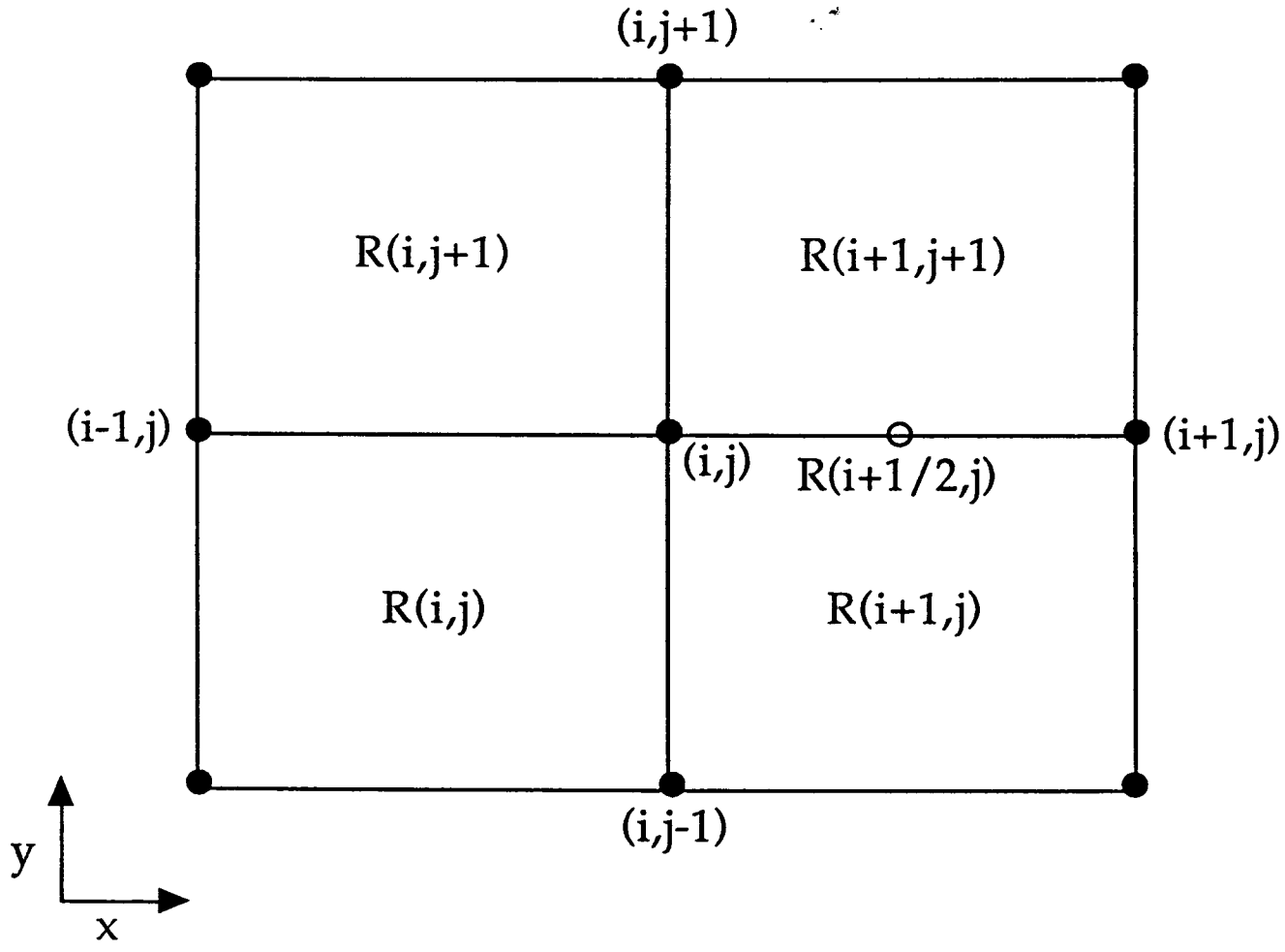

Fig. II.B.1. Computational node (i,j) and adjacent nodes and cells in a mesh-centered finite difference formulation.

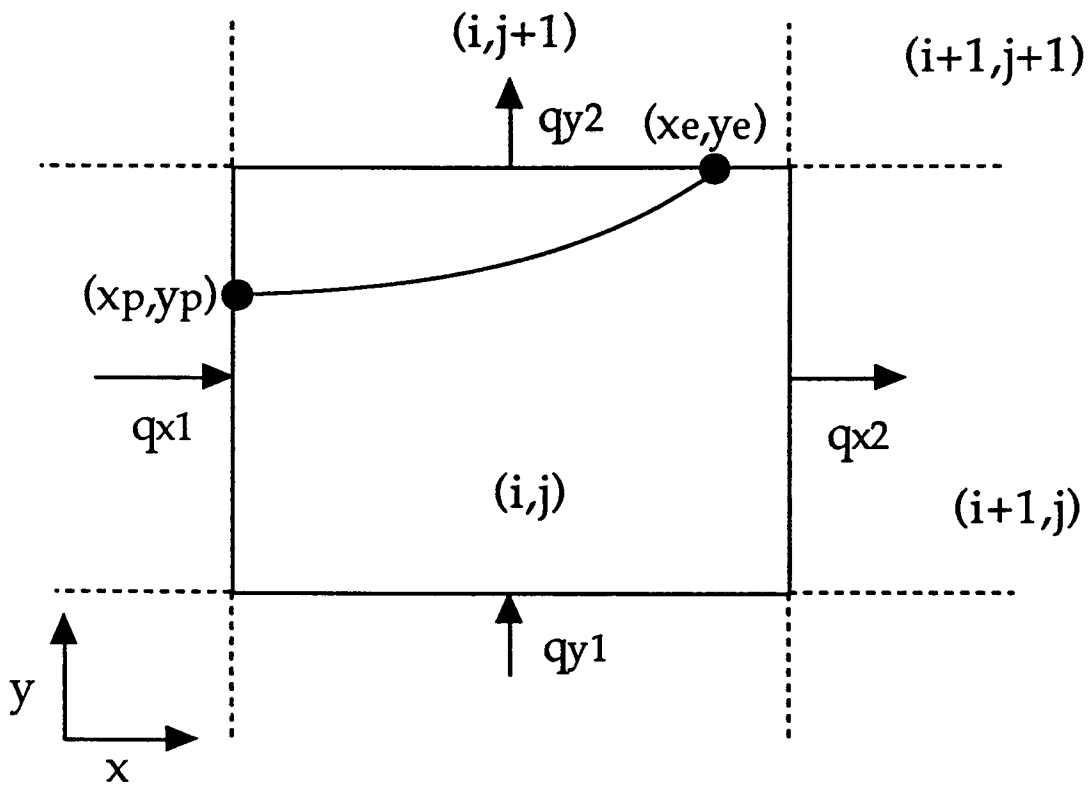

Fig. II.B.2. Typical finite difference cell, with one possible pathline shown. [After *Pollock*, 1988, Figure 2.]

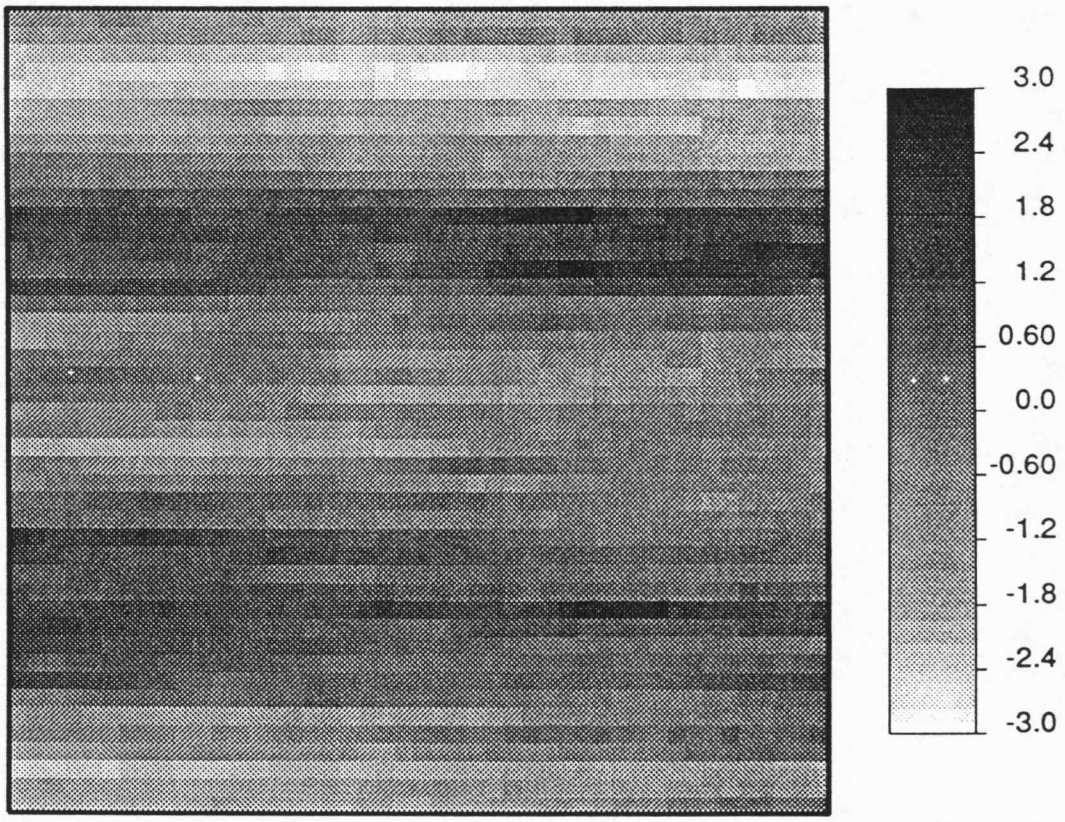

Fig. II.B.3. Natural log of true hydraulic resistivity in tested region, nine units on a side. Grid cells are 0.2 units on a side, resulting in a 45X45 array of grid cells.

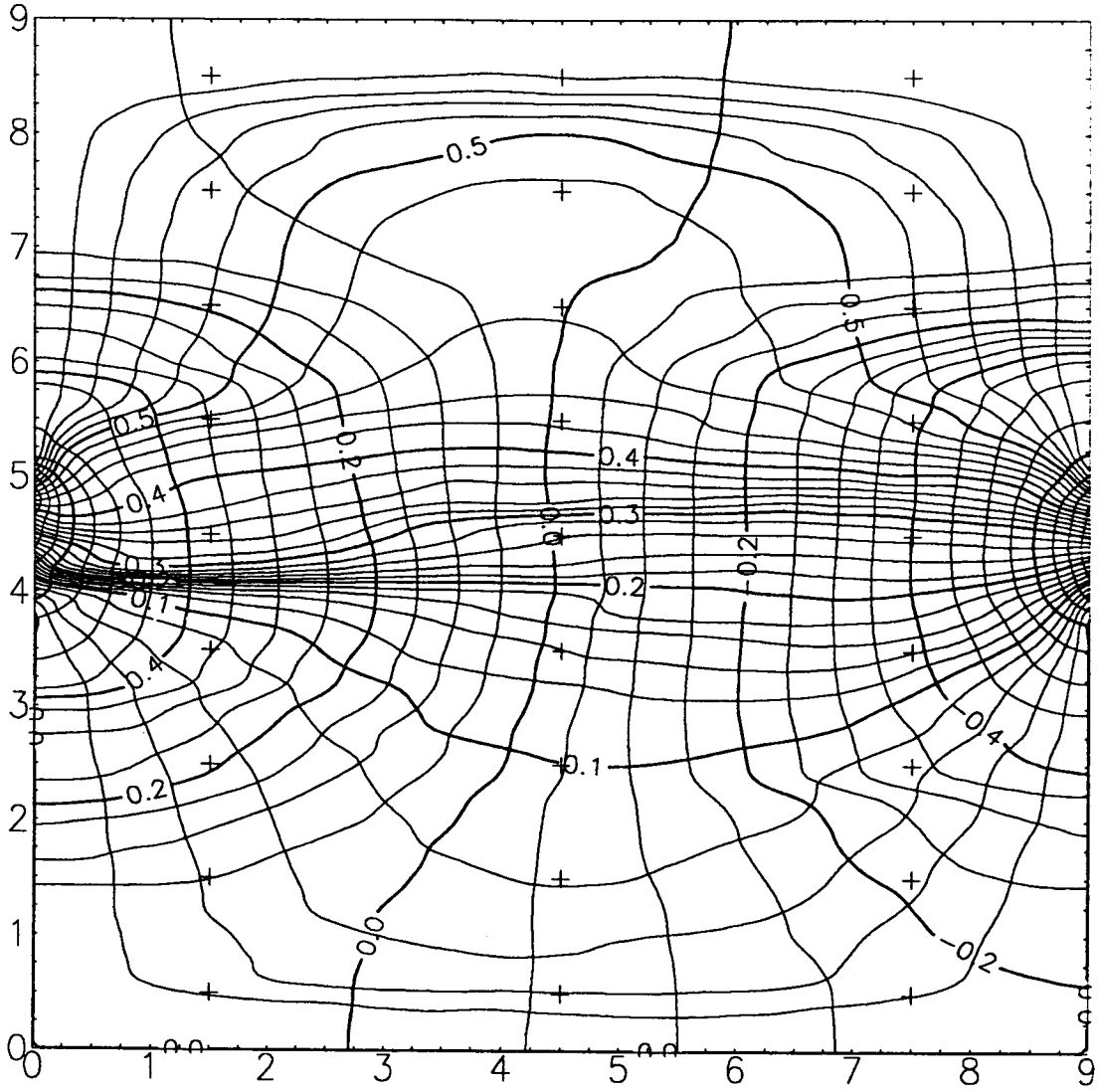

Fig. II.B.4. Contours of head solution (contours near vertical in center of domain) and stream function solution (contours near horizontal in center of domain) for a single test in the resistivity field shown in Figure II.B.3. Plus signs represent data points used in single-test forward run.

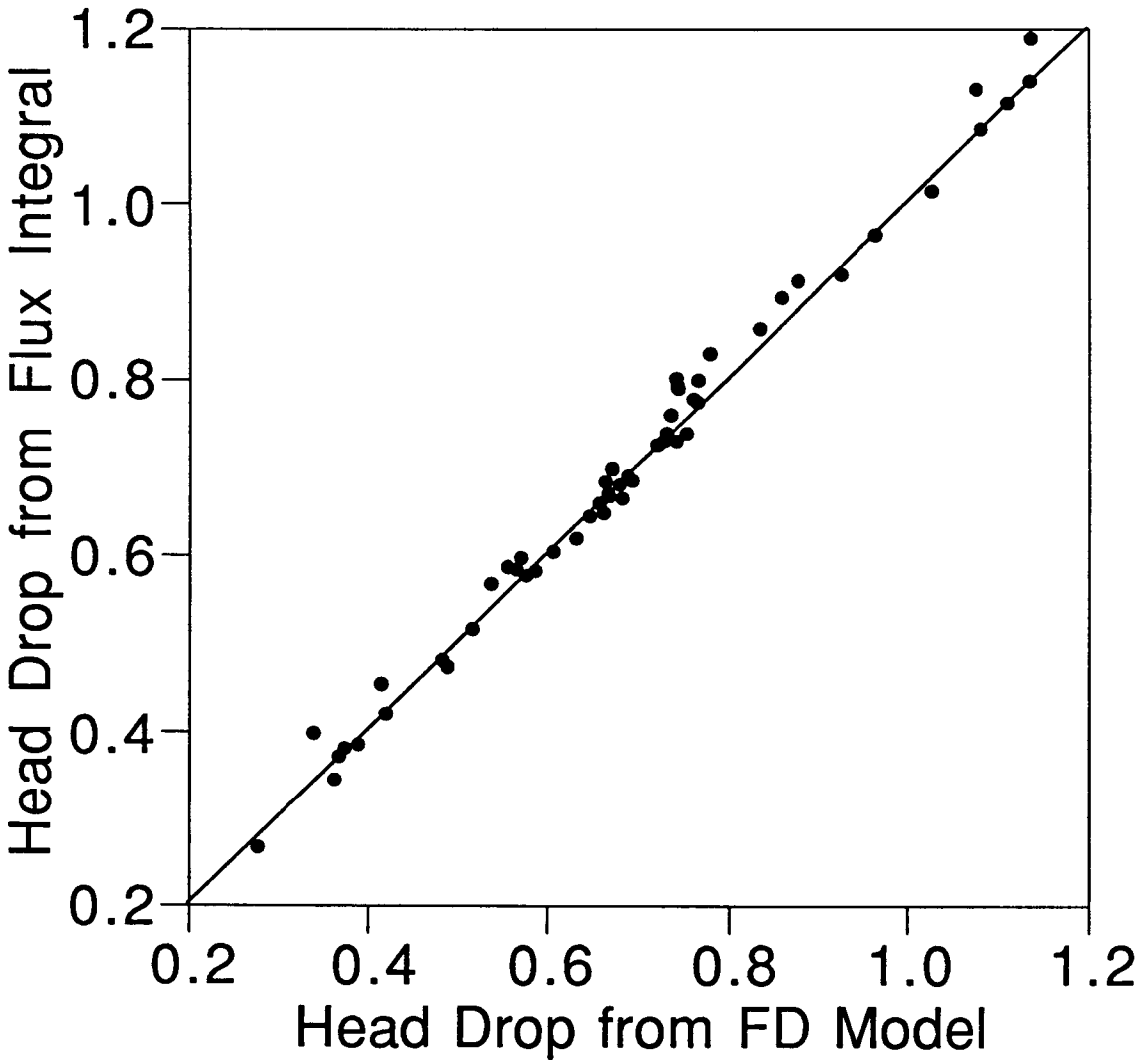

Fig. II.B.5. Head drops calculated from flux integrals along streamlines versus head drops computed from differences of heads computed at finite difference model nodes at each end of streamline.

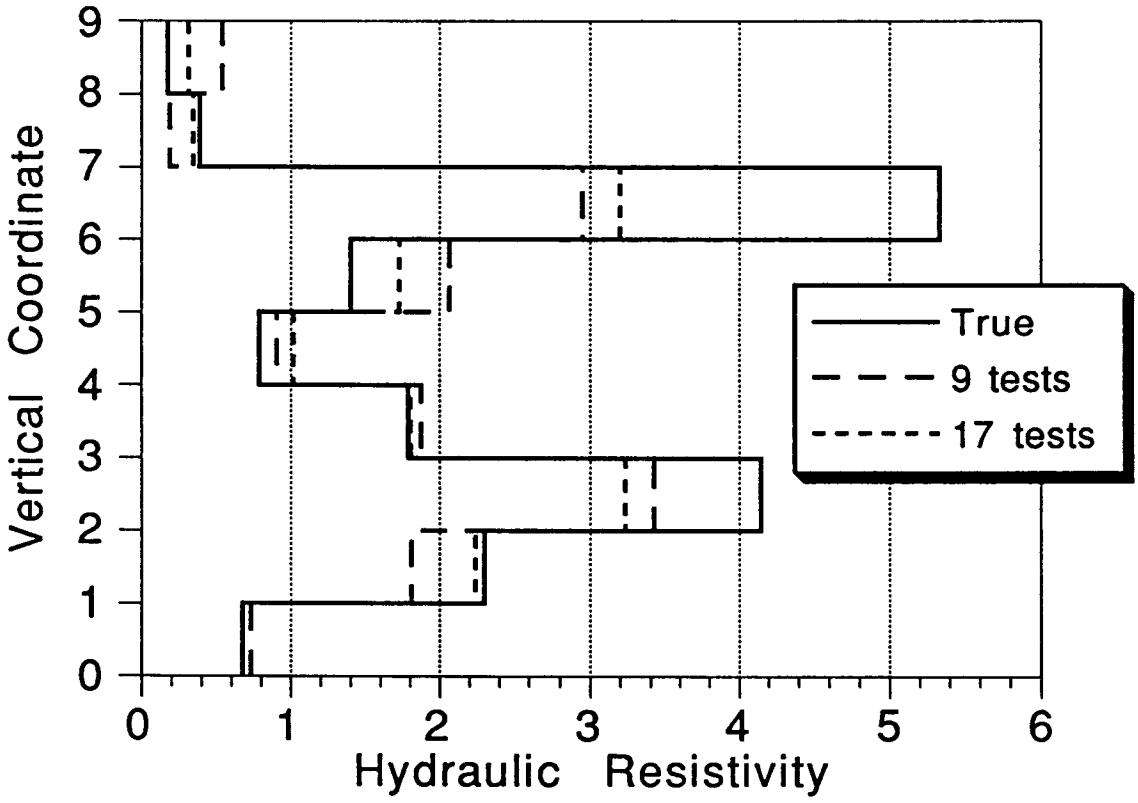

Fig. II.B.6. True and estimated hydraulic resistivities for tests in simple nine-layer aquifer versus height above aquifer base; estimates from nine- and 17-test inverse runs using nine observation points for each test.

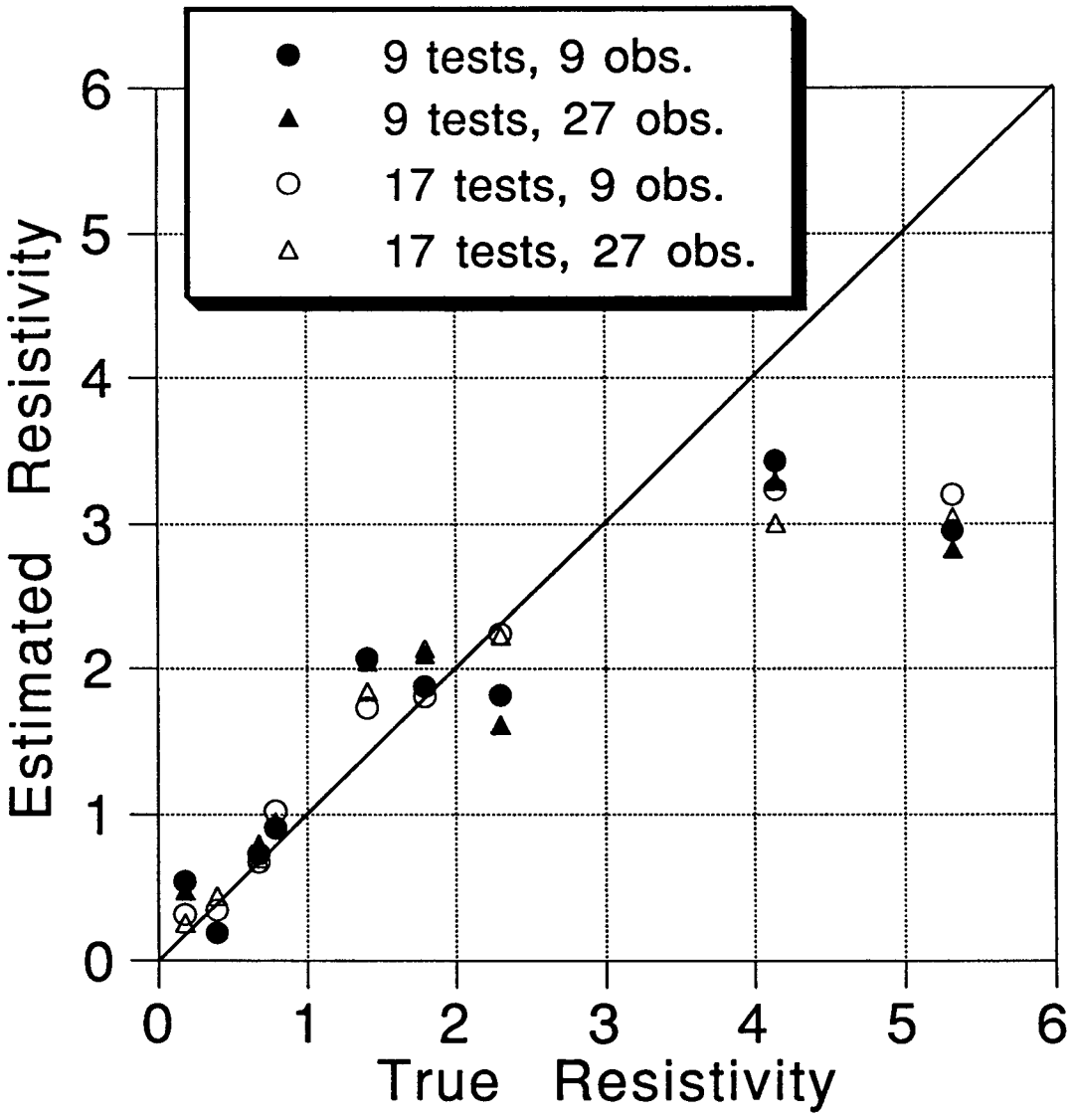

Fig. II.B.7. Crossplots of true and estimated resistivities for tests in nine-layer aquifer using different test scenarios.

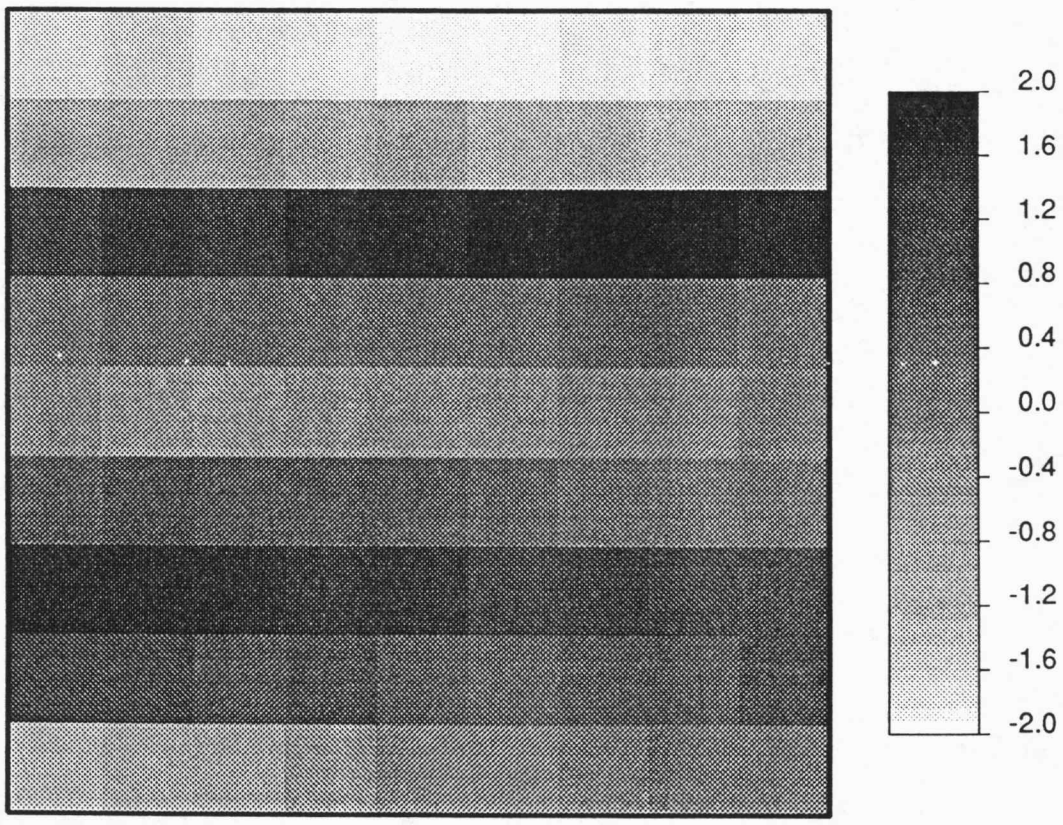

Fig. II.B.8. Natural log of true hydraulic resistivity in 81-block aquifer. Each block consists of a 5X5 array of cells.

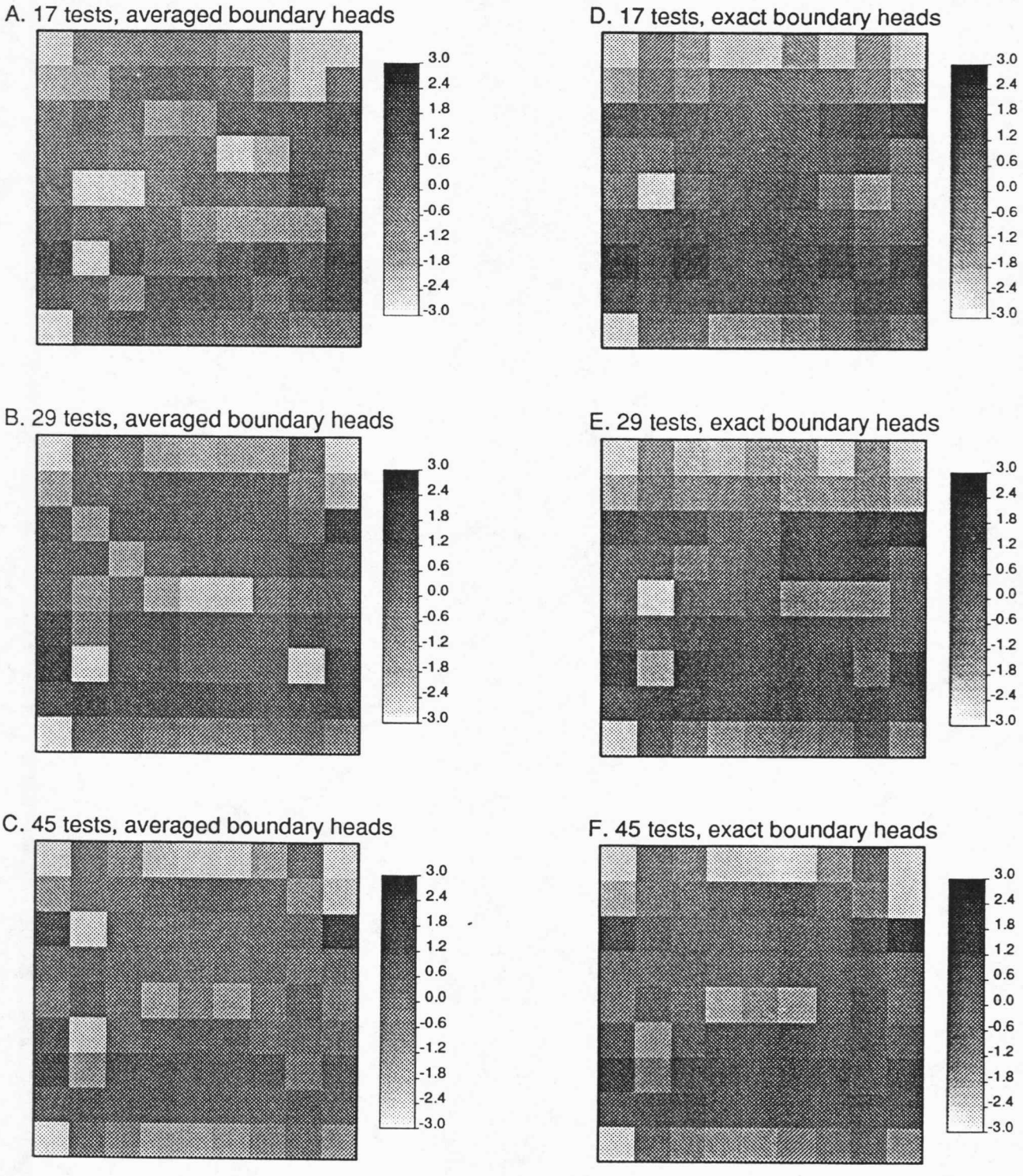

Fig. II.B.9. Spatial distributions of natural logs of estimated hydraulic resistivities for different test scenarios in 81-block aquifer, all using 27 observation points per test. Results of inverse runs using averaged heads along the pumping and injection intervals are shown on the left and those using exact heads are shown on the right.

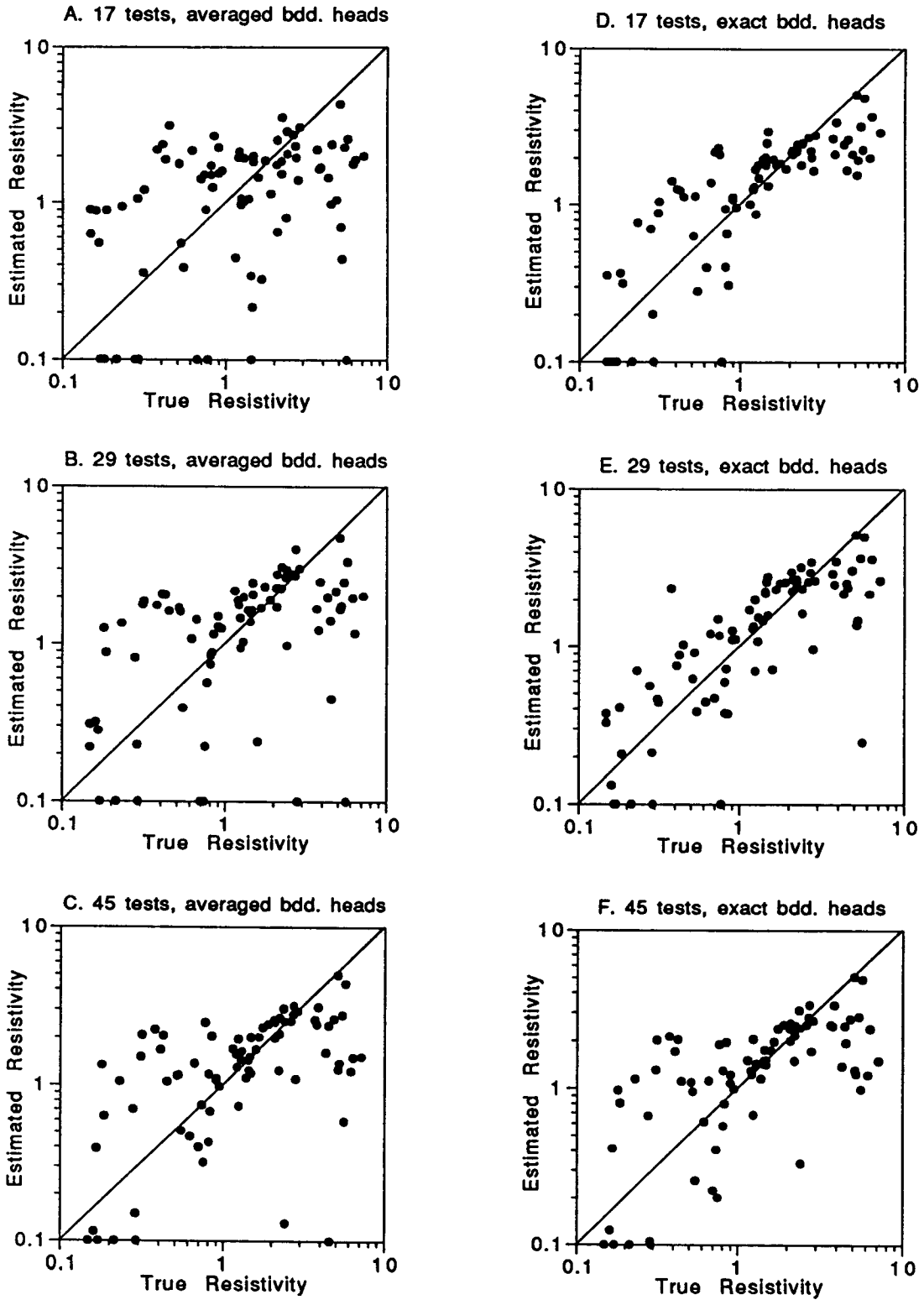

Fig. II.B.10. Crossplots of true and estimated hydraulic resistivities for different test scenarios in 81-block aquifer, all using 27 observation points per test.

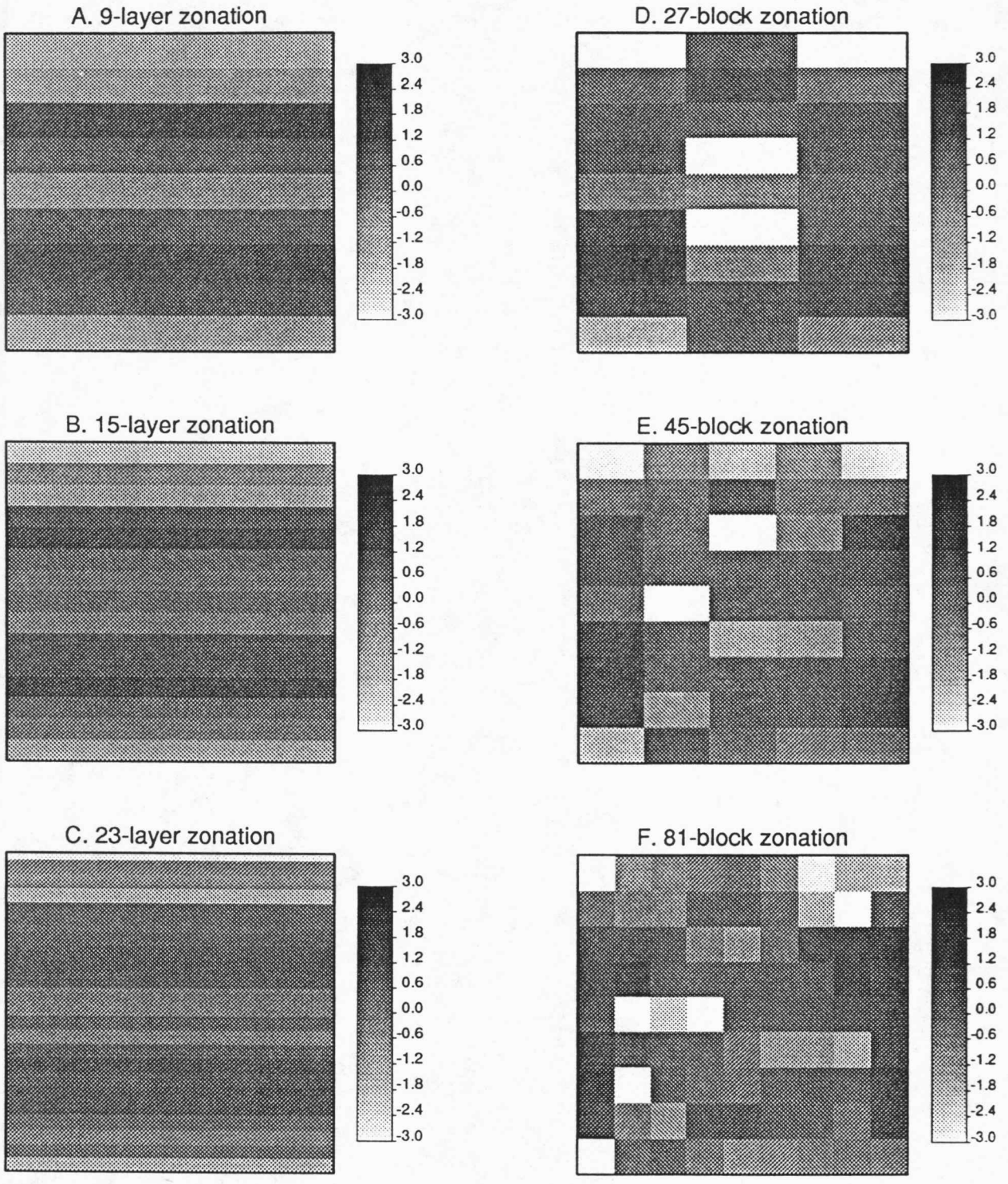

Fig. II.B.11. Natural logs of estimated resistivities using different zonations and a single test scenario (17 tests, 27 data points, averaged boundary heads) in the fully heterogeneous aquifer (shown in Figure II.B.3).

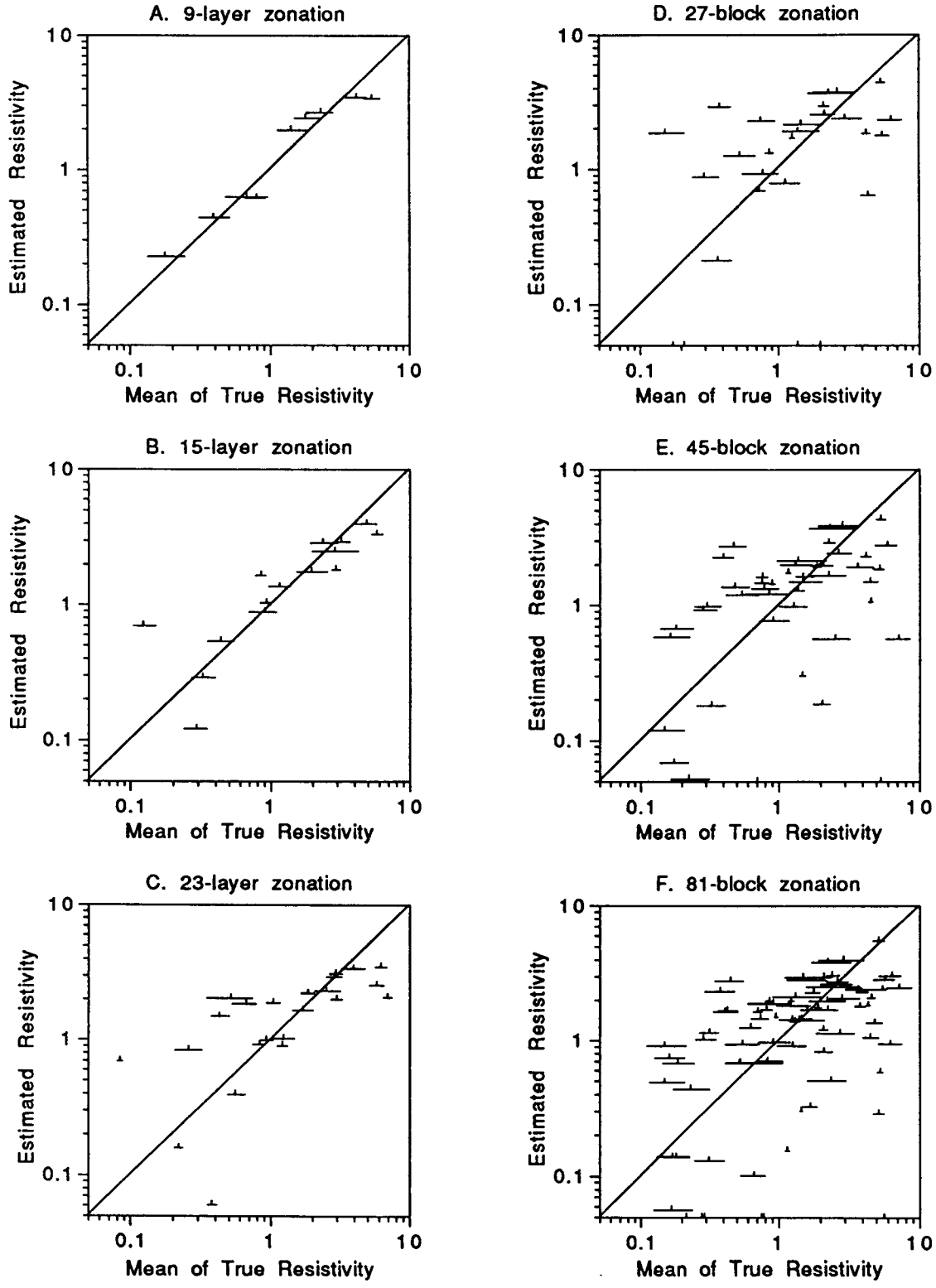

Fig. II.B.12: Estimated zonal resistivities versus range of mean resistivities for all cells in each zone. The lines representing the range of means extend from the harmonic mean (left end) to the arithmetic mean (right end), with the geometric mean represented by the small vertical line in between.

C. AN ASSESSMENT OF THE NGUYEN AND PINDER METHOD FOR SLUG TEST ANALYSIS

Abstract

The Nguyen and Pinder method is one of four techniques commonly used in the field for the analysis of response data from slug tests. Limited field research has raised questions about the reliability of the parameter estimates obtained using this method. In this section, a theoretical evaluation of this technique is described. This evaluation reveals that errors were made in the derivation of the analytical solution upon which the technique is based. Simulation and field examples show that the errors result in parameter estimates that can differ from actual values by orders of magnitude. These findings indicate that the Nguyen and Pinder method should no longer be a tool in the repertoire of the field hydrogeologist. If data from a slug test performed in a partially penetrating well in a confined aquifer need to be analyzed, recent work has shown that the method of Hvorslev is the best alternative among the commonly used techniques.

Introduction

At sites of suspected groundwater contamination, the slug test is often the preferred method for obtaining in-situ estimates of hydraulic conductivity. In addition to its clear logistical and economic advantages over alternative approaches such as pumping tests, the slug test can also provide useful information about spatial variations in flow properties. Such information about the degree of heterogeneity that exists at a site, which is quite difficult to obtain from conventional constant-rate pumping tests (e.g., Butler and Liu, 1993), can be very valuable for the prediction of contaminant movement and the design of remediation schemes.

Currently, most analyses of response data from slug tests are performed using one of four techniques. These techniques are 1) the method of Hvorslev (1951) for slug tests in fully and partially penetrating wells in confined aquifers, 2) the method of Bouwer and Rice (Bouwer and Rice, 1976; Bouwer, 1989) for slug tests in wells in unconfined aquifers screened below the water table, 3) the method of Cooper et al. (1967) for slug tests in fully penetrating wells in confined aquifers, and 4) the method of Nguyen and Pinder (1984) for slug tests in partially penetrating wells in confined aquifers. Note that the first two methods are based on approximate representations of the slug-induced flow system, while the latter two techniques utilize more complete descriptions of the relevant physics.

The focus of this section is on the Nguyen and Pinder method for slug-test

analysis. At the time of its publication, the Nguyen and Pinder method appeared to be the first rigorous approach for the analysis of response data from slug tests in partially penetrating wells in confined aquifers. Analytical solutions for slug tests in partially penetrating wells that have been developed since the introduction of this method (e.g., Dougherty and Babu, 1984; Hayashi et al., 1987) have not been widely adopted for parameter estimation, so the Nguyen and Pinder method is still considered by many to be the most appropriate approach for analysis of slug tests in partially penetrating wells in confined aquifers (e.g., Palmer and Johnson, 1989). Although the method is used by field practitioners, currently taught in industry short courses on aquifer-test analysis (e.g., NGWA, 1993), and recommended in technology transfer publications of the Environmental Protection Agency (e.g., Palmer and Johnson, 1989), the Nguyen and Pinder method has not undergone the same degree of theoretical and field evaluation as the other three commonly used approaches. The limited field research on the technique that has been reported has raised questions about the reliability of the resulting parameter estimates (e.g., Nichols, 1985; Campbell et al., 1990; Brother and Christians, 1993). These researchers reported that the Nguyen and Pinder estimates of hydraulic conductivity were not consistent with those obtained using other approaches. Given that this method is currently being used in the field and that there are questions concerning the reliability of the estimated parameters, it is clear that a more thorough assessment of this approach is needed. Such an assessment is the primary objective of the work reported here.

In this section, a complete theoretical evaluation of the Nguyen and Pinder method is presented. This evaluation demonstrates that the parameter estimates obtained using this method are of very low quality due to errors in the derivation of the solution upon which the technique is based. A field evaluation will also be presented in order to substantiate the results of the theoretical assessment. The section will conclude with recommendations concerning the field applicability of the technique and possible alternative approaches.

Overview of Nguyen and Pinder Model

Model Definition

Although Nguyen and Pinder present a general mathematical model that can be employed for both pumping and slug tests, the focus of this work will be on the slug-test case. Therefore, the problem of interest here is that of the head response produced by

the instantaneous introduction of a slug of water into the screened or open section of a well partially penetrating a confined aquifer, as shown in Figure II.C.1. For the purposes of this development, the aquifer of Figure II.C.1 is considered homogeneous and isotropic. The partial differential equation representing the flow of groundwater in response to an instantaneous introduction of a slug at a central well can be written in cylindrical coordinates as

$$\frac{\partial^2 s}{\partial r^2}+\frac{1}{r}\frac{\partial s}{\partial r}+\frac{\partial^2 s}{\partial z^2}=\left(\frac{S_s}{K}\right)\frac{\partial s}{\partial t} \qquad \text{(II.C.1)}$$

where

s = change in head relative to static, [L];
K = hydraulic conductivity, [L/T];
S_s = specific storage, [1/L];
t = time, [T];
r = radial direction, [L];
z = vertical direction, z=0 at the bottom of the aquifer and increases upward, [L].

Note that, except for the designation of spatial and temporal derivatives, the notation employed here will be that of Nguyen and Pinder.

The initial and boundary conditions are as follows:

$$s(r,z,0) = 0,\ r_s<r<\infty,\ 0\le z\le b \qquad \text{(II.C.2)}$$

$$\frac{\partial s(r,0,t)}{\partial z} = \frac{\partial s(r,b,t)}{\partial z} = 0,\ r_s<r<\infty,\ t>0 \qquad \text{(II.C.3)}$$

$$s(\infty,z,t) = 0,\ 0\le z\le b,\ t>0 \qquad \text{(II.C.4)}$$

$$\frac{1}{(z_2-z_1)}\int_{z_1}^{z_2} s(r_s,z,t)dz = H(t),\ t>0 \qquad \text{(II.C.5)}$$

$$2\pi r_s K\int_{z_1}^{z_2}\frac{\partial s(r_s,z,t)}{\partial r}dz = \pi r_c^2\frac{dH(t)}{dt} \qquad \text{(II.C.6)}$$

where

b = aquifer thickness, [L];

r_s = radius of well screen, [L];

r_c = radius of well casing, [L];

z_1 = distance from the bottom of the aquifer to the bottom of the screen, [L];

z_2 = distance from the bottom of the aquifer to the top of the screen, [L];

$z_2 - z_1$ = screen length, [L];

$H(t)$ = head in well relative to static, [L].

Note that equation (II.C.6), which is the flow boundary at the well screen, is presented in an integral form. Most contributions in the well hydraulics literature concerned with the transient response of partially penetrating wells have assumed a constant horizontal hydraulic gradient along the well screen as a mathematical convenience (e.g., Hantush, 1964; Dougherty and Babu, 1984). The error that is introduced by this assumption has been shown to be very small for wells commonly employed in field applications (e.g., Butler et al., 1993). In addition, this simplification allows a solution to be readily found, thus avoiding the problems that are discussed in the following section.

Although not explicitly stated, the following additional initial and boundary conditions are also employed in the later mathematical development:

$$H(0) = H_0 \qquad \text{(II.C.7)}$$

$$\frac{\partial s(r_s,z,t)}{\partial r} = 0,\ 0<z<z_1,\ z_2<z<b,\ t>0 \qquad \text{(II.C.8)}$$

where

H_0 = height of initial slug, [L].

Model Solution

Equations (II.C.1)-(II.C.8) describe the flow conditions modeled by Nguyen and Pinder. These authors attempted to derive an analytical solution to this mathematical model using conventional integral transform methodology. The key points of their derivation are given in Appendix A. In summary, a Laplace transform in time followed by a finite Fourier cosine transform in the z direction produces a modified Bessel equation in Fourier-Laplace space. Transform-space analogues of boundary conditions (II.C.4) and (II.C.6) are then employed to evaluate the equation constants. The basic problem with the Nguyen and Pinder method for slug-test analysis is that equation (II.C.6) is undefined (i.e. cannot be written in terms of the dependent variable) in Fourier-Laplace space. As shown in Appendix A, Nguyen and Pinder attempted to circumvent this problem by performing an inverse Fourier transform prior to evaluating one of the constants. This step introduced an error that causes the remainder of the mathematical manipulations described by Nguyen and Pinder to be incorrect.

The problems produced by the undefined boundary condition prevented Nguyen and Pinder from presenting a solution in the conventional sense. All of their equations are given in terms of the deviation from static being a function of the temporal derivative of this same deviation. However, they were able to manipulate these equations to obtain expressions for use in estimation of specific storage and hydraulic conductivity. Their expressions for parameter estimation are

$$S_s = \frac{r_c^2 C_3}{r_s^2 (z_2 - z_1)} \qquad \text{(II.C.9)}$$

$$K = \frac{r_c^2 C_3}{4 C_4 (z_2 - z_1)} \qquad \text{(II.C.10)}$$

where

C_3 = the absolute value of the slope of a log-log H(t) versus t plot;

C_4 = the absolute value of the slope of a semilog -dH(t)/dt versus 1/t plot.

The estimation procedure proposed by Nguyen and Pinder is quite straightforward. The slope of a log-log H(t) versus time plot is used to estimate specific storage from equation (II.C.9). That slope along with the slope of a semilog -dH(t)/dt versus 1/t plot is then used to estimate hydraulic conductivity with equation (II.C.10). In the field example presented by Nguyen and Pinder, a straight line is fit to the large-time data and the early-time data are ignored. Unfortunately, because of the errors in the model derivation, the estimates produced by the procedure outlined above must be viewed with considerable skepticism. Furthermore, Nichols (1985) shows that there is a theoretical inconsistency (deviation from static is independent of hydraulic conductivity) that follows from equation (II.C.9). This inconsistency, which is undoubtedly a product of the model error, casts further doubt on the reliability of estimates obtained using equations (II.C.9) and (II.C.10).

Ramifications of the Model Error

In order to explore the ramifications of the model error for parameter estimation, a simple numerical experiment was performed in which a slug test in a partially penetrating well in a confined aquifer was simulated using a semianalytical solution. Parameter estimates were computed from the simulated response data using equations (II.C.9) and (II.C.10), and then compared to the original parameter values employed in the semianalytical solution. In this work, the semianalytical solution of Hyder et al. (in press), which has been extensively checked using both analytical (e.g., Dougherty and Babu, 1984) and numerical (e.g., Butler et al., 1994) approaches, was employed for the simulation of the slug test. The aquifer and well-construction parameters given in Table II.C.1 were used for this simulation. A well of a small aspect ratio (screen length/well radius) was employed in order to accentuate the partially penetrating nature of the well. Figure II.C.2a displays a log-log H(t) versus time plot of the simulated responses. Straight lines have been fit to the steepest (late time) and flattest (early time) portions of the plot in order to bound the specific storage estimates that might be obtained using equation (II.C.9). Specific storage estimates of .00743 ft^{-1} and 3.64 ft^{-1} were obtained using the early and late time slopes, respectively. Note that the estimate obtained from the late time slope, which is the slope used by Nguyen and Pinder in their example, lies outside the range of physical plausibility.

A semilog -dH(t)/dt versus 1/t plot of the simulated responses is given in Figure II.C.2b. Again, straight lines have been fit to the steepest (late time or early inverse time) and flattest (early time) portions of the plot in order to bound the hydraulic conductivity estimates that might be obtained using equation (II.C.10). Note that four

separate estimates of hydraulic conductivity can be obtained from combinations of the specific storages estimated from Figure II.C.2a using equation (II.C.9) and the two slope choices on Figure II.C.2b. Table II.C.2 lists the parameter estimates obtained using the various approaches. Based on the procedure outlined by Nguyen and Pinder, the most appropriate conductivity value would be 1.20 ft/d, which is 42% of the hydraulic conductivity employed in the semianalytical solution. However, given the lack of a clear cut slope on Figure II.C.2b, the fact that a physically implausible specific storage estimate (3.64 ft^{-1}) was employed for the conductivity estimate, and the considerable spread of estimates shown on Table II.C.2, it is apparent that the relative close agreement between the conductivity estimate and the actual value is simply a function of chance.

This numerical experiment shows that the estimates obtained using equations (II.C.9) and (II.C.10) can be quite different from the actual parameter values. Thus, the ramifications of the model error appear to be of practical significance.

Field Evaluation

The theoretical findings of the previous section can be substantiated using field data. Recently, a program of well testing was carried out by the Kansas Geological Survey as part of a regional study of the Dakota aquifer in Kansas. At one site in Lincoln County, Kansas, two wells (0.167 ft and 0.083 ft in radius (r_c), $r_s=r_{sk}=2r_c$, effective screen radius set equal to radius of gravel pack because gravel pack is much more permeable than formation), screened over similar depth intervals, are located 21.2 feet apart. A series of slug tests was carried out in order to obtain estimates of both the hydraulic conductivity and specific storage of the Dakota aquifer at this site. These tests consisted of introducing a slug at the larger of the two wells and measuring the responses both at the test well and at the observation well. Measurements from the observation well were taken using a transducer placed below a packer located just above the top of the screen. The packer enabled effects associated with wellbore storage at the observation well to be kept very small. Note that an observation well was employed in these tests as a result of the theoretical work of McElwee et al. (in press), which shows that use of observation wells with slug tests can greatly improve the reliability of the parameter estimates.

The response data were analyzed using an augmented version of the method of Cooper et al. (1967) that allows inclusion of observations from points other than the test well. Plots of the measured data and the best-fit Cooper et al. model for both the test and observation wells are given in Figure II.C.3. The small difference between the

measured data and the best-fit model, in conjunction with the results of the theoretical work of McElwee et al. (in press), indicates that the reliability of the parameter estimates (given in Table II.C.3) is quite good. The model fitting, which was done using an automated well-test analysis package developed at the Kansas Geological Survey (Bohling and McElwee, 1992), also produces approximate confidence intervals for the estimated parameters. Those confidence intervals are given in Table II.C.3.

Figure II.C.4a presents the log-log normalized head versus time plot of the data from the test well. As with Figure II.C.2a, straight lines have been fit to the steepest (late time) and flattest (early time) portions of the plot in order to bound the specific storage estimates that might be obtained using equation (II.C.9). Table II.C.4 lists the two specific storage estimates. The specific storage estimate obtained using the late-time straight line (0.0218 ft^{-1}) is close to four orders of magnitude larger than the specific storage estimated from the Cooper et al. analysis.

Figure II.C.4b displays the semilog normalized -dH(t)/dt versus 1/t plot of the data. Again, straight lines have been fit to the steepest (late time) and flattest (early time) portions of the plot in order to bound the hydraulic conductivity estimates that might be obtained using equation (II.C.10). Note that, as with the numerical example, four separate estimates of hydraulic conductivity can be obtained from combinations of the specific storages estimated from Figure II.C.4a using equation (II.C.9) and the two slope choices on Figure II.C.4b. Table II.C.4 lists the parameter estimates obtained using the various approaches. Based on the procedure outlined by Nguyen and Pinder, the most appropriate conductivity value would be 0.039 ft/d, which is about two orders of magnitude smaller than the hydraulic conductivity estimated using the Cooper et al. solution. Note that some difference should be expected between Cooper et al. model estimates and those of the Nguyen and Pinder model as a result of differences in the assumptions of these two models concerning vertical flow in response to the slug-induced disturbance. The model of Cooper et al. assumes that the well is fully screened across the tested formation, so there is no possibility of vertical flow in this model. The Nguyen and Pinder model, on the other hand, assumes a well that is partially screened across an isotropic formation. Thus, in this model, there will be a component of vertical flow. Extensive theoretical work (Hyder et al., in press), however, has shown that such dissimilar representations of the slug-induced vertical flow will produce a difference in hydraulic conductivity estimates of less than a factor of two for aspect ratios of the well used in this test ($(z_2-z_1)/r_s \approx 66$). This is a far cry from the discrepancy of two orders of magnitude found here. Thus, the large difference in the computed parameters must be considered an illustration of the ramifications of the error in the Nguyen and Pinder

model. As with the numerical experiment, the ramifications of the model error appear to be of practical significance.

Summary and Conclusions

A theoretical and field evaluation of the Nguyen and Pinder method for the analysis of response data from slug tests in partially penetrating wells in confined aquifers was presented here. The major results of this evaluation are as follows:

1) The Nguyen and Pinder method is not on a firm theoretical foundation as a result of the use of a boundary condition that is undefined in the transform space in which a solution was proposed. An attempt to circumvent this undefined boundary condition introduces further error that propagates into the expressions used for parameter estimation;
2) The errors in the theoretical development produce parameter estimates that may differ from the actual parameter values by orders of magnitude. The limited assessment done here indicates that the specific storage estimates tend to be too high while the hydraulic conductivity estimates are spread over a wide range.

The major conclusion of this evaluation is that the Nguyen and Pinder method should not be used for slug-test analysis. If response data from a slug test performed in a partially penetrating well in a confined aquifer are to be analyzed, the best approach would be to use one of the existing analytical solutions that consider variants of this configuration (e.g., Dougherty and Babu, 1984; Hayashi et al., 1987; Hyder et al., in press). Since these solutions are not widely available, the next best approach would be to employ the model of Hvorslev (1951). Recent work (Hyder et al., in press) shows that the Hvorslev method should produce very reasonable approximations of hydraulic conductivity for the same conditions covered by the Nguyen and Pinder method. The Hvorslev method, however, is not a panacea and must be used with care in cases of high specific storage, low-permeability well skins, and anisotropy (Chirlin, 1989; Demir and Narasimhan, 1994; Hyder et al., in press).

TABLE II.C.1 - PARAMETER SET FOR SLUG TEST SIMULATION

$K = 2.83$ ft/day
$S_s = 3.05e\text{-}6$ ft^{-1}
$r_w = r_c = .082$ ft
$z_2 - z_1 = .82$ ft
$b = 52.5$ ft
$H_0 = 1.0$ ft
$z_1 = 25.84$ ft

TABLE II.C.2 - NGUYEN AND PINDER ESTIMATES FROM SIMULATED SLUG TEST

Parameter Estimates	Slopes Employed in Calculation
$S_s = .00743$ ft^{-1}	C_{31}
$S_s = 3.64$ ft^{-1}	C_{32}
$K = .00245$ ft/day	C_{31}, C_{41}
$K = 12.8$ ft/day	C_{31}, C_{42}
$K = 1.20$ ft/day	C_{32}, C_{41}
$K = 630.$ ft/day	C_{32}, C_{42}

TABLE II.C.3 - COOPER ET AL. ESTIMATES FROM LINCOLN COUNTY SLUG TEST

	Estimated Value[a]	Lower Bound[b]	Upper Bound[b]
K	3.81 ft/day	3.79 ft/day	3.83 ft/day
S_s	2.85e-6 ft^{-1}	2.78e-6 ft^{-1}	2.91e-6 ft^{-1}

[a] Root-mean-squared deviation of .0035 ft. Well screened for 20 ft.

[b] Lower and upper bounds represent approximate 95% confidence intervals.

TABLE II.C.4 - NGUYEN AND PINDER ESTIMATES FROM LINCOLN COUNTY SLUG TEST

Parameter Estimates	Slopes Employed in Calculation
S_s = .000595 ft^{-1}	C_{31}
S_s = .0218 ft^{-1}	C_{32}
K = .00107 ft/day	C_{31}, C_{41}
K = 1.58 ft/day	C_{31}, C_{42}
K = .0393 ft/day	C_{32}, C_{41}
K = 58.0 ft/day	C_{32}, C_{42}

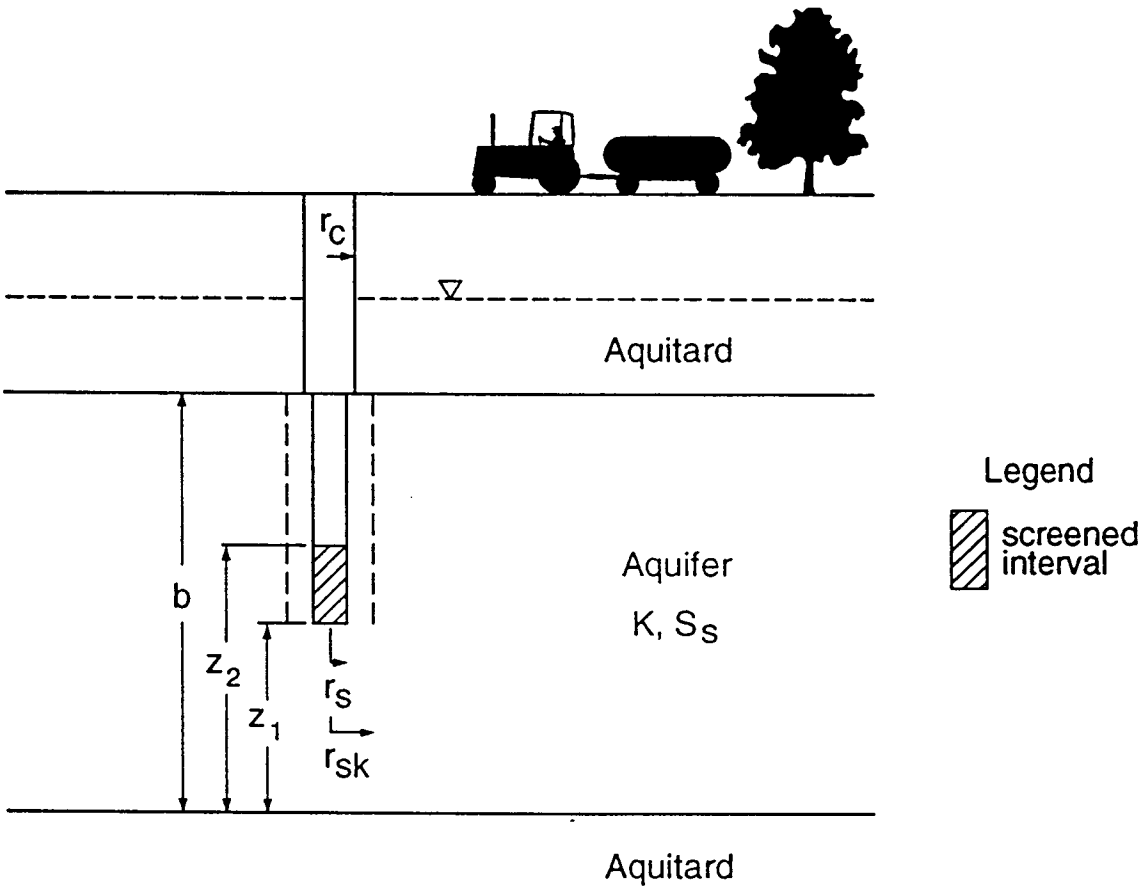

Figure II.C.1 - Cross-sectional view of a hypothetical confined aquifer (notation explained in text except for r_{sk}, the radius of the gravel pack).

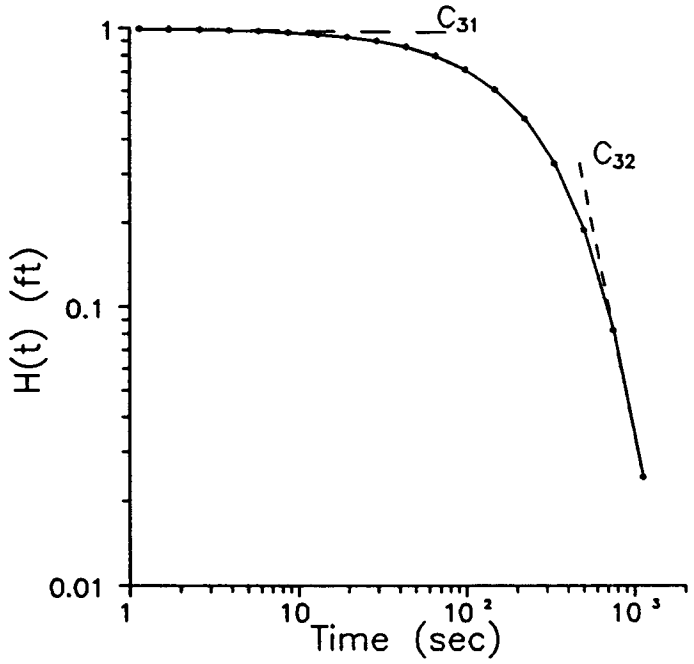

Figure II.C.2 - Nguyen and Pinder data plots for simulated slug test: a) Log-log H(t) versus time plot (C_{31} and C_{32} designate the absolute values of the slopes of straight lines fit to the early and late-time portions of the plot, respectively);

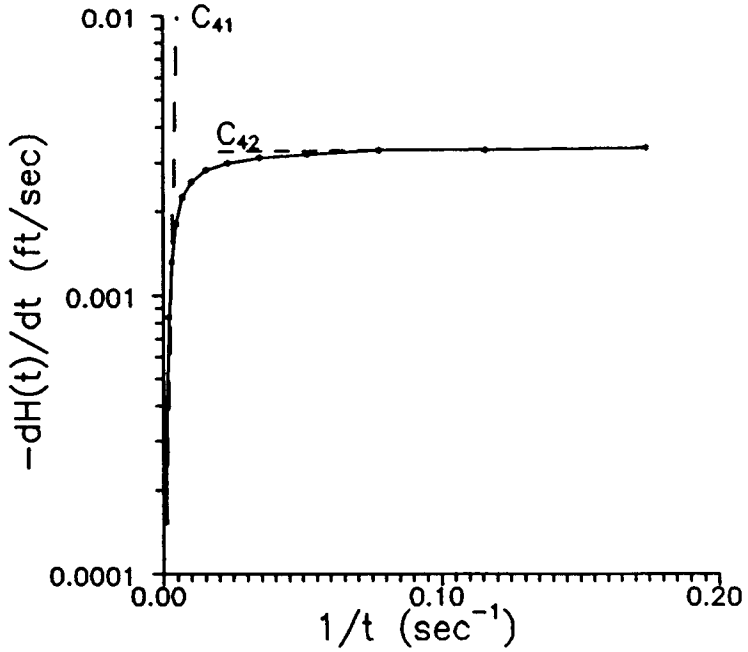

b) Semilog negative head derivative (-dH(t)/dt) versus inverse time plot (C_{41} and C_{42} designate the absolute values of the slopes of straight lines fit to the small and large inverse time portions of the plot, respectively).

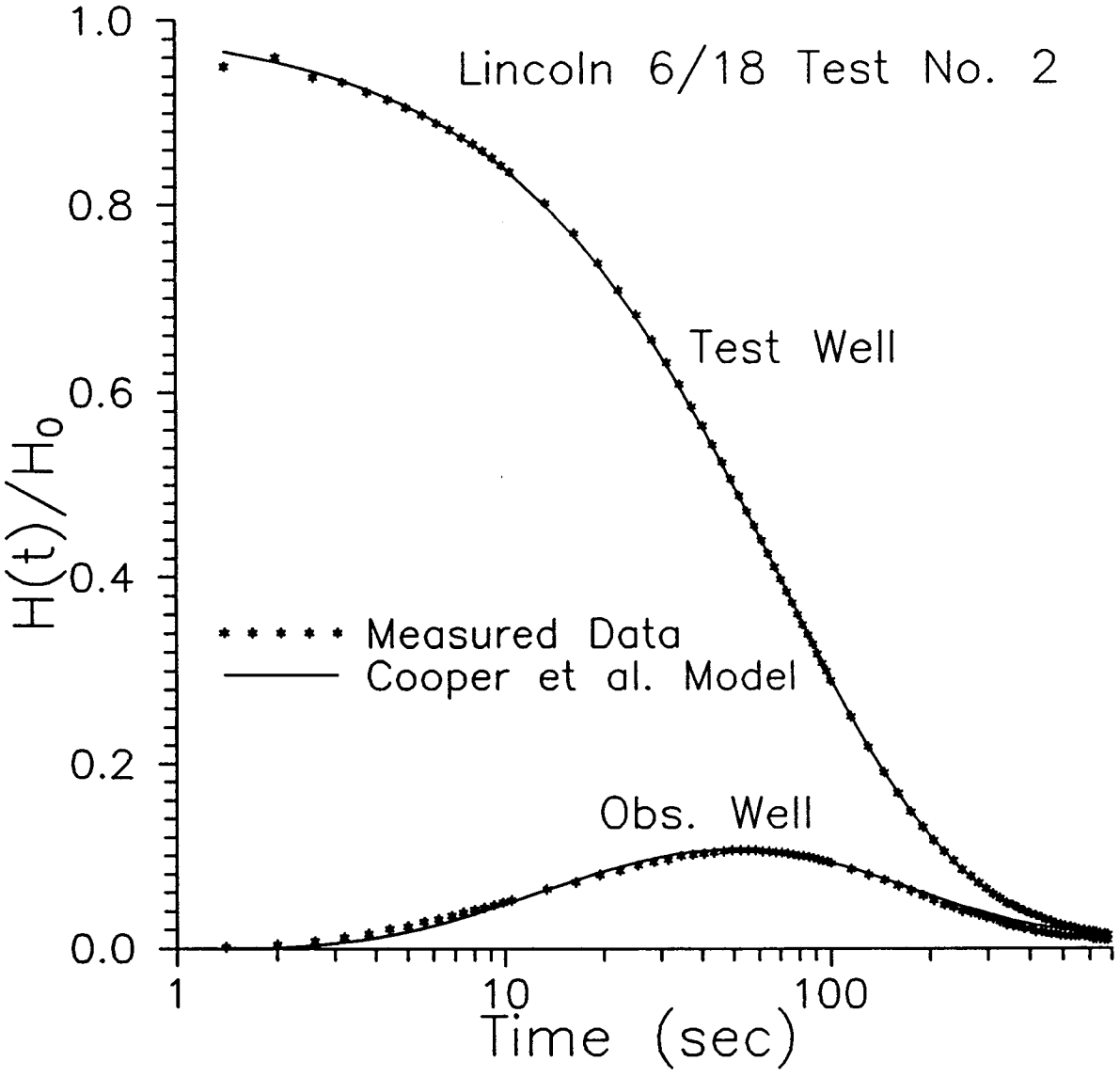

Figure II.C.3 - Semilog normalized head ($H(t)/H_0$) versus time plot of Lincoln County slug-test data and best-fit Cooper et al. model.

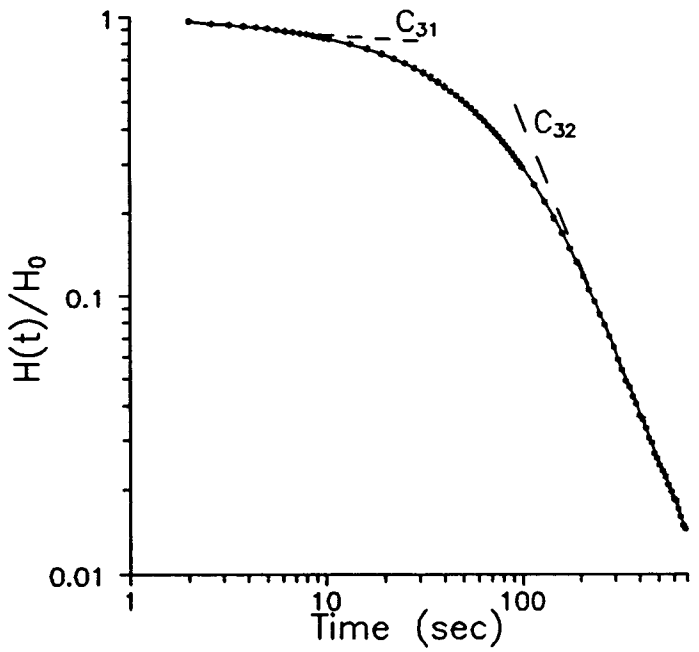

Figure II.C.4 - Nguyen and Pinder data plots for Lincoln County slug test: a) Log-log normalized head ($H(t)/H_0$) versus time plot (C_{31} and C_{32} designate the absolute values of the slopes of straight lines fit to the early and late-time portions of the plot, respectively);

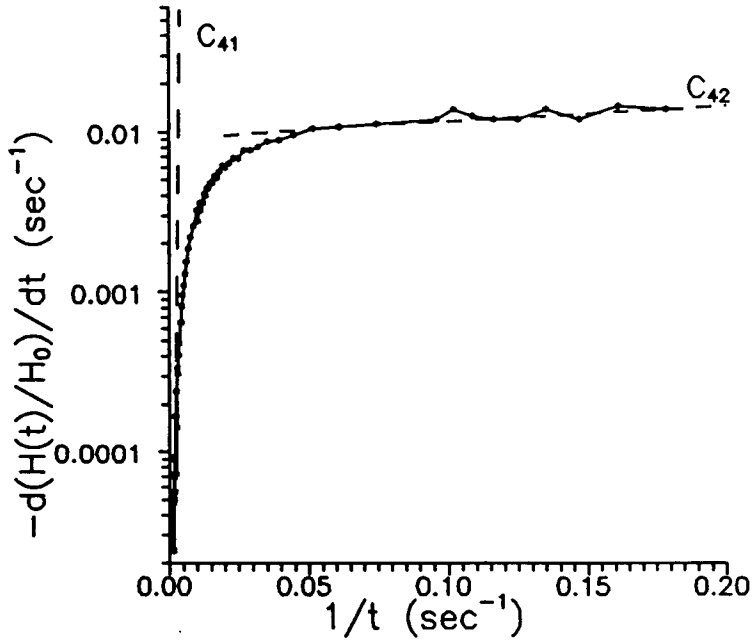

b) Semilog negative normalized head derivative ($-d(H(t)/H_0)/dt$) versus inverse time plot (C_{41} and C_{42} designate the absolute values of the slopes of straight lines fit to the small and large inverse time portions of the plot, respectively).

III. FIELD INVESTIGATIONS OF SLUG TESTS

A. SLUG TESTS WITH OBSERVATION WELLS

Introduction

Traditionally, slug tests have been performed using a single well as both the site of the stress and the site at which measurements are taken. In the first year of this project, theoretical and field results were reported that demonstrated the benefits of using observation wells other than the stressed well in slug tests. The most noteworthy of the reported results was the finding that the reliability of the parameter estimates can be improved through the use of observation wells. In the case of the storage parameter, the improvement is quite dramatic. The field experiment described in the first year's report involved wells approximately 6.5 meters apart. The transmission of the slug-induced pressure disturbance over that distance indicates that the estimated parameters from slug tests are reflective of conditions over a much larger volume of the formation than is normally considered to be influencing the results of a slug test. In cases where large volumetric averages of formation parameters are desired, slug tests may provide an alternative to pumping tests. Clearly, slug tests present several advantages to conventional pumping tests. These include the small amount of equipment and manpower required to perform a test, the relatively short duration of the test, and the need for only a small amount of water (if any) to be added/removed from the well during the course of the test. As discussed in Section II.A, the advantage of being able to initiate a slug test without adding or removing water from the well is very important for testing at sites of known or suspected contamination. However, if information about the hydraulic boundaries of a flow system is desired, slug tests do not provide a viable alternative to pumping tests.

To date, there has been very little work on the use of observation wells with slug tests (henceforth designated as multiwell slug tests). One of the few contributions in this area outside of the research of this project has been the work of Novakowski (1989) in which he presents a semianalytical solution for the response in an observation well to a pressure disturbance introduced instantaneously at a central well. Both the observation well and the stressed well are assumed to be fully screened across the aquifer. Well-bore storage is accounted for at the stressed well and, in an approximate fashion, at the observation well. Recently, van Dyke et al. (1993) describe the use of multiwell slug tests at a monitoring site in New Jersey. Unfortunately, the method that they employ for the analysis of the response data ignores well-bore storage effects at the

stressed and observation wells, thereby introducing a large amount of error into the parameter estimates.

In this section, additional field and theoretical work concerning multiwell slug tests is reported. A program of multiwell slug tests at the Geohydrologic Experimental and Monitoring Site (GEMS) is described. The estimated parameters obtained from these tests were considerably larger than expected. A theoretical examination of multiwell slug tests using a recently developed semianalytical solution is then presented. The results of this theoretical investigation provide one explanation for the larger than expected parameter estimates.

Field Testing at GEMS

Well 10-1 (depth 17.32 m, screen length 0.76 m) was selected as the test well for a program of multiwell slug tests because of its proximity to several groups of wells that could be used as observation wells (see Figure IV.A.1). The tests reported here involved using well 6-2 (depth = 21.55 m, screen length = 11.55 m, distance from 10-1 = 5.62 m) and well 00-1 (depth = 17.04 m, screen length = 0.76 m, distance from 10-1 = 6.61 m) as observation wells. In all cases, the slug test was initiated at 10-1 using the slug-test packer system described in the report of the first year of this project (Butler and McElwee, 1992). Measurements at the observation wells were taken using a transducer attached to the bottom of a packer located beneath the static water level in the well. The packer enabled effects associated with wellbore storage at the observation well to be kept very small. The response data could thus be analyzed without considering the effects of wellbore storage at the observation well.

Figures III.A.1 and III.A.2 display the responses observed at wells 6-2 and 00-1, respectively, for a slug test performed at well 10-1. In all cases, the responses at the stressed well exhibited the nonlinear behavior discussed in Section III.B of this report. Note the very low normalized heads measured at the two observation wells. The head changes at the observation wells were so small that the effective resolution of the transducers produced a stepped pattern in the measured responses. Note that the responses at well 6-2 were approximately 33% smaller than those at 00-1, even though 6-2 is one meter closer to 10-1 than 00-1. Several explanations can be advanced for the difference between the responses at 6-2 and 00-1: 1) the well at 6-2 is screened for a considerable length, so head increases at the same vertical interval as the stressed well are dampened by vertical movement of water in the well; 2) the resolution of the transducers causes the measured difference in the responses to be greater than the actual difference; and 3) spatial variations (heterogeneities) in flow properties produce a lower

diffusivity (K/S_s) between wells 10-1 and 6-2 than that between wells 10-1 and 00-1. Additional testing with a higher resolution pressure transducer and use of additional wells is currently being carried out to evaluate which of these explanations is the most reasonable.

Figures III.A.3 and III.A.4 display the results of an analysis of the response data using the fully penetrating slug-test model of Cooper et al. (1967). Although the fits appear relatively good (especially considering the stepped nature of the measured responses), the parameter estimates are much larger than the results obtained from the single-well slug tests discussed in Section III.B of this report. In addition, the parameter values exceed the maximum values (for both K and S_s) that would be plausible for the sand and gravel aquifer at GEMS (e.g., Anderson and Woessner, 1992). In an attempt to explain the anomalously high parameter values that were obtained in the field tests, a further theoretical investigation of multiwell slug tests was initiated at the end of the second year of this project. The results of the initial portion of this work are reported below.

Theoretical Investigation of Multiwell Slug Tests

The Cooper et al. model that was used in the analysis of the responses at wells 6-2 and 00-1 is based on the assumption that both the stressed well and the observation well are fully screened across the aquifer. Since well 10-1 is screened for only .76 meters of a 10.7 meter sequence of sand and gravel, the fully screened assumption of the Cooper et al. model is clearly being violated. In order to assess the error that is introduced into parameter estimates through use of a fully penetrating well model to analyze results from multiwell slug tests performed in partially penetrating wells, a recently developed semianalytical solution for slug tests in partially penetrating wells (Hyder et al., in press, henceforth designated as the KGS model) was extended to the case of observation points at other than the stressed well. The head at an observation point anywhere in the aquifer for the case of a slug test performed in a well with a finite-radius well skin in an anisotropic confined aquifer can be written in a non-dimensional form as

$$\phi_1(\xi,\eta,p)=\frac{\frac{\gamma}{\alpha}\Omega_2}{[1+\frac{\gamma}{\alpha}p\Omega_1]},\ \xi\le\xi_{sk} \qquad \text{(III.A.1a)}$$

$$\phi_2(\xi,\eta,p)=\frac{\frac{\gamma}{\alpha}\Omega_3}{[1+\frac{\gamma}{\alpha}p\Omega_1]},\ \xi_{sk}\le\xi \qquad \text{(III.A.1b)}$$

where

$\phi_i(\xi,\eta,p)$ = the nondimensional Laplace transform of $h_i(t)$, the head in zone i;

i = zone designator, for $r \le r_{sk}$, i=1, and for $r_{sk} \le r$, i=2;

r_w = screen radius, [L];

r_{sk} = outer radius of skin, [L];

r = radial direction, [L];

$\xi = r/r_w$;

$\eta = z/b$;

z = vertical position of observation point, z=0 at the top of the aquifer and increases downward, [L];

b = screen length of stressed well, [L];

p = Laplace-transform variable;

$\alpha = (2r_w^2 S_{s2} b)/r_c^2$;

$\gamma = K_{z2}/K_{r1}$;

S_{si} = specific storage of zone i, [1/L];

K_{zi}, K_{ri} = vertical and radial components, respectively, of the hydraulic conductivity of zone i, [L/T];

r_c = radius of well casing, casing and screen do not have to be of equal radius, [L];

$$\Omega_i = \int_{\varsigma}^{\varsigma+1} (F_c^{-1}(F_c(\omega)f_1))d\zeta, \; i = 1,$$

$$= F_c^{-1}(F_c(\omega)f_i), \; i = 2,3;$$

ω = the Fourier-transform variable = $(n\pi)/\beta$, n=0,1,2,..;

β = B/b;

B = aquifer thickness, [L];

$F_c(\omega)$ = finite Fourier cosine transform of $\Pi(z)$

$$= \frac{2}{\omega}\sin(\frac{\omega}{2})\cos(\frac{\omega(1+2\varsigma)}{2}), \; \omega = n\pi/\beta, \; n=1,2,3...,$$

$$= 1, \; \omega = 0;$$

$\Pi(z)$ = boxcar function = 0, $z < d$, $z > b+d$,

= 1, elsewhere;

d = distance from the top of the aquifer to the top of the screen, [L];

F_c^{-1} = inverse finite Fourier cosine transform;

$$f_1 = \frac{[\Delta_2 K_0(\nu_1) - \Delta_1 I_0(\nu_1)]}{\nu_1[\Delta_2 K_1(\nu_1) + \Delta_1 I_1(\nu_1)]};$$

$$f_2 = \frac{[\Delta_2 K_0(\nu_1\xi) - \Delta_1 I_0(\nu_1\xi)]}{\nu_1[\Delta_2 K_1(\nu_1) + \Delta_1 I_1(\nu_1)]};$$

$$f_3 = \frac{N[K_0(\nu_1\xi_{sk})I_1(\nu_1\xi_{sk}) + K_1(\nu_1\xi_{sk})I_0(\nu_1\xi_{sk})]K_0(\nu_2\xi)}{\gamma\nu_1[\Delta_2 K_1(\nu_1) + \Delta_1 I_1(\nu_1)]}.$$

$\varsigma = d/b;$

$\nu_i = (\psi_i^2\omega^2 + R_i p)^{.5};$

$\psi_i = (A_i/a^2)^{.5};$

$A_i = K_{zi}/K_{ri};$

$a = b/r_w;$

$R_i = \gamma\alpha/2\lambda$, i = 1,
$= \alpha/2$, i = 2;
$\lambda = S_{s2}/S_{s1}$;

$$\Delta_1 = K_0(\nu_1\xi_{sk})K_1(\nu_2\xi_{sk}) - [\frac{N}{\gamma}]K_0(\nu_2\xi_{sk})K_1(\nu_1\xi_{sk});$$

$$\Delta_2 = I_0(\nu_1\xi_{sk})K_1(\nu_2\xi_{sk}) + [\frac{N}{\gamma}]K_0(\nu_2\xi_{sk})I_1(\nu_1\xi_{sk});$$

$I_i(\ )$ = modified Bessel function of the first kind of order i;
$K_i(\ )$ = modified Bessel function of the second kind of order i;
$N = \nu_1/\nu_2$;
$\xi_{sk} = r_{sk}/r_w$.

Note that the inverse Fourier transforms in the numerator of Equations (III.A.1a) and (III.A.1b) are performed for η in the observation well, while the inverse Fourier transforms in the denominator are performed over the screened interval of the well at which the test is initiated.

Equation (III.A.1b) was employed to simulate a series of slug tests in a hypothetical aquifer with a hydraulic conductivity of 1.0e-3 m/s and a specific storage of 1.0e-5 m^{-1}. For the initial analysis discussed here, the well skin was assumed to have the same properties as the aquifer and the formation was considered isotropic with respect to hydraulic conductivity. This series of tests was designed to examine the effect of the fully screened assumption of the Cooper et al. model. A slug test was simulated for the case of a test well that is fully screened across a one-meter thick aquifer. A second simulation was performed in which the slug test was performed in a well, with a screen one meter in length, that is at the center of a very thick aquifer. Figure III.A.5 displays the simulated responses for an observation point located ten meters in the radial direction from the stressed well. In both cases, the observation point is at the same vertical position as the center of the screen. Note that the responses in the partially penetrating case are close to an order of magnitude smaller than those in the fully penetrating case. An analysis of the partially penetrating responses using the Cooper et al. model produced the results displayed in Figure III.A.6. Note that the estimated hydraulic conductivity and specific storage are 7.8 and 33 times, respectively, larger than

the actual parameters employed in the simulations. Clearly, the misapplication of the Cooper et al. model to data from a partially penetrating well can produce parameter estimates that are much larger than the actual formation parameters.

Given this result, it is clear that the data from the multiwell slug tests at GEMS must be reanalyzed using the partially penetrating slug test model. Figure III.A.7 displays the results of the reanalysis of the test at well 00-1. Note that the estimated hydraulic conductivity and specific storage values are 22 and 38 times, respectively, smaller than the parameters obtained in the fully penetrating case. Note also that the estimated conductivity of 3.4e-4 m/s (29.4 m/d) is in keeping with the results of the core analyses reported in Section IV.B. In the early part of the third year of this project, the remainder of the multiwell slug test data will be reanalyzed using the partially penetrating model.

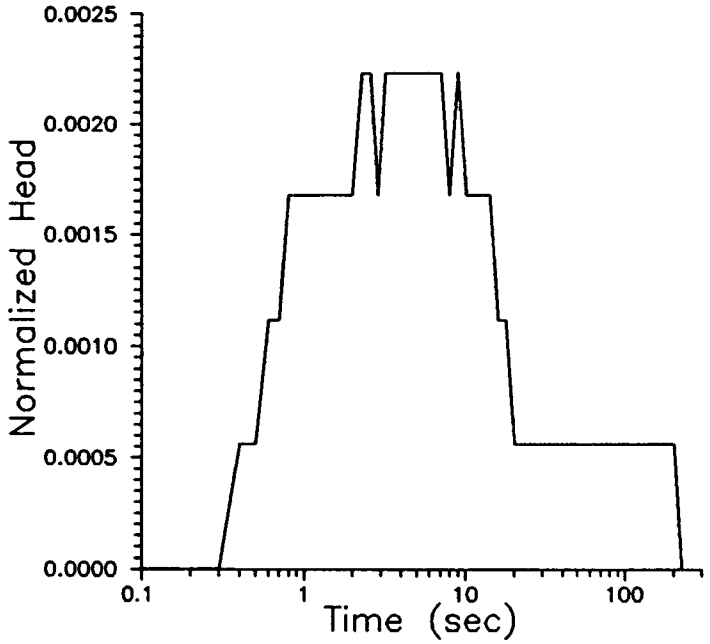

FIGURE III.A.1 - Normalized head ($h(t)/H_0$) versus time plot for well 6-2.

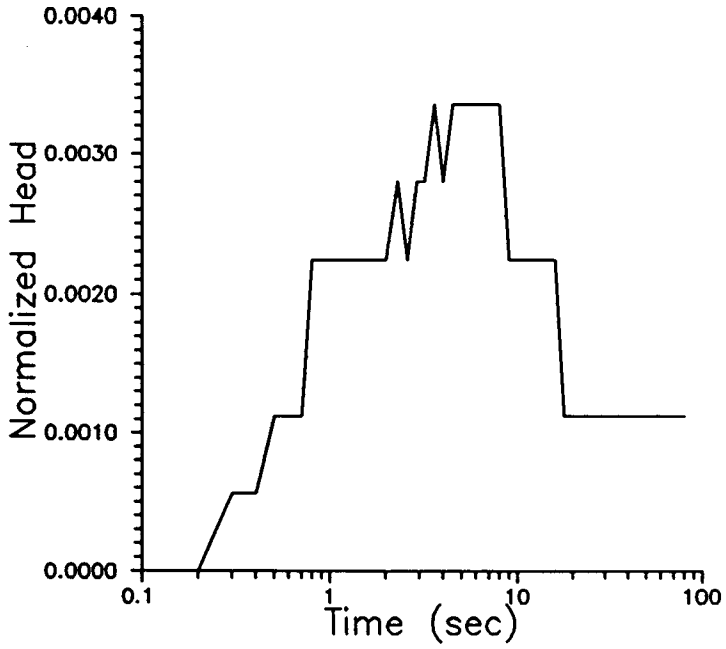

FIGURE III.A.2 - Normalized head ($h(t)/H_0$) versus time plot for well 00-1.

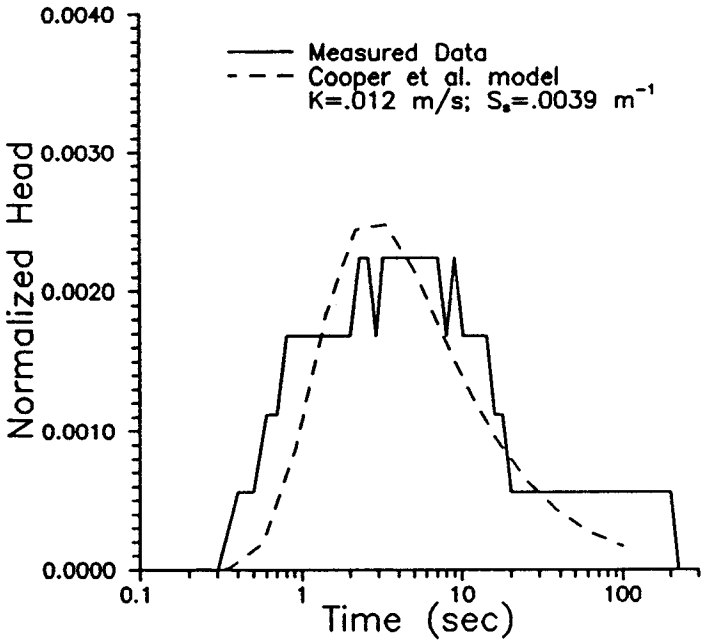

FIGURE III.A.3 - Normalized head versus time plot and the best-fit Cooper et al. model for well 6-2.

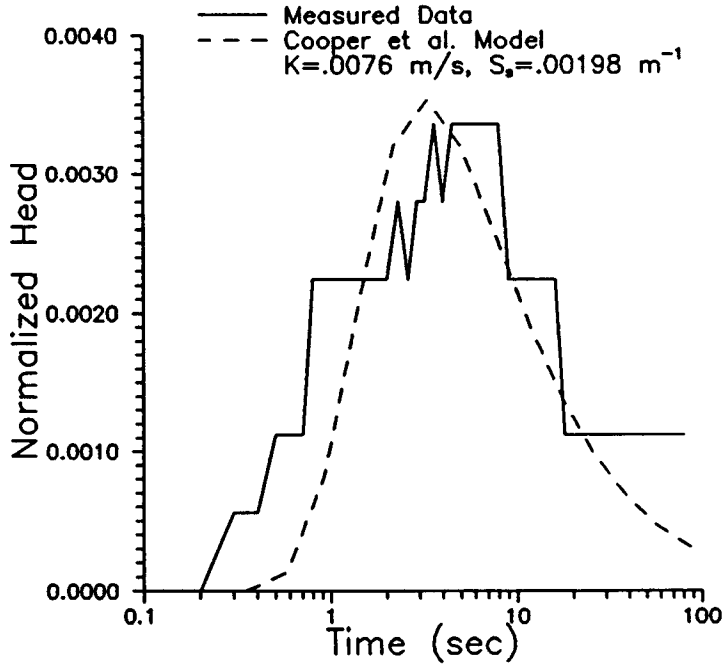

FIGURE III.A.4 - Normalized head versus time plot and the best-fit Cooper et al. model for well 00-1.

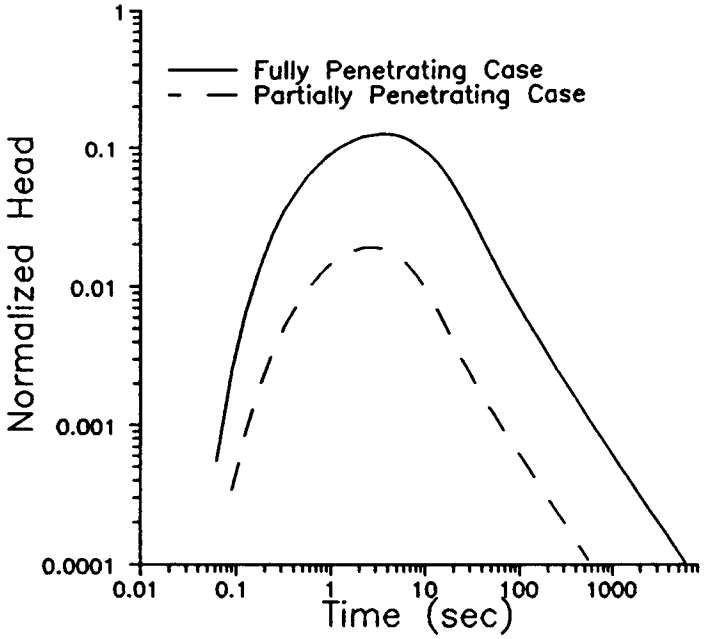

FIGURE III.A.5 - Normalized head versus time plot of simulated slug-test data (simulations employ the KGS model (Hyder et al., in press)).

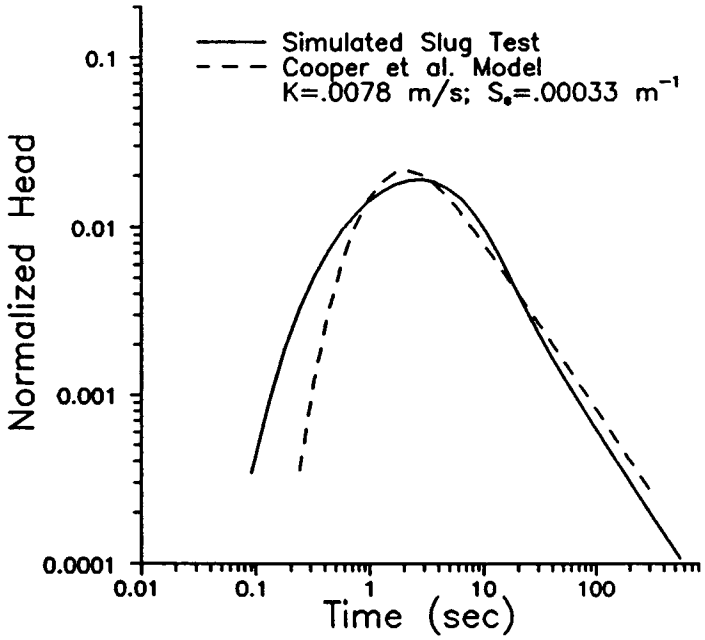

FIGURE III.A.6 - Normalized head versus time plot and the best-fit Cooper et al. model for the simulated partially penetrating well data of Figure III.A.5.

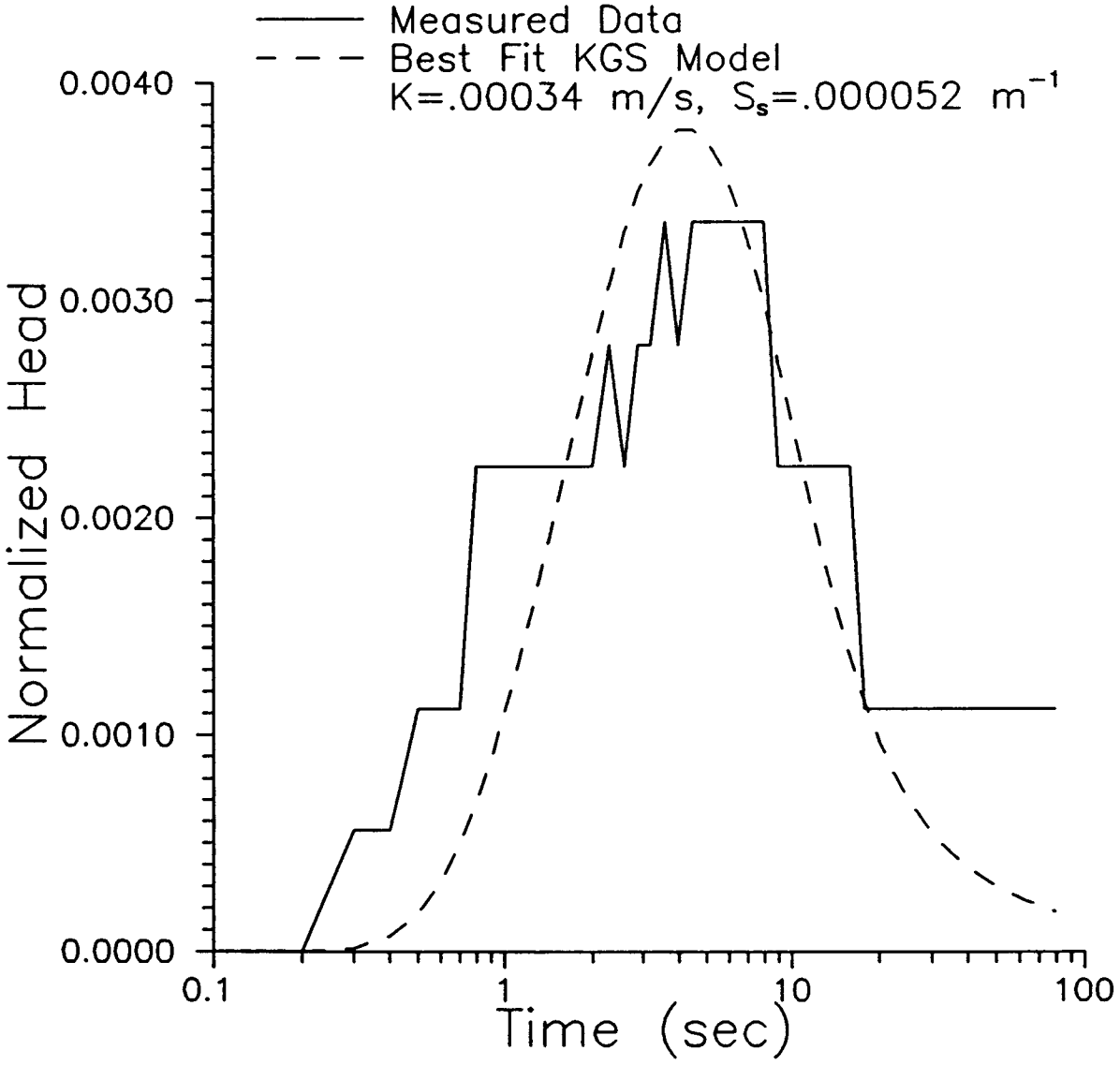

FIGURE III.A.7 - Normalized head versus time plot and the best-fit KGS model (Hyder et al., in press) for well 00-1.

B. UNIFIED ANALYSIS OF SLUG TESTS INCLUDING NONLINEARITIES, INERTIAL EFFECTS, AND TURBULENCE

Introduction

Slug tests are frequently used to characterize the flow properties of an aquifer. In highly permeable aquifers, however, problems arise when conventional techniques (e.g., Hvorslev (1951) and Cooper et al. (1967)) are employed for the analysis of slug-test response data. At a field site in an aquifer consisting of coarse sand and gravel overlain by silt and clay (the Geohydrologic Experimental and Monitoring Site (GEMS)), we have consistently observed slug-induced responses that are not in agreement with linear theoretical models. Typically, we see a systematic lack of fit of the measured data to conventional linear models, and a dramatic dependence of the duration of the slug test on the magnitude of the initial displacement (Figures III.B.1. and III.B.2.).

Figure III.B.1 shows some typical slug test data from a GEMS well. There are two noteworthy aspects of the data shown in Figure III.B.1: 1) test duration is dependent on the initial head (H_0), and 2) attempts to fit the data with the Hvorslev (1951) and Cooper et al. (1967, henceforth designated as the CBP model) models produce a systematic deviation between the measured data and the theoretical models. In all linear theories, the responses data from a series of slug tests initiated using different initial heads should coincide when plotted in a normalized (response data normalized by H_0) format. Clearly, this is not the case in Figure III.B.1. Also, as we shall see later, a plot of the field data in the semilog Hvorslev format displays a pronounced concave downward curvature. This is in contrast to the concave upward curvature that Chirlin (1989) shows should result when data from a fully penetrating well are plotted in the Hvorslev format. The implication is that this well is exhibiting behavior in the "critically damped" region. Since the Hvorslev and CBP models have been formulated for the "overdamped" region, it is not surprising that systematic deviations between the measured data and theoretical models are observed.

In other wells at GEMS, we have also observed oscillatory behavior (Figure III.B.2). Although some existing theories describe oscillatory behavior in slug tests, it has been difficult to analyze tests that are in the so-called "critically damped" region. One of the earliest attempts to analyze oscillatory data was by Van der Kamp (1976). He, however, invoked a number of assumptions to make the theory linear. Kipp (1985) has also dealt with the linear theory of oscillatory slug test responses by using Laplace transforms and numerical inversions to generate type curves. Kabala et al. (1985) are

among the first to consider the use of a nonlinear equation to describe the oscillatory behavior. However, after considerable numerical study, they state that "the linear model is sufficiently accurate in all practical cases." The data in Figure III.B.2 show that their conclusion is not valid for this well. Very recently, Stone and Clarke (in press) have used a nonlinear model to study hydraulic properties in glacial flow systems.

We have developed a unified model for slug tests that includes the effects of nonlinear terms, inertia, turbulence (spatial velocity distributions), viscosity and differing casing and screen radii. We have obtained a numerical solution, using a similar set of assumptions to those of Hvorslev (1951), to this model that should be valid over the whole range from "overdamped" to "underdamped" conditions. There are two interesting aspects that come to light in analyzing the GEMS data. First, most investigators (Van der Kamp (1976); Kabala et al. (1985); and Stone and Clarke (in press)) find that the effective water column height may be different than that measured in the field. We think we may have found an explanation for this phenomena. Second, some nonlinear effects are much stronger than most investigators have suggested and the magnitude of their strength is not easily predicted from the theory. For this reason, we use the magnitude of these effects as a fitted parameter.

Navier-Stokes Equation for the Borehole

The motion of the water in the borehole can be described by the Navier-Stokes equations (Eskinazi, 1967). If we consider the borehole as a streamtube with average flow in the z direction the z component equation is

$$\frac{\partial V}{\partial t} + V\frac{\partial V}{\partial z} = -g - \frac{\nabla P}{\rho} + \frac{\mu}{\rho}\nabla^2 V \qquad \text{(III.B.1)}$$

where V is the average velocity of the water in the borehole in the z direction, g is the acceleration of gravity, P is the pressure, ρ is the density and μ is the viscosity. This equation is basically a force balance equation per unit fluid mass and can be integrated in the z direction over the length of the borehole shown in Figure III.B.3 to obtain an energy or work balance equation:

$$\int\frac{\partial V}{\partial t}dz + \int V dV = -g(h + z_o + b) - \int\frac{dP}{\rho} + \int\frac{\mu}{\rho}\nabla^2 V dz \qquad \text{(III.B.2)}$$

Note that in the remainder of this development we will assume that the length of the screen (b) is negligible in comparison with the water column length,

$$b << z_o + h(t) \tag{III.B.3}$$

the water is incompressible (ρ is constant), and that the viscosity is constant. Integrating from the bottom of the screen to the top of the water in the borehole gives

$$\int \frac{\partial V}{\partial t} dz + \frac{V_T^2 - V_s^2}{2} = -g(h + z_o + b) + \frac{P_s - P_a}{\rho} + \int \frac{\mu}{\rho} \nabla^2 V dz \tag{III.B.4}$$

where P_s and P_a are the pressures in the screen and at the top of the water column, respectively, and V_T and V_s are the water velocities at the top of the column and in the screen, respectively. The average velocity at the top of the water column is simply dh/dt. Thus, the velocities can be related by the conservation of mass flow:

$$\pi r_c^2 V_T = \pi r_c^2 \frac{dh}{dt} = 2\pi r_s b V_s \tag{III.B.5}$$

where r_c and r_s are the casing and screen radii, respectively. Using equation (III.B.5) in equation (III.B.4) results in

$$\int \frac{\partial V}{\partial t} dz + \frac{1}{2}\left[1 - \left(\frac{r_c^2}{2r_s b}\right)^2\right]\left(\frac{dh}{dt}\right)^2 = -g(h + z_o + b) + \frac{P_s - P_a}{\rho} + \int \frac{\mu}{\rho} \nabla^2 V dz \tag{III.B.6}$$

The first and last terms of equation (III.B.6) require a little more explanation.

The last term in equation (III.B.6) is the work done by viscous forces in the fluid column. Writing out the Laplacian operator gives

$$\int \frac{\mu}{\rho} \nabla^2 V dz = \frac{\mu}{\rho} \int \left[\frac{\partial^2 V}{\partial r^2} + \frac{1}{r} \frac{\partial V}{\partial r} + \frac{1}{r^2} \frac{\partial^2 V}{\partial \theta^2} + \frac{\partial^2 V}{\partial z^2} \right] dz \qquad \text{(III.B.7)}$$

If we assume that the flow is unchanging in the θ direction and that the cross section of the borehole is uniform and the fluid is incompressible then

$$\frac{\partial V}{\partial \theta^2} = 0 \ , \ \frac{\partial^2 V}{\partial z^2} = 0 \qquad \text{(III.B.8)}$$

and equation (III.B.7) becomes

$$\int \frac{\mu}{\rho} \nabla^2 V dz = \frac{\mu}{\rho} \int \left[\frac{\partial^2 V}{\partial r^2} + \frac{1}{r} \frac{\partial V}{\partial r} \right] dz \qquad \text{(III.B.9)}$$

Of course, if we have varying radii in the borehole due to changes in casing radius or the presence of an obstruction such as a packer or other equipment, then equation (III.B.8) is no longer correct and additional terms need to be added to equation (III.B.9) due to viscous work being performed at those locations. If we assume a parabolic distribution of velocities across the borehole radius as shown in Figure III.B.4, we can write

$$V = V_o \left[1 - \frac{r^2}{r_c^2} \right] . \qquad \text{(III.B.10)}$$

This allows equation (III.B.9) to be written as

$$\int \frac{\mu}{\rho} \nabla^2 V dz = - \frac{4\mu}{r_c^2 \rho} V_o \int dz = - \frac{4\mu}{r_c^2 \rho} V_o (h + z_o + b) \qquad \text{(III.B.11)}$$

The average vertical water velocity is given by the rate of change of the height of the water column and is related to the maximum of the parabolic velocity distribution as

follows

$$Q = \pi r_c^2 \frac{dh}{dt} = \int V dA = 2\pi \int_0^{r_o} V_o \left[1 - \frac{r^2}{r_c^2}\right] r dr = \frac{\pi r_c^2 V_o}{2}$$

$$V_o = 2\frac{dh}{dt} \qquad \text{(III.B.12)}$$

where Q is the rate of water flow through the borehole. The final form for equation (III.B.11) is

$$\int \frac{\mu}{\rho} \nabla^2 V dz = -\frac{8\mu}{r_c^2 \rho}(h + z_o + b)\frac{dh}{dt} \qquad \text{(III.B.13)}$$

The first term in equation (III.B.6) can be manipulated as follows

$$\int \frac{\partial V}{\partial t} dz = \frac{\partial}{\partial t} \int V dz = \frac{\partial}{\partial t}\left[\frac{dh}{dt} \int \frac{\pi r_c^2}{A(z)} dz\right] \qquad \text{(III.B.14)}$$

by remembering that conservation of water flow requires that

$$\pi r_c^2 \frac{dh}{dt} = A(z)V(z) \qquad \text{(III.B.15)}$$

where dh/dt is the velocity in the casing with normal radius r_c and V(z) is the velocity where the cross sectional area is A(z). If the cross sectional areas do not change with time and if the cross sectional area is uniform in the z direction, then equation (III.B.14) becomes

$$\int \frac{\partial V}{\partial t} dz = (h + z_0 + b)\frac{d^2h}{dt^2} \qquad \text{(III.B.16)}$$

Additional acceleration work terms must be added to this equation if there are significant restrictions in the cross sectional area in the borehole. Our calculations show that these additional terms are usually negligible if the restrictions in cross sectional area are not too great.

Substitution of equations (III.B.16) and (III.B.13) into (III.B.6) yields the following expression

$$(h + z_0 + b)\frac{\partial^2 h}{\partial t^2} + \frac{1}{2}[1 - (\frac{r_c^2}{2r_s b})^2](\frac{\partial h}{\partial t})^2$$
$$= -g(h + z_0 + b) + \frac{P_s - P_a}{\rho} - \frac{8\mu}{r_c^2 \rho}(h + z_0 + b)\frac{\partial h}{\partial t} \qquad \text{(III.B.17)}$$

which is an ordinary differential equation for the height of the water column in the borehole as a function of time. Notice that this equation is nonlinear in h.

Borehole and Aquifer Interaction

The pressure at the screen will depend on the head in the aquifer, which in turn depends on the aquifer parameters. If H(r) is the head in the aquifer relative to the static level shown in Figure III.B.3, we can write

$$P_s = P_a + g\rho[H(r_s,t) + z_o + b] \qquad \text{(III.B.18)}$$

(assuming that b is small so that the pressure across the screen is nearly constant in the vertical). Substitution of equation (III.B.18) into equation (III.B.17) yields the final form for the borehole equation which couples to the aquifer equation through H(r,t).

$$(h + z_0 + b)\frac{\partial^2 h}{\partial t^2} + \frac{1}{2}[1 - (\frac{r_c^2}{2r_s b})^2](\frac{\partial h}{\partial t})^2 +$$
$$\frac{8\mu}{r_c^2 \rho}(h + z_0 + b)\frac{\partial h}{\partial t} + g[h - H(r_s,t)] = 0 \qquad \text{(III.B.19)}$$

The general aquifer equation

$$\nabla[bK\nabla H(r,t)] = S_s b\frac{\partial H}{\partial t} \qquad \text{(III.B.20)}$$

where K and S_s are the aquifer hydraulic conductivity and specific storage, respectively, must be solved for H(r,t) concurrently with equation (III.B.19) to obtain the complete solution. The screen is the boundary between these two solutions and the following boundary condition applies.

$$Q(t) = -\pi r_c^2\frac{dh(t)}{dt} = -2\pi bK[r\frac{\partial H(r,t)}{\partial r}]_{r_s} \qquad \text{(III.B.21)}$$

Hvorslev Style Approximation

The system of equations (III.B.19)-(III.B.21) is difficult to solve in general, so an approximation that simplifies the solution would be welcome. Following Hvorslev (1951) and Bouwer and Rice (1976), we assume that the storage in the aquifer is negligible and consider the aquifer as going through a series of quasi steady states in response to the slug in the borehole. With this assumption, equation (III.B.21) can be taken to hold at any radius, not just at the screen. In that case, the following equation for H(r,t) can be obtained by integrating equation (III.B.21) over r:

$$H(r,t) = \left(\frac{r_c^2}{2bK}\right)\left(\frac{dh}{dt}\right)\ln\left(\frac{r}{r_e}\right) \qquad \text{(III.B.22)}$$

where r_e, which is the effective radius at which the effect of the slug goes to zero, is

treated as an empirical parameter. Evaluating equation (III.B.22) at r_s and substituting into equation (III.B.19) gives a single ordinary differential equation that must be solved for h(t).

$$(h + z_0 + b)\frac{\partial^2 h}{\partial t^2} + \frac{1}{2}[1 - (\frac{r_c^2}{2r_s b})^2](\frac{\partial h}{\partial t})^2 + [\frac{8\mu}{r_c^2 \rho}(h + z_0 + b) + g(\frac{r_c^2}{2bK})\ln(\frac{r_e}{r_s})]\frac{\partial h}{\partial t} + gh = 0 \qquad \text{(III.B.23)}$$

Equation (III.B.23) is the nonlinear equivalent to the usual linear Hvorslev equation. Dropping the nonlinear, inertial, and viscous terms in equation (III.B.23) gives

$$\left[g\left(\frac{r_c^2}{2bK}\right)\ln\left(\frac{r_e}{r_s}\right)\right]\left(\frac{dh}{dt}\right) + gh = 0 \qquad \text{(III.B.24)}$$

which is equivalent to the Hvorslev equation

$$Q = -\pi r_c^2 \frac{dh}{dt} = FKh \qquad \text{(III.B.25)}$$

if we identify the Hvorslev shape factor (F) as

$$F = \frac{2\pi b}{\ln\left(\frac{r_e}{r_s}\right)} \qquad \text{(III.B.26)}$$

Both F and r_e are empirical factors, so it does not matter which we use. In order to stay consistent with the widely used Hvorslev theory, we will write equation (III.B.23) as

$$(h + z_0 + b)\frac{\partial^2 h}{\partial t^2} + \frac{1}{2}[1 - (\frac{r_c^2}{2r_s b})^2](\frac{\partial h}{\partial t})^2 + [\frac{8\mu}{r_c^2 \rho}(h + z_0 + b) + g(\frac{\pi r_c^2}{FK})]\frac{\partial h}{\partial t} + gh = 0 \qquad \text{(III.B.27)}$$

If we use the usual Hvorslev expressions for F, this equation only has one unknown parameter, K. The rest of the physical parameters in equation (III.B.27) can be measured directly in the field or laboratory. Therefore, a least squares fit of the numerical solution of equation (III.B.27) to field data for h(t) should yield a value for K, the hydraulic conductivity of the aquifer.

To conserve writing effort we use the usual definition of the Hvorslev time lag

$$t_o = \frac{\pi r_c^2}{FK} \qquad \text{(III.B.28)}$$

and define two more quantities

$$A = \frac{\left[1 - \left(\frac{r_c^2}{2r_s b}\right)^2\right]}{2g\pi r_c^2} \qquad \text{(III.B.29)}$$

and

$$M = \frac{8\mu}{g t_o r_c^2 \rho} \qquad \text{(III.B.30)}$$

With these definitions and dividing by gt_o, equation (III.B.27) can be written as

$$\frac{(h + z_o + b)}{gt_o}\frac{d^2h}{dt^2} + FKA\left(\frac{dh}{dt}\right)^2 + [M(h + z_o + b) + 1]\left(\frac{dh}{dt}\right) + \frac{h}{t_o} = 0 \qquad \text{(III.B.31)}$$

When the acceleration term is negligible and M =0, this is the same model as presented by McElwee et al. (1992) for the nonoscillatory case.

Limiting Case Solutions

Analytical solutions to equation (III.B.31) can be obtained in a couple of limiting cases. At t=0, the water column is at rest and dh/dt = 0. The velocity of the water column will be small at early times, so the velocity dependent terms of equation (III.B.31) can be dropped to give

$$(h_o + z_o + b)\frac{d^2h}{dt^2} + gh_o = 0 \qquad \text{(III.B.32)}$$

where h_o is the initial height. Equation (III.B.32) can only be used for very early times before the water column has moved much because we are assuming the column height is approximately constant at h_o. With these assumptions the solution to equation (III.B.32) is

$$h - h_o = \frac{g}{2}\left(\frac{h_o}{h_o + z_o + b}\right)t^2 \qquad \text{(III.B.33)}$$

This is simply the normal equation for a falling body under the action of gravity. However, the acceleration is not g but some fraction based on the quantities h_o, z_o, and b. In the case where $h_o >> z_o + b$, the column acceleration approaches g at early times.

Dropping only the velocity squared term (assuming small velocities) in equation (III.B.31) gives

$$(h + z_o + b)\frac{d^2h}{dt^2} + gt_o\,[M(h + z_o + b) + 1]\left(\frac{dh}{dt}\right)^2 + gh = 0 \qquad \text{(III.B.34)}$$

which would be the usual damped harmonic oscillator equation except for the expression (h + z_o + b) which occurs in the coefficients and makes the equation nonlinear. In the case where $h_o << z_o + b$ (initial displacements are small), equation (III.B.34) can be approximated by

$$(z_o + b)\frac{d^2h}{dt^2} + gt_o\,[M(z_o + b) + 1]\left(\frac{dh}{dt}\right)^2 + gh = 0 \qquad \text{(III.B.35)}$$

which is exactly the damped harmonic oscillator equation (Kreyszig, 1983). Three cases can be identified. The overdamped case is the classical one usually treated in older geohydrology literature:

$$g^2t_o^2\,[M(z_o + b) + 1]^2 > 4g(z_o + b) \qquad \text{(III.B.36)}$$

In this case the water column does not oscillate at all. In these overdamped cases, the viscosity effects represented by M are usually much smaller than the damping due to the aquifer hydraulic conductivity, and thus can usually be ignored. If the quantities on both sides of equation (III.B.36) are equal, then critical damping is said to occur and there is no oscillation.

The third case to be identified is underdamping and occurs when

$$g^2t_o^2\,[M(z_o + b) + 1]^2 < 4g(z_o + b) \qquad \text{(III.B.37)}$$

In this case we have an exponentially decaying oscillation given by

$$h(t) = CExp\,[-\alpha t]\cos(\omega^* t - \delta) \qquad \text{(III.B.38)}$$

where

$$\alpha = \frac{gt_o\,[M(z_o + b) + 1]}{2(z_o + b)} \qquad \text{(III.B.39)}$$

and

$$\tilde{\omega}^* = \sqrt{\frac{g}{z_o + b} - \alpha^2} \qquad \text{(III.B.40)}$$

C and δ are given by the initial conditions on the displacement and the velocity of the water column. If $\alpha = 0$ in equation (III.B.40), which corresponds to no damping either by viscous forces or the aquifer, then $\tilde{\omega}^*$ is just the natural frequency of an undamped water column. A number of papers in recent years have dealt with this case (e.g., Van der Kamp (1976); Kabala et al. (1985), etc.). However, little has been done to treat the general case which might lie anywhere in the domain from overdamped to underdamped. Clearly what is needed is a general solution to equation (III.B.31).

Numerical Solution

Since the fully nonlinear equation (III.B.31) can not be solved analytically, we must resort to numerical techniques. Evaluating equation (III.B.31) at time n and using central difference formulas for the time derivatives results in

$$\frac{(h^n + z_o + b)}{gt_o}\left[\frac{h^{n+1} - 2h^n + h^{n-1}}{\Delta t^2}\right] + FKA\left(\frac{h^{n+1} - h^{n-1}}{2\Delta t}\right)^2 + [M(h^n + z_o + b) + 1]\left(\frac{h^{n+1} - h^{n-1}}{2\Delta t}\right) + \frac{h^n}{t_o} = 0 \qquad \text{(III.B.41)}$$

We have had good results applying a point iterative method to equation (III.B.41). In order to apply this iterative method, an iteration index (m+1) will be introduced as a superscript in all single appearances of h at time level n+1. In all terms where h squared at time level n+1 appears we must evaluate one h at the new iteration level

(m+1) and one h at the old iteration level (m).

$$\frac{(h^n + z_o + b)}{gt_o}\left[\frac{h^{n+1(m+1)} - 2h^n + h^{n-1}}{\Delta t^2}\right] + FKA\left(\frac{h^{n+1(m)} - h^{n-1}}{2\Delta t}\right)\left(\frac{h^{n+1(m+1)} - h^{n-1}}{2\Delta t}\right) + [M(h^n + z_o + b) + 1]\left(\frac{h^{n+1(m+1)} - h^{n-1}}{2\Delta t}\right) + \frac{h^n}{t_o} = 0$$

(III.B.42)

Rearranging equation (III.B.42) gives

$$h^{n+1(m+1)} = \frac{coef(n-1,m)h^{n-1} + coef(n)h^n}{coef(n+1,m)}$$

(III.B.43)

where

$$coef(n+1,m) = \left[1 + \left(M + \frac{2}{gt_o\Delta t}\right)(h^n + z_o + b) + FKA\left(\frac{h^{n+1(m)} - h^{n-1}}{2\Delta t}\right)\right],$$

(III.B.44)

$$coef(n-1,m) = \left[1 + \left(M - \frac{2}{gt_o\Delta t}\right)(h^n + z_o + b) + FKA\left(\frac{h^{n+1(m)} - h^{n-1}}{2\Delta t}\right)\right],$$

(III.B.45)

and

$$coef(n) = \left[\frac{4(h^n + z_o + b)}{g t_o \Delta t} - \frac{2\Delta t}{t_o} \right] . \qquad \text{(III.B.46)}$$

Equation (III.B.43) can now be solved iteratively for h at the new time level n+1.

This numerical solution has been incorporated into an automated well test analysis package called SUPRPUMP (Bohling and McElwee, 1992). As mentioned earlier, K, the hydraulic conductivity of the aquifer, is really the only parameter available for fitting in equation (III.B.31). We discovered a number of things when we tried to fit the field data. First of all, it was impossible to fit the overall shape of the oscillatory field data with only one parameter. The values of A and M in equations (III.B.29) and (III.B.30) were quite small and did not seem to fit the field data. The value of A calculated from equation (III.B.29) for our field data was about .7 sec^2/ft^2. The kinematic viscosity (μ/ρ) is about 10^{-5} ft^2/sec. Therefore, neither of these parameters played an important role in the analysis of our data. We decided to treat A as an adjustable parameter to be determined by fitting the data. McElwee et al. (1992) had pretty good success using this kind of model when no oscillating water column was observed. Unfortunately, when applied to oscillatory data, the model with two parameters (A and K) still did not give a good overall fit to the shape of the curve and most troubling of all, a constant set of values for A and K did not seem to predict the head dependence of the slug test properly. In the process of trying to fit the data, it was observed that if the length of the water column in the borehole was adjusted to larger values the general shape of the field data could be fit much better. So, it appeared that something was missing in the physical model.

Revision of the Model

An alternate method of deriving the equation of motion of the water column in a slug test can be obtained by considering an energy balance equation (Hansen, 1967). Consider the water column inside the borehole (Figure III.B.3) to be a control volume. The change of energy within the control volume over time is determined by the work done at the free surface and the amount of energy that flows out the screen. In equation form this is

$$\frac{d}{dt}\int_{V_{cv}}\left(\frac{V^2}{2}+gz\right)\rho dV_{cv}+\int_{A_s}\left(\frac{P_s}{\rho}+\frac{V_s^2}{2}\right)V_m\rho dA_s+\int_{A_T}P_a V_a dA_T=0 \qquad \text{(III.B.47)}$$

The first term is the rate of change of kinetic and potential energy in the borehole (control volume,V_{cv}). The second term is the rate at which energy flows out the screen area (A_s) due to a radial velocity (V_m), where P_s and V_s are the screen pressure and velocity (V_m will be assumed equal to V_s for the remainder of this derivation), respectively. The third term is the rate at which work is done by atmospheric pressure (P_a) on the moving upper surface. This equation neglects viscous forces.

Assume that the pressure is constant over the screen area ($2\pi r_s b$) and on the upper surface (πr_c^2). In addition, assume that the velocity is uniform over the screen area (V_s) and the upper free surface (V_a). If we consider the water incompressible, the average screen velocity is related to the average borehole velocity (dh/dt).

$$V_s=-\frac{r_c^2}{2r_s b}V_a=-\frac{r_c^2}{2r_s b}\frac{dh}{dt} \qquad \text{(III.B.48)}$$

Using the mean value theorem to average equation (III.B.47) over the control volume gives the result

$$\frac{d}{dt}\left\{\left[\frac{\overline{V^2}}{2}+\frac{g}{2}(h+z_o+b)\right]\pi r_c^2\rho(h+z_o+b)\right\}$$
$$-\left\{\frac{P_s}{\rho}+\left(\frac{r_c^2}{2r_s b}\right)^2\frac{1}{2}\left(\frac{dh}{dt}\right)^2\right\}\left(\frac{r_c^2}{2r_s b}\frac{dh}{dt}\right)2\pi r_s b\rho+P_a\pi r_c^2\frac{dh}{dt}=0$$

(III.B.49)

The term involving $\overline{V^2}$ is the average kinetic energy per unit volume of the borehole and needs further consideration. In actual fact, there will be velocity components inside the borehole other than the average vertical velocity describing the

drop of the water column. These velocity components may be random in nature (turbulence) or axially circular (curl of velocity not zero), but when averaged over the borehole they do not contribute to the net flow of water out the screen. However, these velocity components may carry significant energy and must be considered when averaging the kinetic energy over the control volume, which is the entire borehole. Assume that the velocity field can be represented by a vertical component and a random component.

$$V = V_z + V_r \tag{III.B.50}$$

Using this form for the velocity in equation (III.B.49) gives

$$\begin{aligned}\overline{V^2}\rho\pi r_c^2(h + z_o + b) &= \int_{V_{cv}} V^2 \rho dV_{cv} = \int_{V_{cv}} (V_z + V_r)^2 \rho dV_{cv} \\ &= \int_{V_{cv}} (V_z^2 + 2V_z V_r + V_r^2)\rho dV_{cv}\end{aligned} \tag{III.B.51}$$

Since V_r is a random velocity component, we assume that the following integral will average to zero over the control volume.

$$\int_{V_{cv}} V_z V_r \rho dV_{cv} = 0 \tag{III.B.52}$$

Assume that V_z is given by a radial velocity distribution defined by equations (III.B.10) and (III.B.12).

$$V_z = 2\frac{dh}{dt}\left[1 - \frac{r^2}{r_c^2}\right] \tag{III.B.53}$$

The first term in equation (III.B.51) can now be evaluated. The last term in equation (III.B.51) requires some addition assumptions about the random component. Since the random component is zero in a static situation and could logically be expected to increase proportionally to the average vertical velocity, it is reasonable to assume that

$$V_r = \alpha \frac{dh}{dt} \tag{III.B.54}$$

With these assumptions equation (III.B.51) can be written as

$$\overline{V^2} \rho \pi r_c^2 (h + z_o + b) = \left(\frac{dh}{dt}\right)^2 \int_{V_{cv}} \left(4\left[1 - \frac{r^2}{r_c^2}\right]^2 + \alpha^2 \right) \rho dV_{cv}$$

$$= \left(\frac{dh}{dt}\right)^2 \left[\frac{4}{3} + \alpha^2\right] \rho \pi r_c^2 (h + z_o + b) \tag{III.B.55}$$

which shows that the average square velocity is larger than the square of the average velocity by a factor greater than one.

$$\overline{V^2} = \left(\frac{dh}{dt}\right)^2 \left[\frac{4}{3} + \alpha^2\right] \tag{III.B.56}$$

This implies that the kinetic energy of the water column can be significantly larger than one might suspect based on the average vertical velocity (dh/dt).

With the above considerations, equation (III.B.49) can now be written as

$$\frac{d}{dt}\left\{\left[\frac{1}{2}\left(\frac{dh}{dt}\right)^2\left(\frac{4}{3} + \alpha^2\right) + \frac{g}{2}(h + z_o + b)\right] \pi r_c^2 \rho (h + z_o + b)\right\}$$

$$- \left\{\left[\frac{P_s}{\rho} + \left(\frac{r_c^2}{2 r_s b}\right)^2 \frac{1}{2}\left(\frac{dh}{dt}\right)^2\right]\left(\frac{r_c^2}{2 r_s b}\frac{dh}{dt}\right) 2\pi r_s b \rho + P_a \pi r_c^2 \frac{dh}{dt} = 0 \right. \tag{III.B.57}$$

Performing the differentiation and rearranging slightly shows that this is identical to

equation (III.B.17) except for the viscous terms which have been neglected and the factor multiplying the kinetic energy:

$$(\frac{dh}{dt})[(h + z_0 + b)(\frac{4}{3} + \alpha^2)\frac{d^2h}{dt^2} + \frac{1}{2}[(\frac{4}{3} + \alpha^2) - (\frac{r_c^2}{2r_s b})^2](\frac{dh}{dt})^2 + g(h + z_0 + b) - \frac{P_s - P_a}{\rho} = 0 \qquad \text{(III.B.58)}$$

By considering an energy based approach, we have derived the same basic equation as is obtained starting from the Navier-Stokes equation. However, since the kinetic energy contribution of velocity components other than those in the vertical direction may be considerable, a new parameter (α) has been added to the model. The generalization of equation (III.B.58) to include a viscous term or the addition of the factor multiplying the acceleration term into equation (III.B.17) gives the final form for the mathematical model.

$$(h + z_0 + b)(\frac{4}{3} + \alpha^2)\frac{d^2h}{dt^2} + \frac{1}{2}[(\frac{4}{3} + \alpha^2) - (\frac{r_c^2}{2r_s b})^2](\frac{dh}{dt})^2 + g(h + z_0 + b) - \frac{P_s - P_a}{\rho} + \frac{8\mu}{r_c^2 \rho}(h + z_0 + b)\frac{dh}{dt} = 0 \qquad \text{(III.B.59)}$$

Data Analysis

The numerical method presented earlier can easily be adapted to the model presented by equation (III.B.59) simply by adding the factor which multiplies the acceleration term. The point iterative formula for the head at the latest time level is still given by equation (III.B.43).

$$h^{n+1(m+1)} = \frac{coef(n-1,m)h^{n-1} + coef(n)h^n}{coef(n+1,m)} \qquad \text{(III.B.43)}$$

Only the coefficients are changed slightly.

$$coef(n+1,m) = 1 + \left(M + \frac{2\left(\frac{4}{3} + \alpha^2\right)}{gt_o \Delta t} \right) (h^n + z_o + b) + FKA\left(\frac{h^{n+1(m)} - h^{n-1}}{2\Delta t} \right) , \quad \text{(III.B.60)}$$

$$coef(n-1,m) = 1 + \left(M - \frac{2\left(\frac{4}{3} + \alpha^2\right)}{gt_o \Delta t} \right) (h^n + z_o + b) + FKA\left(\frac{h^{n+1(m)} - h^{n-1}}{2\Delta t} \right) , \quad \text{(III.B.61)}$$

and

$$coef(n) = \frac{4\left(\frac{4}{3} + \alpha^2\right)(h^n + z_o + b)}{gt_o \Delta t} - \frac{2\Delta t}{t_o} . \quad \text{(III.B.62)}$$

Note that the A parameter in these equations is slightly different from the definition given in (III.B.29):

$$A = \frac{[(\frac{4}{3} + \alpha^2) - (\frac{r_c^2}{2r_s b})^2]}{2g\pi r_c^2} \qquad \text{(III.B.63)}$$

The model represented by equation (III.B.43) and equations (III.B.60)-(III.B.62) has three parameters (α, A, K) which may be adjusted to fit the field data. We have had good results fitting this model to the GEMS data. Figures III.B.5 and III.B.6 show the fitted theoretical model values as stars on the field data plots. The theory describes the head dependence and the general shape of the field data very well. Both the nonoscillatory (Figure III.B.5) and oscillatory (Figure III.B.6) data are predicted very well by the fitted values. Field data for a variety of initial slug heights are reproduced well for a single set of parameters (α, A, K). Earlier models (McElwee et al., 1992) fit the non oscillatory data fairly well, but the parameters had some dependence on the initial slug height. In general, the effect of the viscosity term in the model appears to be insignificant. The factor $(4/3 + \alpha^2)$ in the model implies that the velocity components not in the z direction carry about 15% of the kinetic energy since $\alpha = .5$ is the best fit value. The 4/3 arises from the assumption that there is a parabolic distribution of velocities along the radius. Any other radial distribution will give a slightly different result. However, the important point is that the column is usually carrying more kinetic energy than would be predicted by simply using the average vertical velocity (dh/dt). These two contributions together increase the kinetic energy about 60% over the uniform velocity case. The other parameter, A, was fitted with a magnitude of 55-70 for this field data. This is much larger than would be calculated from equation (III.B.63) for A. Clearly, some physical mechanism has been left out of the model. It apparently has the same mathematical form as the term involving A in equation (III.B.31), but with a much larger magnitude. Further research is needed to shed light on the nature of this mechanism.

Figures III.B.7 and III.B.8 are plots of the field data and theoretical model for one particular value of the initial slug height. These plots allow one to better assess the quality of the fit of the theoretical model to the experimental data. In general, the fit is very good. Figure III.B.9 is a Hvorslev type plot of the field data and the theoretical model for a non oscillatory well. Notice that the data are becoming very noisy after about 12 seconds, so little quantitative information is available beyond that time. Also notice that the curve for the theoretical model is approaching a straight line whose slope is proportional to K at large time (McElwee et al., 1992). However, there is little hope

that data could ever be collected in this region since the response is so small. Only in the overdamped case will this straight line portion move into the range where it is measurable. In the case of wells in the critically damped region, this characteristic downward curvature on a Hvorslev plot can be considered an indication that a model more complex than the conventional linear models must be used to analyze the data.

Conclusions

Generally, the effects of viscosity and changing casing-screen radii are negligible on slug test responses. However, the effects of nonlinearities, inertia, and velocity distributions can be quite important. The nonlinear terms make slug test results dependent on the initial head, inertial effects are important when oscillatory behavior is observed, and nonuniform velocity distributions cause the effective water column length to be greater than expected. We have developed a general model incorporating all these features. This general model can be reduced to a Hvorslev type model by assuming no storage in the aquifer. We have obtained an iterative numerical solution to this model and have applied it to field data from our research site. The results are quite good both for oscillatory and non oscillatory situations, and give consistent values for the physical parameters with various initial displacements. The theory predicts the general shape and head dependence observed in the field data. Further research in needed to identify the source of the strong nonlinearity represented by one parameter.

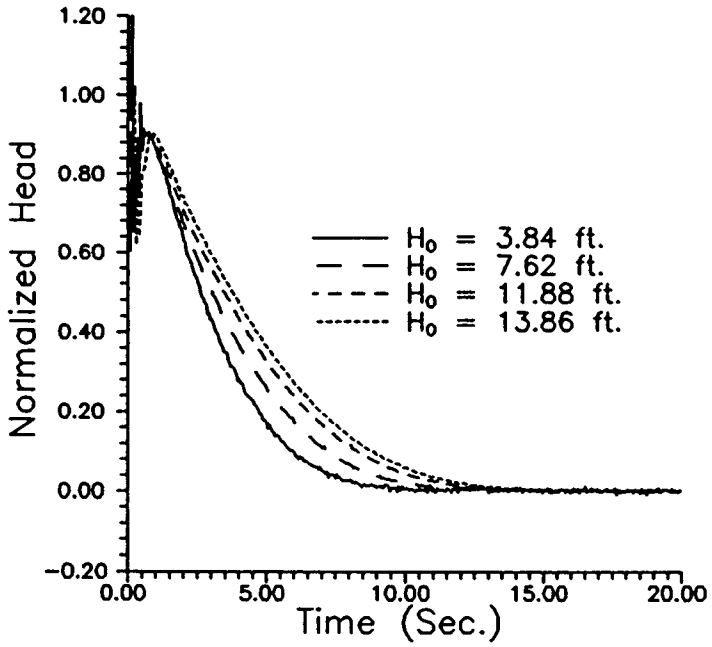

Figure III.B.1 - Normalized head versus time plot for GEMS well 02.

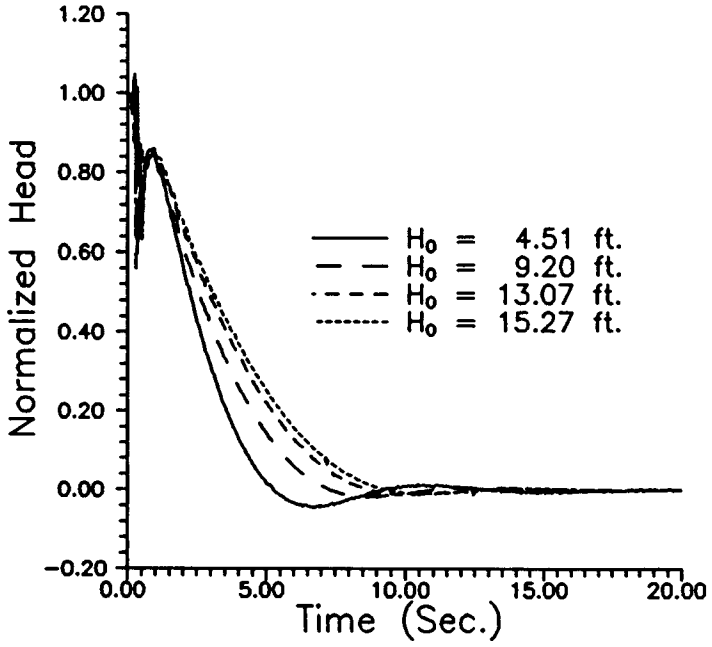

Figure III.B.2 - Normalized head versus time plot for GEMS well 07.

Figure III.B.3. Schematic of the Slug Test Wellbore

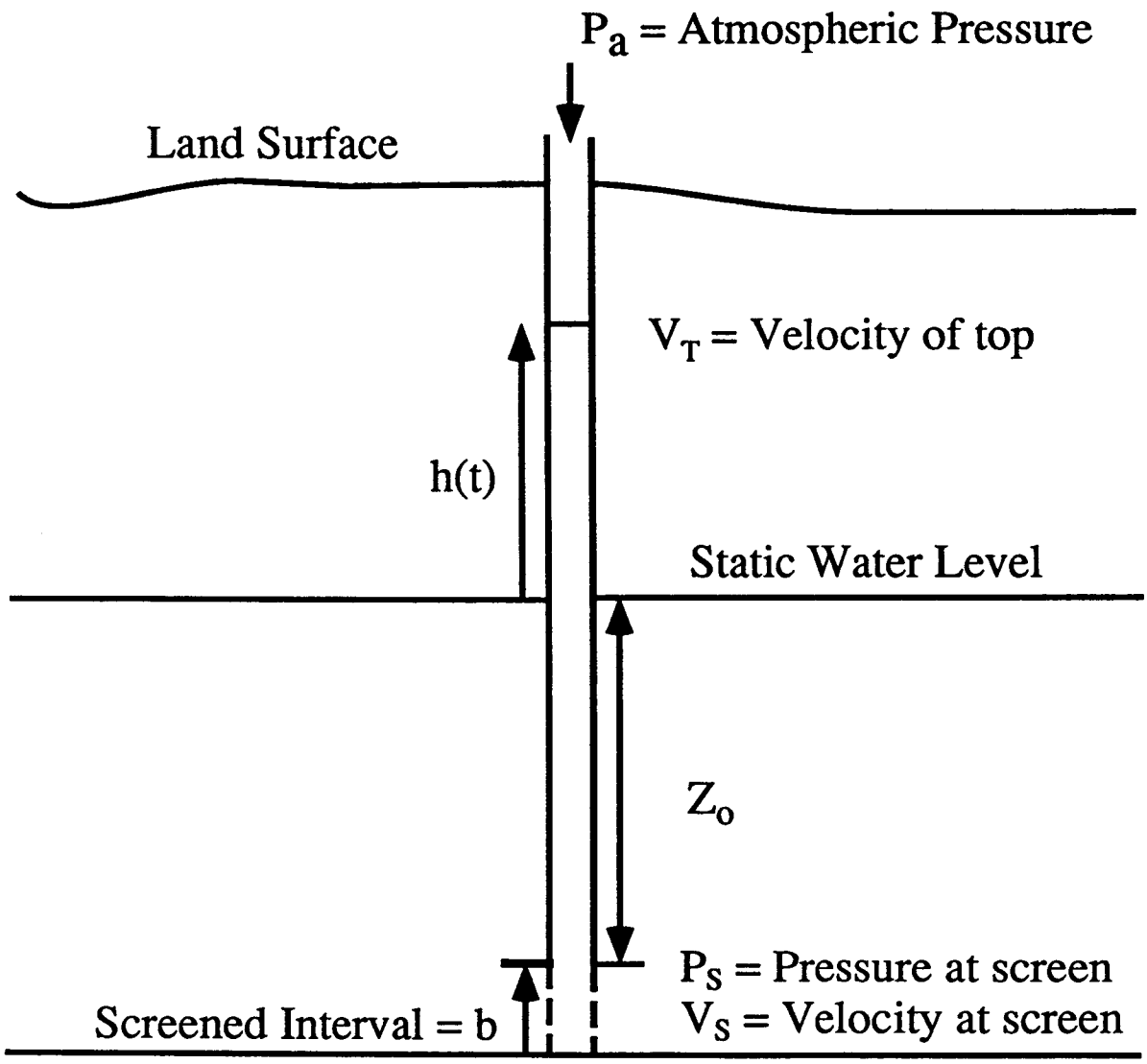

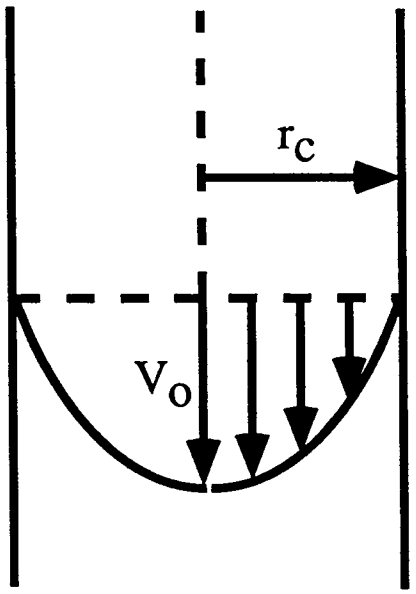

Figure III.B.4. Assumed Radial Velocity Distribution

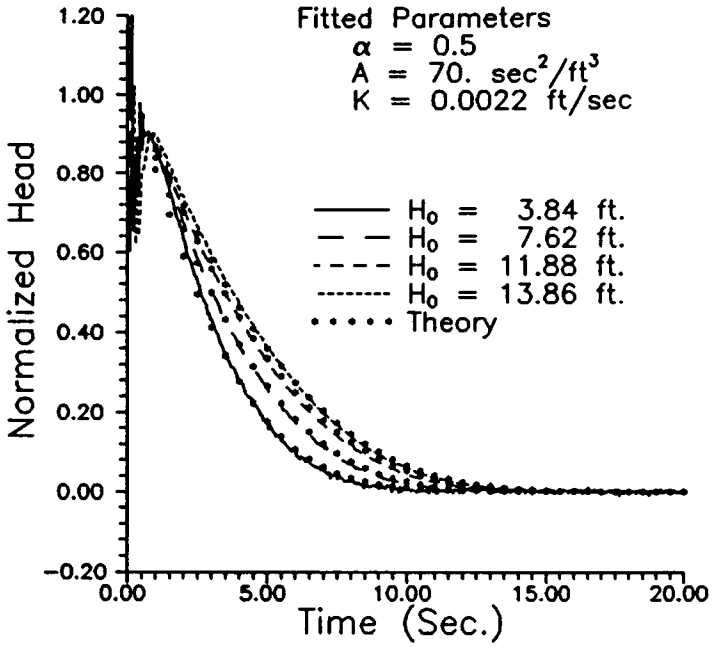

Figure III.B.5 - Normalized head versus time plot and the best-fit nonlinear model for a series of slug tests at GEMS well 02.

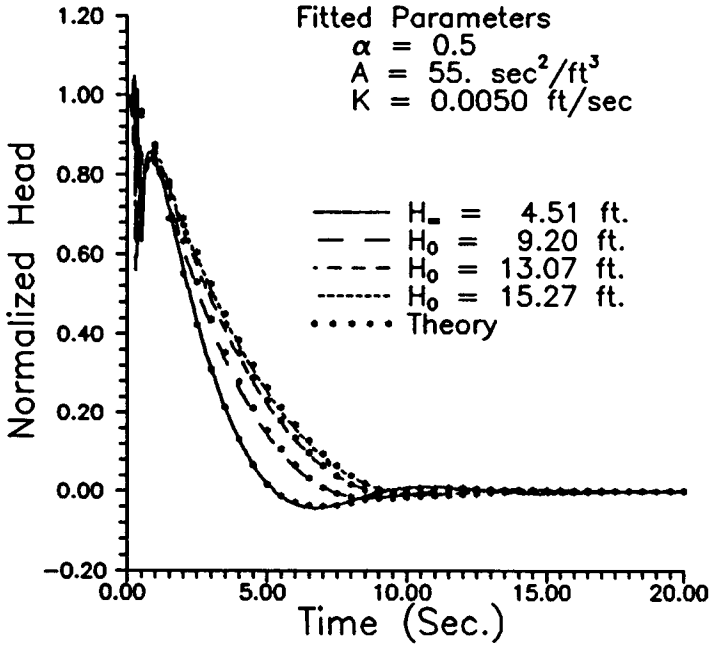

Figure III.B.6 - Normalized head versus time plot and the best-fit nonlinear model for a series of slug tests at GEMS well 07.

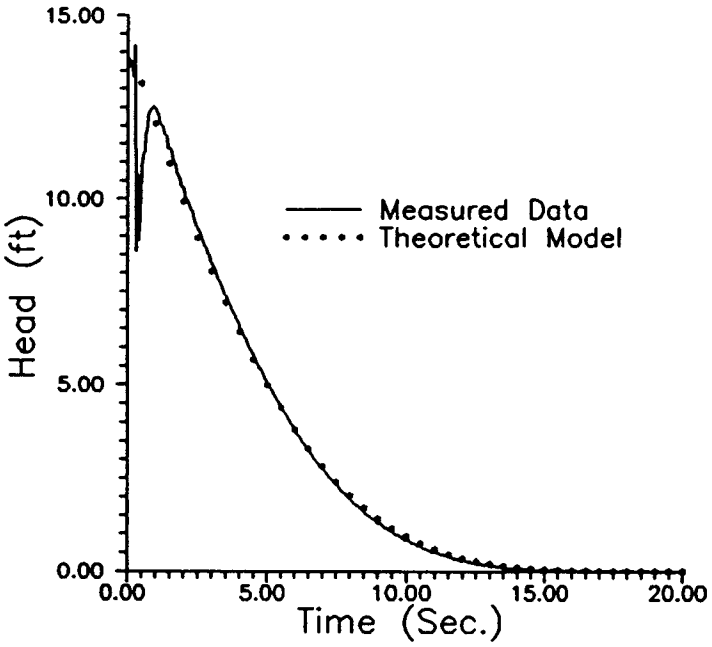

Figure III.B.7 - Head versus time plot and the best-fit nonlinear model for a single slug test at GEMS well 02 (fitted parameters as in Figure III.B.5).

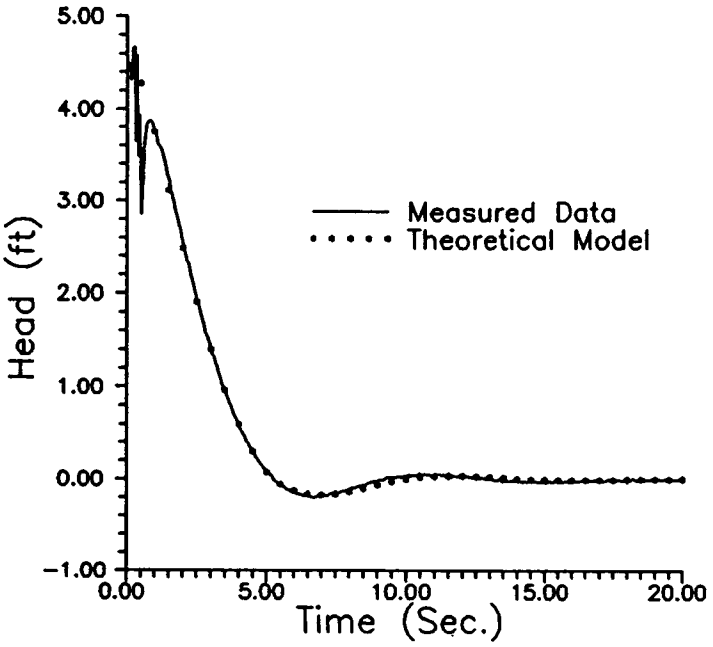

Figure III.B.8 - Head versus time plot and the best-fit nonlinear model for a single slug test at GEMS well 07 (fitted parameters as in Figure III.B.6).

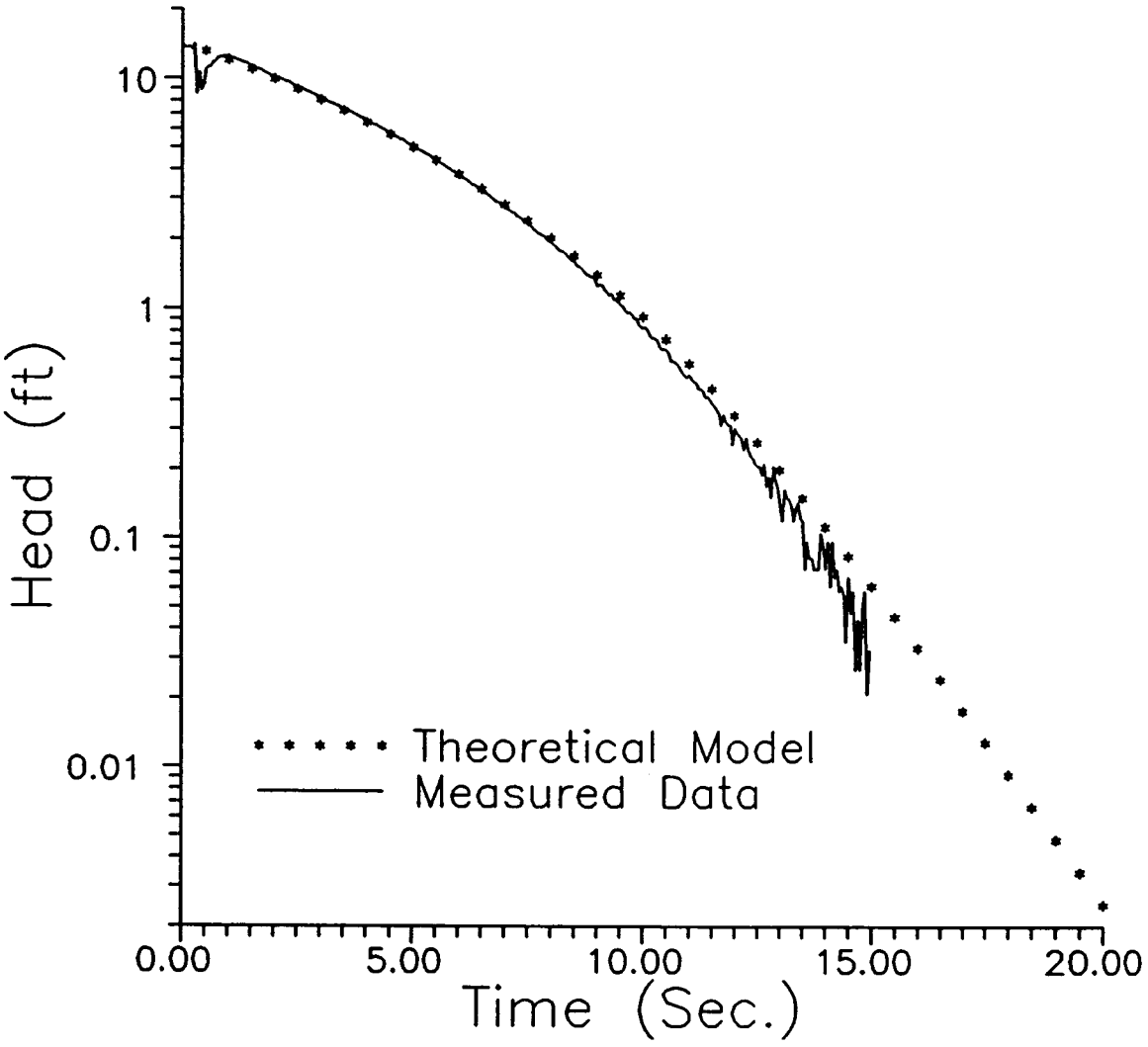

Figure III.B.9 - Semilog head versus time plot and the best-fit nonlinear model for a single slug test at GEMS well 02 (fitted parameters as in Figure III.B.5).

IV. SITE CHARACTERIZATION ACTIVITIES

A. DRILLING AND SAMPLING ACTIVITIES

Introduction

Prior to the work period covered by this report, thirty five wells had been installed at GEMS. Samples from the sand and gravel interval (10.7-21.3 meters below land surface) were taken at ten of these wells using various techniques (McElwee et al., 1991). A modified Waterloo sampler (Zapico, 1987; Zapico et al., 1987) was employed with good success when drilling mud was used in the auger flights to control heaving sands and to help prevent the sediment from falling out the bottom of the sampler. The use of drilling muds, however, has disadvantages (potential to contaminate the formation and the cores) and recovery without sample loss is difficult since the recovery procedure is very sensitive to vibration and other mechanical forces. Without the use of drilling muds, the modified Waterloo sampler performed unsatisfactorily due to a large percentage of the sediment falling out the bottom of the sampler. In order to address this limitation, new sampler designs were developed and field tested in the first year of this project (Butler and McElwee, 1992). The most promising design did not require drilling mud, achieved a very high recovery percentage, and was not very sensitive to vibration and other mechanical forces during recovery. In addition to the piston used in the Waterloo sampler, the new design incorporates an inflatable bladder, located in the drive shoe, which closes off the end of the sampler (McElwee et al., 1991). In the initial phase of the sampling, the rubber bladder lies deflated behind a plastic sample liner as the core enters the sampler. Near the end of the 1.52 meter sample drive, an extension at the upper end of the piston triggers a release mechanism and allows a .102 meter retraction of the plastic liner, resulting in the bladder being in direct contact with the sediment. The bladder is then inflated from the surface with nitrogen gas, closing off the bottom of the sampler and allowing recovery with minimal opportunity for sediment to fall out. After recovery, the cores are taken to the laboratory for storage until measurement of hydraulic conductivity, porosity, density, and particle-size fraction, which is described in subsection IV.B, can be done.

Drilling and Sampling Procedures

All except one of the monitoring wells at GEMS have been installed with hollow-stem auger techniques (Hackett, 1987). Auger flights with an inside diameter

of 0.083 meters and an outside diameter of 0.168 meters were used in all cases. As noted earlier, the near-surface stratigraphy at GEMS consists of approximately 10.6 meters of clay and silt overlying approximately 10.6 meters of sand and gravel. If samples from the clay and silt interval are desired, a split-spoon sampler with an overshoot mechanism for attachment inside the auger flights is used. The split-spoon samplers are 0.61 meters in length and must be retrieved after every 0.61 meters of drilling. Retrieval is done using a wire line on the drill rig.

Although we have taken continuous samples through the clay and silt interval at four well locations scattered over the site, our primary interest at GEMS is in the sand and gravel interval. One of the biggest problems faced in obtaining samples from the sand and gravel interval is heaving sands or sandblows (Minning, 1982; Perry and Hart, 1985; Keely and Boateng, 1987; and Hackett, 1987). It is absolutely essential to maintain greater hydrostatic pressure inside the auger flights than in the formation when working in heaving sands. The water level inside the auger flights is maintained higher than the ambient water level by adding water at critical times (i.e. any time when tools are moved within the open flights or the open flights themselves are moved). If a greater hydrostatic head is not maintained within the auger flights at these critical times, up to one or more meters of sediment may quickly enter the flights, making it impossible to obtain an undisturbed sample at that depth. Adding water to maintain a higher head in the flights may affect the chemistry and biota of an aquifer, so one must balance this concern with the need to control heaving sands. At GEMS, we simply pump water from a nearby well in the sand and gravel interval into the flights. There is no known contamination at GEMS, so we are adding water of a similar composition to the flights. This procedure seems appropriate for our purposes.

Samples are obtained from the sand and gravel interval using the sampler described earlier (McElwee et al., 1991). If samples are not taken in the overlying clay and silt interval, we first drill down to approximately 10.7 meters. The pilot bit is withdrawn via a wireline and the sampler emplaced at the bottom of the flights. The sampler is then driven 1.52 meters in advance of the flights. The sampler is retrieved using drill rods or a wireline, after which the pilot bit is reinserted and the augers advanced to the depth for the next sample. Note that due to the close fit of the pilot bit and the sampler in the interior of the flights, there is great potential to induce heaving sands during removal of the pilot bit and retrieval of the sampler. Special care must be taken to add water to the flights during these procedures.

If no samples are to be obtained during drilling, a knock-out plate is installed

in the auger head in place of a pilot bit (Perry and Hart, 1985; Hackett, 1987). The plate is left in place until the completion depth is achieved. At that point, the plate is knocked out of the bottom of the flights using the casing string. The plate is then left in the formation below the well. Stainless steel, PVC, and aluminum knock-out plates have been used at GEMS. Note that water must be added to the flights when the plate is knocked out in order to prevent movement of sediment into the interior of the flights and possible binding of the casing string in the flights.

Drilling and Sampling - Year Two

During the second year of this project, six additional wells were drilled and completed. Four of these wells were cored from the surface to the bedrock using the techniques outlined above. The split-spoon sampler was used for approximately the first 10.7 meters and then the bladder sampler was used until bedrock was reached at approximately 21.3 meters below land surface.

These six additional wells bring the total number of wells at GEMS to forty one. Table IV.A.1 is a summary of pertinent information about the GEMS wells. Figure IV.A.1 is a map of the GEMS area showing the location of all the wells. The elevation data given in Table IV.A.1 were obtained through a cooperative surveying exercise with the 1st Battalion of the 127th Field Artillery of the Kansas National Guard performed in March of 1992 supplemented by later work by KGS personnel with recently purchased surveying equipment. Note that a reference point was established at a central location on the site during the cooperative exercise. This reference point was used in the following surveys at the site. The elevation as well as the longitude and latitude of the reference point are given in Table IV.A.1.

The samples of silt and clay obtained from the first 10.7 meters using the split-spoon sampler were examined visually and detailed written logs of the visible features were prepared. Although no additional work was done with these samples, in the third year of this project we plan to analyze the cores from this interval for hydraulic conductivity while they are still saturated. We have purchased a permeameter for use with low-conductivity samples (S-480 Permeability Cell and Pressure Control Panel, Brainard-Kilman Co.) and are preparing it for the analysis of these cores.

The bladder sampler was used to collect samples of the sand and gravel interval beginning at approximately 10.7 meters below land surface. Table IV.A.2 summarizes the sample recovery for all holes drilled in the reporting period (5-1, 7-1, 9-1, and 11-1). Other data about these wells can be found in Table IV.A.1. The

overall recovery was about 72%, which is 13% lower than expected. The lower than expected recovery obtained at these wells was due to a number of factors. In several instances, we had problems with large rock fragments blocking the sampler throat. Mechanical problems also plagued us this year. Several times the retraction mechanism failed so that the bladder could not be inflated. In one instance, this resulted in the complete loss of the sample (sample #1 of well 7-1). Since the sampler takes a great deal of punishment while being driven by an air jackhammer, we must expect some mechanical failures.

Two additional wells (0-7 and 0-8) were also drilled during the second year of this project. These wells, both of which are 0.102 m in diameter, were drilled using recently purchased large diameter auger flights (inner diameter 0.165 m, outer diameter 0.254 m). Larger diameter wells were needed so that larger pumps could be used and the aquifer could be stressed more than is currently possible with a pump in a 0.051 m diameter well. These wells should prove invaluable in the pulse testing work of the third year of this project, allowing a larger volume per unit time to be pumped. Note that one of these wells (0-8) is screened with continuous wire-wrap PVC screen, while the other employs standard slotted PVC screen. As part of this work, we also hope to examine the effect of screen type on well testing results.

Table IV.A.1

Well Data

Well Number	Elevation (m)	Depth (m)	Screen Length (m)
00-1	252.724	17.04	0.76
00-2	252.780	14.41	0.76
00-3	252.670	21.37	NA
00-4	252.667	11.18	NA
00-5	252.021	9.74	NA
00-6	252.746	12.91	NA
00-7	252.734	20.34	NA
0-1	252.796	21.74	9.14
0-2	252.756	14.08	0.70
0-3	252.787	11.00	0.74
0-4	252.707	7.94	0.76
0-5	252.793	19.84	0.70
*0-6	252.945	24.66	1.52
**0-7	252.743	16.57	0.70
**0-8	252.827	15.33	0.76
1-1	252.799	14.26	0.76
1-2	252.714	11.22	0.61
1-3	252.814	8.55	0.65
1-4	252.796	6.15	1.45
1-5	252.791	20.33	9.14
1-6	252.899	17.06	0.73
1-7	252.735	21.42	9.14
2-1	252.791	11.92	0.57

2-2	252.785	14.72	0.56
2-3	252.784	8.53	0.63
2-4	252.779	6.04	1.41
2-5	252.791	21.42	9.14
2-6	252.735	20.24	9.14
2-7	252.728	17.17	0.79
4-1	252.724	21.58	9.14
5-1	252.949	21.54	9.14
6-1	252.753	20.34	0.77
6-2	252.754	21.55	11.55
7-1	253.452	17.74	9.14
8-1	252.703	17.44	NA
9-1	252.639	20.93	13.26
10-1	252.566	17.32	NA
11-1	253.412	19.63	13.72
A1	252.511	9.91	0.76
A2	252.931	7.86	0.61
+PW	NA	21.84	6.10

KGS Reference Mark: Latitude-North 39°00' 55.628" Longitude-West 95°12' 21.272" Elevation 252.242 m

* Well diameter is 0.127 m; unmarked wells are 0.051 m in diameter.
** Well diameter is 0.102 m; unmarked wells are 0.051 m in diameter.
\+ High capacity pumping well, screen and casing is 0.254 m in diameter, drop pipe is 0.102 m in diameter.
NA - information not currently available.

Table IV.A.2

Sample Recovery Analysis

Well Number	Sample Number	Sample Length (m)	Head Space (m)	% of Sample Length
5-1	1	1.524	0.088	5.8
5-1	2	1.524	0.137	9.0
5-1	3	1.524	0.076	5.0
5-1	4	1.524	0.107	7.0
5-1	5	1.524	0.171	11.2
5-1	6	1.524	0.472	31.0
5-1	7	1.384	0.165	12.0
5-1 Totals		10.528	1.216	11.6
		Theoretical Recovery		88.4
		Bladder Loss		10.0
		Actual Recovery		78.4
7-1	1*	1.524	1.372	90.0
7-1	2	1.524	0.162	10.6
7-1	3	1.524	0.238	15.6
7-1	4	1.524	0.311	20.4
7-1	5	1.524	0.229	15.0
7-1	6	1.524	0.305	20.0
7-1	7	0.914	0.165	18.0
7-1 Totals		10.058	2.774	27.6
		Theoretical Recovery		72.4
		Bladder Loss		10.0
		Actual Recovery		62.4
9-1	1	1.524	0.107	7.0
9-1	2	1.524	0.083	5.4

9-1	3	1.448*	0.509	35.2
9-1	4	1.524	0.088	5.8
9-1	5	1.472*	0.149	10.1
9-1	6	1.524	0.232	15.2
9-1	7	1.308	0.408	31.2
9-1 Totals		10.324	1.576	15.3
		Theoretical Recovery		84.7
		Bladder Loss		10.0
		Actual Recovery		74.7
11-1	1	1.524	0.579	38.0
11-1	2	1.524	0.134	8.8
11-1	3	1.524	0.125	8.2
11-1	4	1.524	0.235	15.4
11-1	5	1.524	0.210	13.8
11-1	6	1.524	0.552	36.2
11-1	7	1.021	0.189	18.5
11-1 Totals		10.165	2.024	19.9
		Theoretical Recovery		80.1
		Bladder Loss		10.0
		Actual Recovery		70.1
Well Totals		41.075	7.590	18.5
		Theoretical Recovery		81.5
		Bladder Loss		10.0
		Actual Recovery		71.5

The procedure used in obtaining all samples was a pneumatic jackhammer technique.

* Mechanical failure produced some anomalous results.

Bladder Loss - 10% of the total sample length, 4.109 m, is lost due to the bladder mounting dimensions.

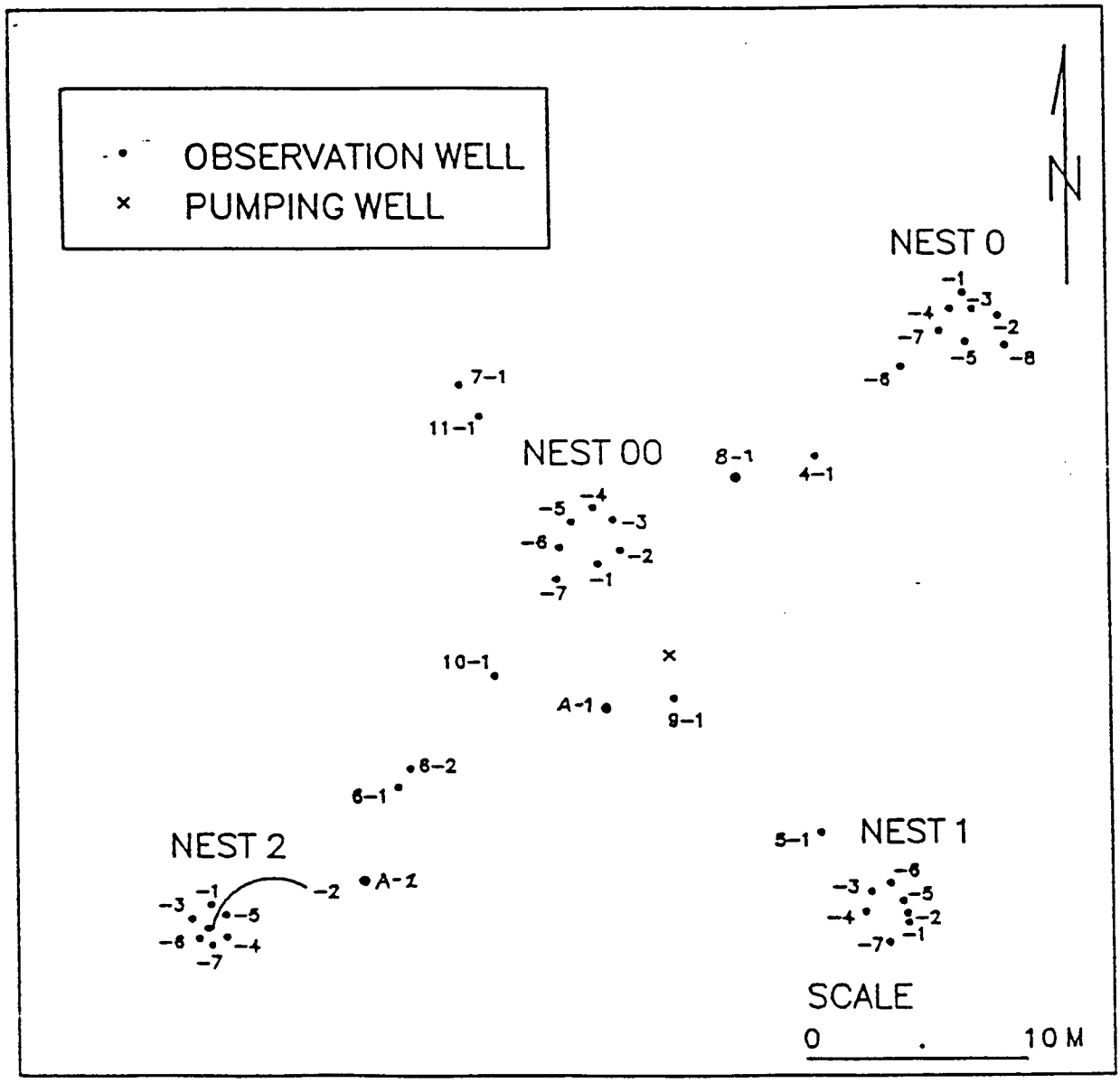

Figure IV.A.1 - Map of wells at GEMS.

B. LABORATORY ACTIVITIES

Laboratory Procedures and Methods

The cores recovered from the drilling and sampling summarized in the previous section of this report were taken to the laboratory for measurement of core properties. The procedures and methods used in analyzing the core samples are essentially the same as those described in the report of the first year of this project (Butler and McElwee, 1992) with the exception of the changes noted below.

Most parts of the permeameter that had been composed of opaque PVC have been replaced with clear PVC in order to more easily assess flow of water, transport of fine sediment, and entrapment of air bubbles within the system.

The hydraulic conductivity of some of the cores is too low to be determined using the constant-head permeameter in any reasonable time frame. In order to determine the hydraulic conductivity of these cores, a permeameter designed for the analysis of low-conductivity cores, the Brainard-Kilman S-480 Permeability Cell, has been purchased. This system is currently being prepared for use in the analysis of cores from GEMS.

As noted in the report of the first year of this project, the decrease in hydraulic conductivity with time that was observed for many of the cores could be a result of the deposition of calcite in pore throats. Another possible explanation would be the expansion and/or dispersion of clays, which would also produce a clogging of pore throats. In an attempt to identify the primary mechanism responsible for the observed decreases in conductivity with time, a series of experiments was conducted using a single core in the permeameter. The chemistry of the water prior to passage through the core and after passage through the core was carefully monitored with the assistance of the Analytical Services Section of the Kansas Geological Survey.

As described in the report of year one, the water circulated in the permeameter is obtained from wells at GEMS that are screened close to or over the same interval from which the core was taken. At the same time water was collected for use in the permeameter experiments, samples were taken in the field for analysis by the Analytical Services Section. The collected water was then transported to the laboratory where it was allowed to sit for two weeks in order to equilibrate with laboratory temperatures and pressures. Additional water samples were taken during this period in order to assess changes occurring with equilibration to laboratory conditions. Once the water was placed in the permeameter, samples were taken several times a day from the water that

had passed through the core and once a day from the permeameter water that had not passed through the core. A subset of these samples was chosen for major cation analysis by the Analytical Services Section using observed changes in hydraulic conductivity as the selection criterion. Note that the permeameter setup used here involves recirculating the water that has passed through the cores. For these experiments, however, no recirculation was allowed so that any chemistry changes occurring in the water passing through a core could be readily identified and not be masked by mixing.

In addition to the major cation analyses performed by the Analytical Services Section, the pH and dissolved oxygen of the water prior to passage through the core (henceforth designated as permeameter water) and after passage through the core (henceforth designated as outflow-tube water) were monitored in the laboratory. The pH was determined using a CARDY Twin pH meter (Horiba Instruments). Measurement of the pH of the outflow-tube water was done several times a day, while measurement of the pH of the permeameter water was done at least once a day. Dissolved oxygen (DO) was measured using a K-7512 CHEMets colorimetric kit (CHEMetrics). DO was determined for outflow-tube water once a day and once every 3 to 4 days for the permeameter water.

Sediment samples from the cores used in these experiments were collected for x-ray analysis of clay mineralogy both before and after being processed in the permeameter.

As a result of the findings of the water chemistry and clay analysis, two further modifications have been made to the laboratory procedure: 1) carbon dioxide gas is being bubbled into the water of the upper reservoir to maintain the pH, which is monitored daily, at a level comparable to that of the water at GEMS; and 2) a different biocide (dichlorophene) is being used to inhibit biologic growth in the system.

Results and Discussion

Core Analyses

Graphs of the original and repacked hydraulic conductivities and porosities, the percent fines (<53 microns), and the mean grain size of core segments from wells 1-7, 5-1, 7-1, and 9-1 are presented in Figures IV.B.1 - IV.B.28. The hydraulic conductivities and porosities for original and repacked core segments from GEMS well 11-1 are presented in Figures IV.B.29 - IV.B.33. The grain size statistics for that well will be given in the report of the third year of this project.

GEMS 1-7

Well 1-7 shows some overlap between the top two samples where an interval was resampled during core recovery.

The undisturbed (original) cores of well 1-7 have an arithmetic mean conductivity of 16.43 m/day, with a sample standard deviation of 20.47 m/day (Figure IV.B.1). Values range from a minimum of 0.83 m/day to a maximum of 129.03 m/day. There is a general increase in hydraulic conductivity with depth.

The repacked cores exhibit a higher mean conductivity and greater variability than the undisturbed cores (Figure IV.B.2). Values range from 0.39 m/day to 171.28 m/day with a mean of 58.26 m/day and a standard deviation of 38.11 m/day. For 52 of the 54 processed segments, the repacked hydraulic conductivity is greater than the original measurement (Figure IV.B.3). Possible explanations for this were discussed in the first year report.

Porosity values were calculated for both the original and repacked cores from the particle density, bulk density and core volume. The original cores from well 1-7 have porosities ranging from 23.1% to 33.1% with an arithmetic mean of 28.2% and a standard deviation of 2.0% (Figure IV.B.4). The porosity of the repacked cores ranges from 23.2% to 32.5% with an arithmetic mean of 28.6% and a standard deviation of 2.1% (Figure IV.B.5).

The differences between the original and repacked porosities for well 1-7 range from 0.00% to 5.07% with an arithmetic mean of 0.98%. For 36 of the 54 processed cores, the repacked porosity is greater than the original porosity; 17 of the repacked cores have lower porosities than the original cores and one core has identical original and repacked porosities. The primary reasons for differences between the original and repacked porosities are 1) inability to repack the cores to exactly the same volume as the original cores, and 2) loss of sediment during the repacking process.

The percent fines (<53 microns) was also calculated for the core segments. The percent fines for well 1-7 ranges from 0.01% to 20.3% with an arithmetic mean of 2.1% and a standard deviation of 3.7% (Figure IV.B.6). The mean phi grain size was calculated using the method of moments. The phi sizes for well 1-7 range from -1.19 to 2.24 with an arithmetic mean of -0.05 and a standard deviation of 0.69 (Figure IV.B.7).

GEMS 5-1

Well 5-1 shows some overlap between the top two samples where an interval was resampled during core recovery.

The undisturbed cores of well 5-1 have an arithmetic mean hydraulic conductivity

of 16.88 m/day, with a sample standard deviation of 15.41 m/day (Figure IV.B.8). Values range from a minimum of 0.12 m/day to a maximum of 65.32 m/day. There is no apparent trend in hydraulic conductivity with depth.

As was observed for well 1-7, the repacked cores of well 5-1 have a higher mean conductivity and greater variability than the undisturbed cores (Figure IV.B.9). Values range from 4.97 m/day to 159.61 m/day with a mean of 44.01 m/day and a standard deviation of 36.59 m/day. For 52 of the 55 processed segments, the repacked hydraulic conductivity is greater than the original measurement (Figure IV.B.10). Sample #4, segment #5 (15.99-16.14 m) was not repacked because it had a very low original permeability and will be processed when the Brainard-Kilman permeability cell is operational.

The original cores have porosities ranging from 20.6% to 32.7% with an arithmetic mean of 26.8% and a standard deviation of 2.3% (Figure IV.B.11). The porosity of the repacked cores ranges from 22.2% to 36.2% with an arithmetic mean of 27.5% and a standard deviation of 2.4% (Figure IV.B.12).

The differences between the original and repacked porosities range from 0.01% to 5.36% with an arithmetic mean of 1.2%. For 37 of the 55 processed cores, the repacked porosity is greater than the original porosity; 18 of the repacked cores have lower porosities than the original cores.

The percent fines for the segments from well 5-1 ranges from 0.1% to 8.6% with an arithmetic mean of 1.9% and a standard deviation of 1.9% (Figure IV.B.13). The phi sizes for well 5-1 range from -1.05 to 2.44 with an arithmetic mean of 0.19 and a standard deviation of 0.76 (Figure IV.B.14). Grain size data for sample #1, segment #4 (11.51-11.69 m) are not available because some of the sediment was lost during sieving. Grain size and porosity data for sample #4, segment #5 (15.99-16.14 m) have not been collected since the segment is being saved to be processed in the low permeability cell.

GEMS 7-1

Sample #1 was not recovered due to the sampler malfunctioning.

The undisturbed cores of well 7-1 (not including the cores through which no water flowed) have an arithmetic mean hydraulic conductivity of 32.38 m/day, with a sample standard deviation of 48.85 m/day (Figure IV.B.15). Values range from a minimum of 0.28 m/day to a maximum of 261.78 m/day. There is no apparent trend in hydraulic conductivity with depth. There was no flow through three segments from this well: sample #6, segments #1, #4, and #5 (18.41-18.56 m, 18.86-19.01 m and 19.01-19.17 m).

The repacked cores of well 7-1 have a higher mean conductivity but less

variability than the undisturbed cores (Figure IV.B.16). Values range from 0.18 m/day to 153.65 m/day with a mean of 39.91 m/day and a standard deviation of 36.94 m/day. For 27 of the 35 processed segments, the repacked hydraulic conductivity is greater than the original measurement (Figure IV.B.17). Sample #5, segment #7 (17.93-18.09 m) and the three cores mentioned in the preceding paragraph were not repacked because of their very low original permeability. They will be processed when the Brainard-Kilman permeability cell is operational.

The original cores have porosities ranging from 19.8% to 36.4% with an arithmetic mean of 25.8% and a standard deviation of 3.4% (Figure IV.B.18). The porosity of the repacked cores ranges from 20.2% to 36.0% with an arithmetic mean of 26.5% and a standard deviation of 3.3% (Figure IV.B.19).

The differences between the original and repacked porosities range from 0.01% to 2.83% with an arithmetic mean of 0.87%. For 25 of the 35 processed cores, the repacked porosity is greater than the original porosity; 10 of the repacked cores have lower porosities than the original cores.

The percent fines for well 7-1 ranges from 0.4% to 20.28% with an arithmetic mean of 3.3% and a standard deviation of 4.1% (Figure IV.B.20). The phi sizes for well 7-1 range from -0.73 to 0.98 with an arithmetic mean of 0.02 and a standard deviation of 0.45 (Figure IV.B.21). Grain size data are not available for segments that have not yet been repacked.

GEMS 9-1

The undisturbed cores of well 9-1 have an arithmetic mean hydraulic conductivity of 27.19 m/day, with a sample standard deviation of 32.59 m/day (Figure IV.B.22). Values range from a minimum of 0.19 m/day to a maximum of 134.73 m/day.

The repacked cores of well 9-1 have a higher mean conductivity and greater variability than the undisturbed cores (Figure IV.B.23). Values range from 0.16 m/day to 233.27 m/day with a mean of 49.19 m/day and a standard deviation of 43.36 m/day. For 44 of the 47 processed segments, the repacked hydraulic conductivity is greater than the original measurement (Figure IV.B.24). Sample #1, segment #1 was not repacked because it was used for x-ray analysis of clay mineralogy.

The original cores have porosities ranging from 21.3% to 36.3% with an arithmetic mean of 26.4% and a standard deviation of 2.8% (Figure IV.B.25). The porosity of the repacked cores ranges from 21.5% to 37.2% with an arithmetic mean of 27.6% and a standard deviation of 3.0% (Figure IV.B.26).

The differences between the original and repacked porosities range from 0.05%

to 4.74% with an arithmetic mean of 1.51%. For 35 of the 47 processed cores, the repacked porosity is greater than the original porosity; 12 of the repacked cores have lower porosities than the original cores.

The percent fines for the segments from well 9-1 ranges from 0.2% to 33.43% with an arithmetic mean of 2.7% and a standard deviation of 5.9% (Figure IV.B.27). The phi sizes for well 9-1 range from -1.05 to 2.07 with an arithmetic mean of 0.19 and a standard deviation of 0.69 (Figure IV.B.28). Grain size and porosity data for sample #1 segment #1 (10.81-10.98 m) are not available because the core was used for x-ray analysis of clay mineralogy. Grain size data for sample #2, segment #3 are not included in the calculations since an error was made in the sieve analysis.

GEMS 11-1

The undisturbed cores of well 11-1 have an arithmetic mean hydraulic conductivity of 29.6 m/day, with a sample standard deviation of 32.51 m/day (Figure IV.B.29). Values range from a minimum of 0.41 m/day to a maximum of 118.57 m/day. Hydraulic conductivity values were not obtained for sample #1, segments #1, #2 and #5 (10.92-11.07, 11.07-11.19 and 11.47-11.61 m); sample #5, segment #6 (17.66-17.81 m); and sample #6, segment #1 (18.50-18.64 m), as there was no flow through these cores under the head gradient produced in the permeameter.

The repacked cores of well 11-1 have a higher mean conductivity and greater variability than the undisturbed cores (Figure IV.B.30). Values range from 1.20 m/day to 166.72 m/day with a mean of 63.93 m/day and a standard deviation of 45.26 m/day. For 30 of 36 processed segments, the repacked hydraulic conductivity is greater than the original measurement (Figure IV.B.31). The samples mentioned in the preceding paragraph, as well as sample #6, segments #5 and #6, were not repacked and have been set aside to process in the low permeability cell. Sample #3, segment #3 and sample #5, segments #3 and #8 were not repacked because they were used for x-ray analysis of clay mineralogy. The repack information from sample #3, segment #4; sample #4 segments #1, #4 and #7; sample #5, segment #4; and sample #7, segment #3 were not included in the graphs and statistics, since a mistake was made when the method of securing the cores in the permeameter was modified, and the sediment from these cores was repacked to a length approximately 1 to 2 cm longer than the original cores.

The original cores have porosities ranging from 22.2% to 33.0% with an arithmetic mean of 26.4% and a standard deviation of 2.7% (Figure IV.B.32). The porosity of the repacked cores ranges from 21.2% to 31.7% with an arithmetic mean of 26.8% and a standard deviation of 3.7% (Figure IV.B.33).

The differences between the original and repacked porosities range from 0.09% to 2.03% with an arithmetic mean of 1.06%. For 20 of the 29 cores considered, the repacked porosity is greater than the original porosity; 9 of the repacked cores have lower porosities than the original cores.

Grain size data for well 11-1 are still being analyzed.

Chemistry Analyses

The pH of GEMS water measured in the field is approximately 7. Monitoring of the pH of water collected for use in the permeameter did not reveal any trend with time while equilibrating to laboratory conditions over a 19 day period. After the water was introduced into the permeameter, the pH rose fairly rapidly to approximately 8 and fluctuated between 8 and 9 while circulating through the permeameter with no apparent trend with time (Figure IV.B.34). There was no significant change in pH after the water had passed through the cores. The measured differences are within the limit of accuracy of the pH meter. The rise in pH when the water started circulating through the permeameter was most likely due to the loss of CO_2. Bubbling CO_2 through the upper reservoir has been successful in maintaining a pH close to 7.

Dissolved oxygen (DO) measurements indicate that the oxygen content of the water increases after the water is placed in the permeameter. Before the water is placed in the permeameter, it has a DO content of 1 to 2 ppm. After the water has been placed in the permeameter, the DO content increases to 5 to 8 ppm. There is no significant change in DO content after the water has passed through a sediment core

Major cation analyses of the water in the permeameter and outflow-tube for the three cores employed in these experiments indicate that the calcium content of the water generally decreases with time (Figure IV.B.35), further demonstrating that precipitation of calcite is occurring within the permeameter apparatus.

The first core placed in the apparatus (GEMS 9-1 sample #1, segment #1) shows a consistently lower calcium content in the outflow-tube water as compared to that in the permeameter (the accuracy of the chemical analysis is better than 1 ppm for calcium). This indicates that calcite is being precipitated in the core and perhaps contributing to a decrease in hydraulic conductivity. The pH rose at the beginning of the period that this core was in the permeameter and the calcium content of the permeameter water remained fairly high.

GEMS 11-1, sample #5, segment #3 was the next core placed in the permeameter. During the period of time that water was flowing through this core the calcium content of the water decreased. No conclusions concerning the relative calcium

content of the outflow tube and permeameter water can be made. Only three analyses of the permeameter water were done, with one having a higher calcium content than the outflow-tube water, one having a lower calcium content, and a third sample (marked by an asterisk) that is probably not representative of the system because circulation had been very slow for some time.

The third core placed in the permeameter for this experiment was GEMS 11-1, sample #3, segment #3. The outflow-tube water from this core had a calcium content consistently higher than that of the permeameter water, suggesting that calcite was being dissolved out of the core. However, the hydraulic conductivity of this core decreased with time, which indicates that deposition of calcite is not the controlling mechanism in reducing hydraulic conductivity during this time period.

X-ray analyses of the clays have determined that the clays are composed primarily of smectite, with some kaolinite and some illite (which is fairly crystalline, bordering on mica). There is no change in the composition of the clays while they are in the permeameter, but there was some deposition of calcite on the clays.

It was noted during preparation of the clays for x-ray analysis, that the clays are easily flocculated and dispersed, and that thymol, which had been used in the system as a biocide, caused the clays to flocculate. This tendency to readily flocculate and disperse could result in the clogging of pore throats and decreases in hydraulic conductivity. Fogler and Vaidya (1993) suggested that if the hydraulic conductivity of a core was reduced due to fines blocking the pore throats, reversing the flow direction through the core should flush out the clogged pore throats and produce an increase in hydraulic conductivity. GEMS 7-1, sample #4, segment #3, which experienced a decrease in hydraulic conductivity, was turned upside down in the permeameter, but no increase in conductivity was observed.

Using a different biocide, dichlorophene, appears to have reduced, but not eliminated, the decreases in hydraulic conductivity with time. Whether this is due to more effective biocidal action in the core (though it appears to be less effective in the permeameter tubing), or due to the fact that the dichlorophene is not reacting with the clays is unclear at this time.

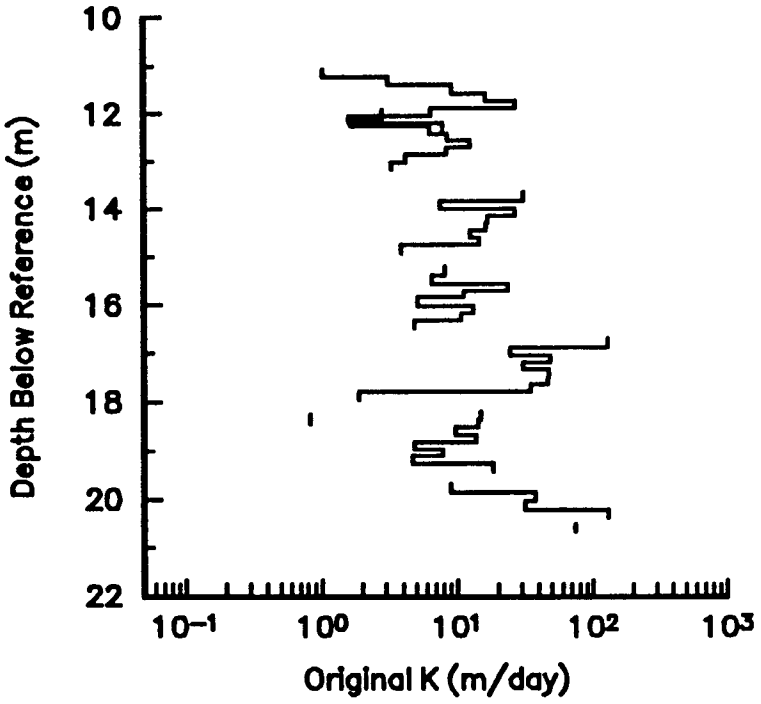

Figure IV.B.1. Original hydraulic conductivity vs. depth for GEMS well 1-7.

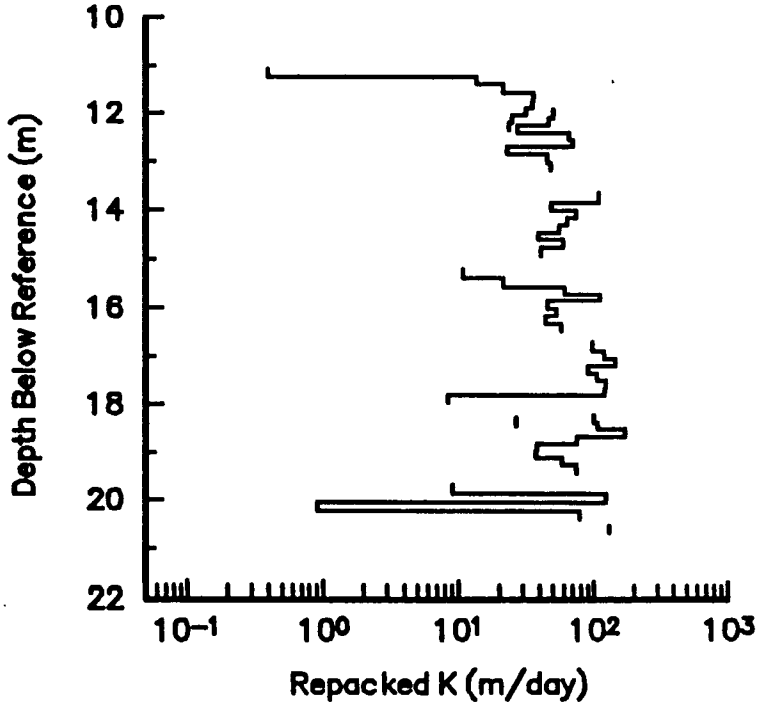

Figure IV.B.2. Repacked hydraulic conductivity vs. depth for GEMS well 1-7.

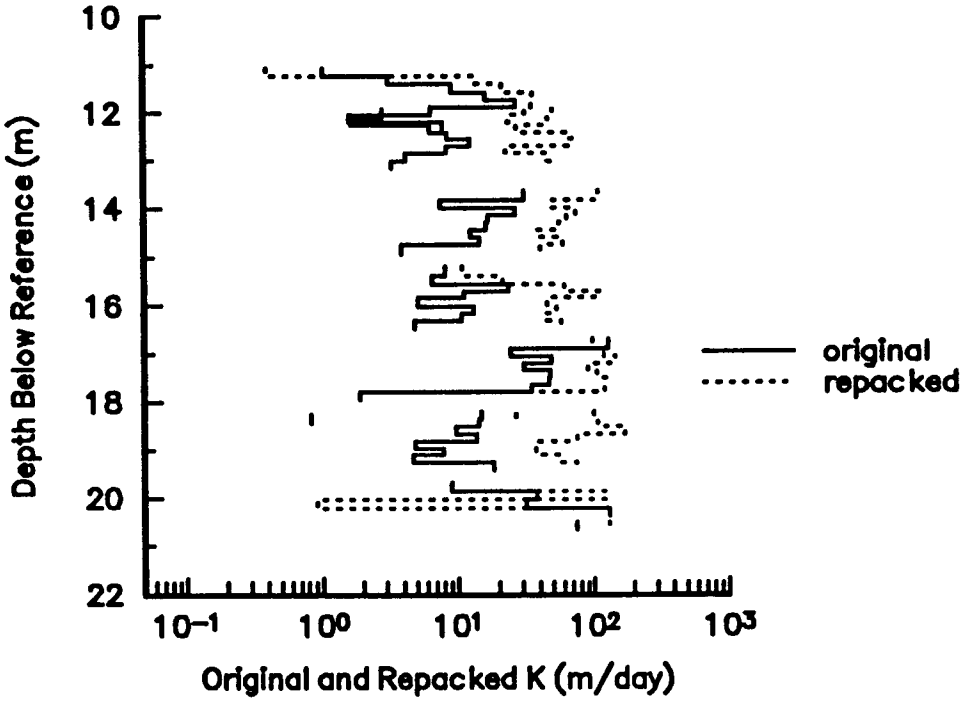

Figure IV.B.3. Original and repacked conductivity vs. depth for GEMS well 1-7.

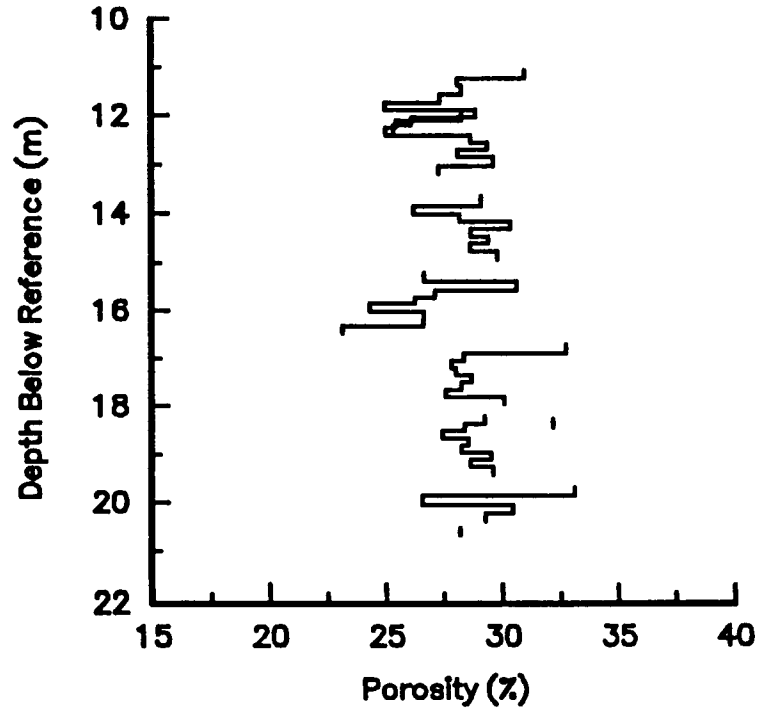

Figure IV.B.4. Original porosity vs. depth for GEMS well 1-7.

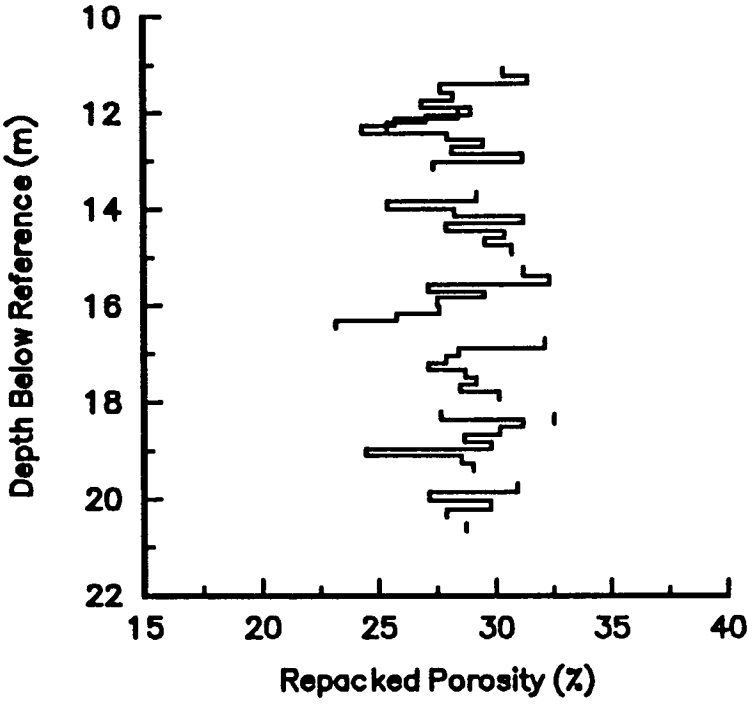

Figure IV.B.5. Repacked porosity vs. depth for GEMS well 1-7.

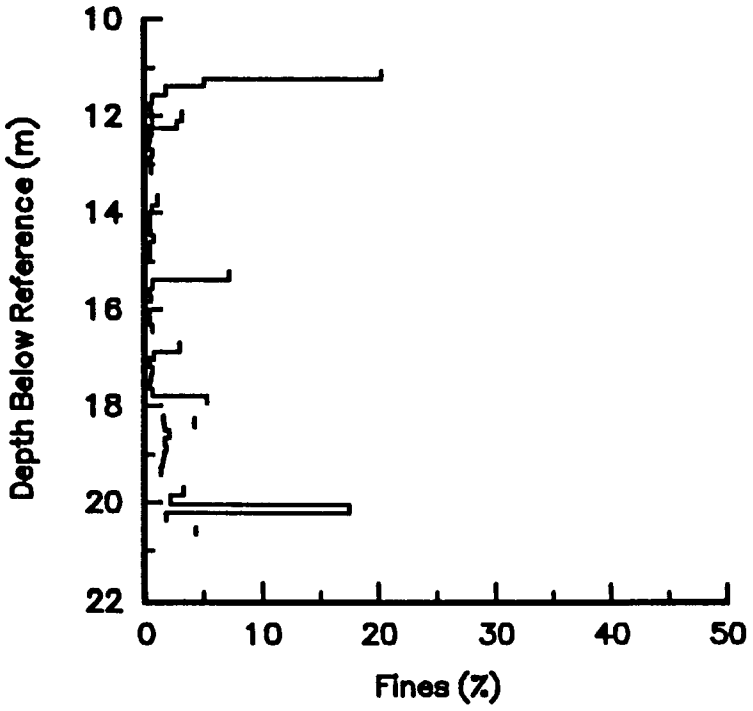

Figure IV.B.6. Percent fines (<.053 mm) vs. depth for GEMS well 1-7.

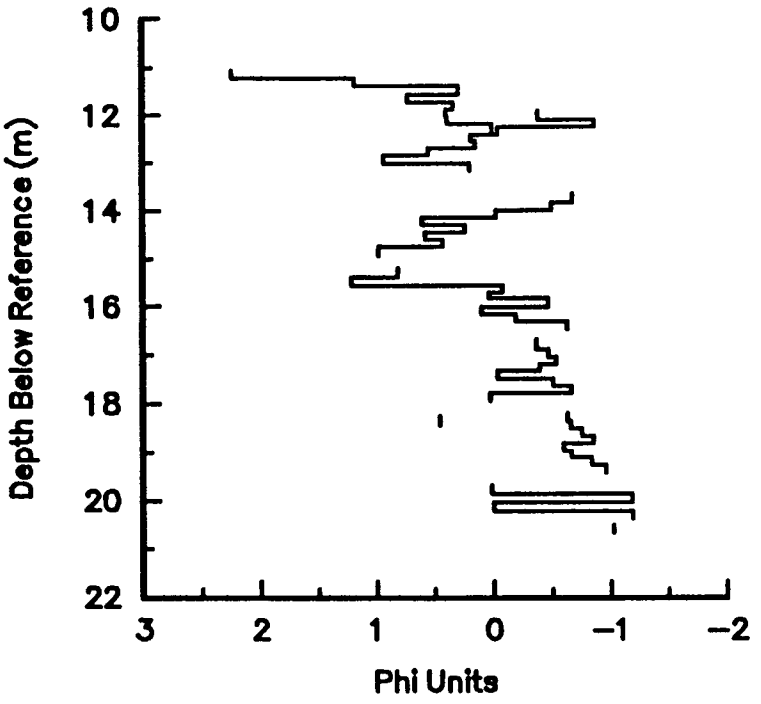

Figure IV.B.7. Mean grain size (in phi units) vs. depth for GEMS well 1-7.

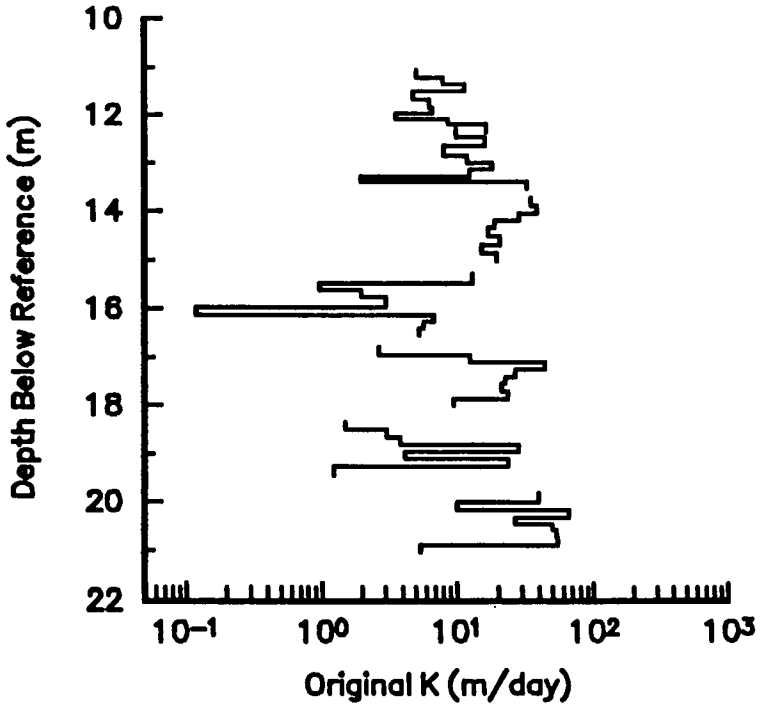

Figure IV.B.8. Original hydraulic conductivity vs. depth for GEMS 5-1.

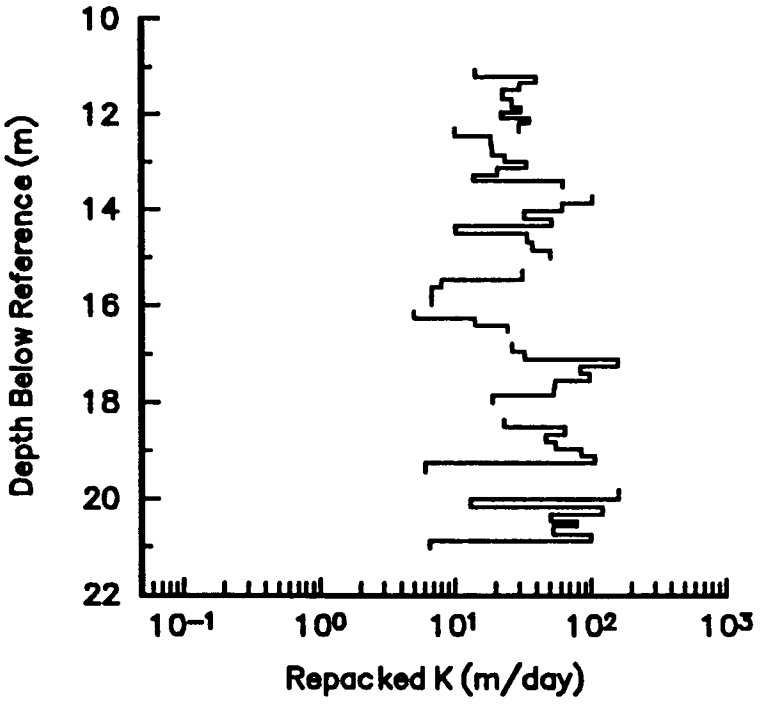

Figure IV.B.9. Repacked hydraulic conductivity vs. depth for GEMS well 5-1.

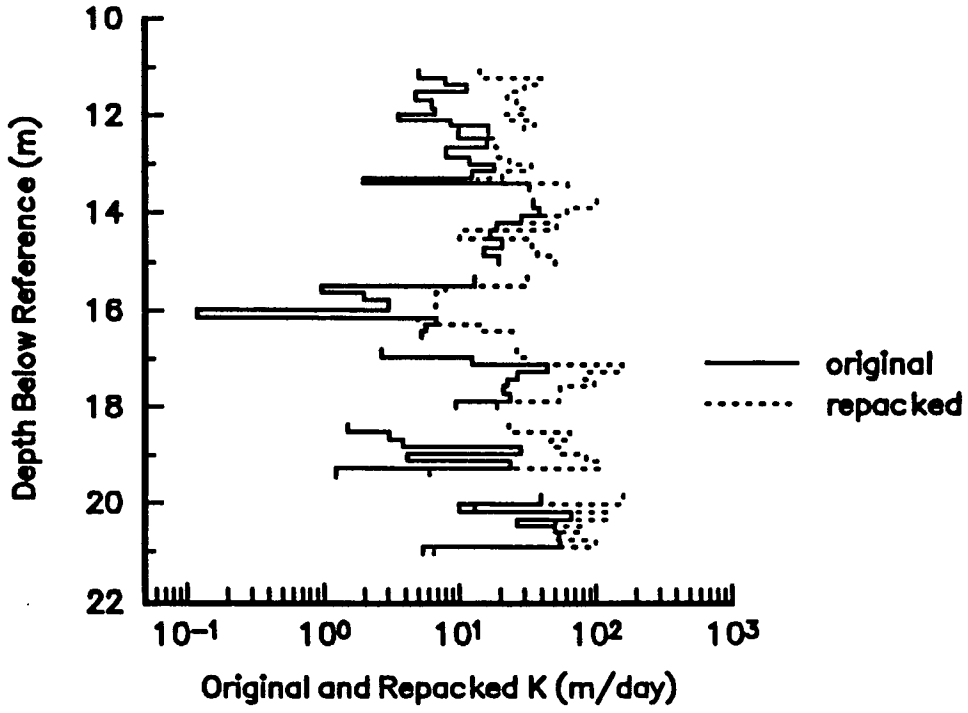

Figure IV.B.10. Original and repacked conductivity vs. depth for GEMS well 5-1.

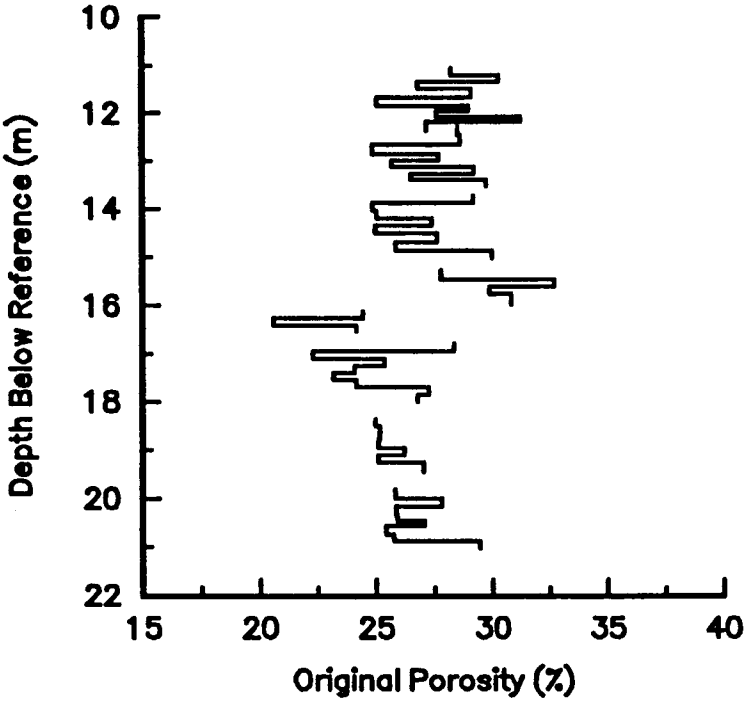

Figure IV.B.11. Original porosity vs. depth for GEMS well 5-1.

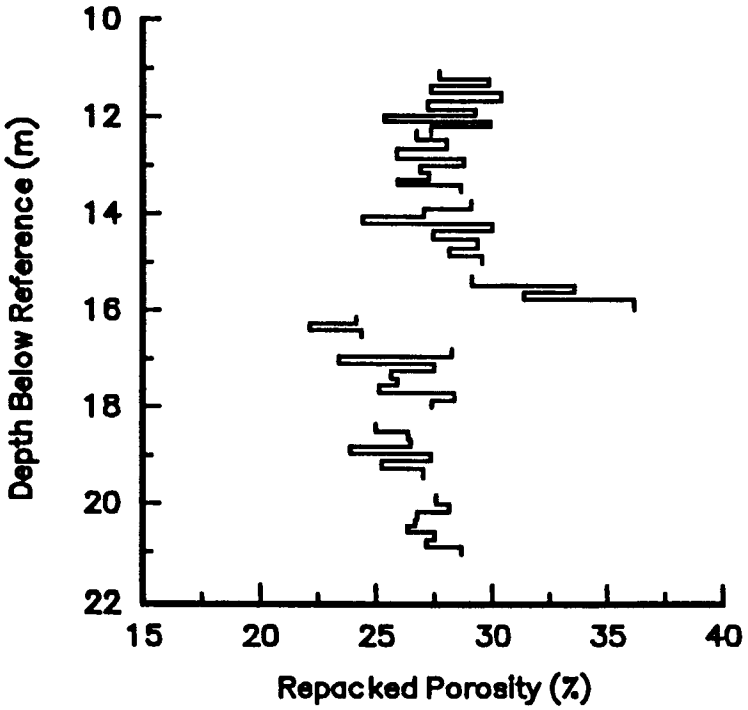

Figure IV.B.12. Repacked porosity vs. depth for GEMS well 5-1.

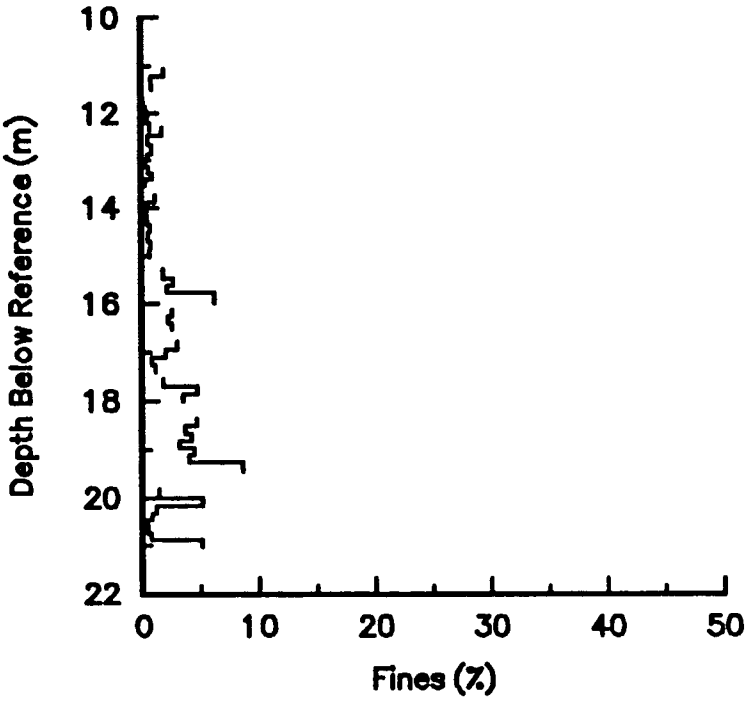

Figure IV.B.13. Percent fines (<.053 mm) vs. depth for GEMS well 5-1.

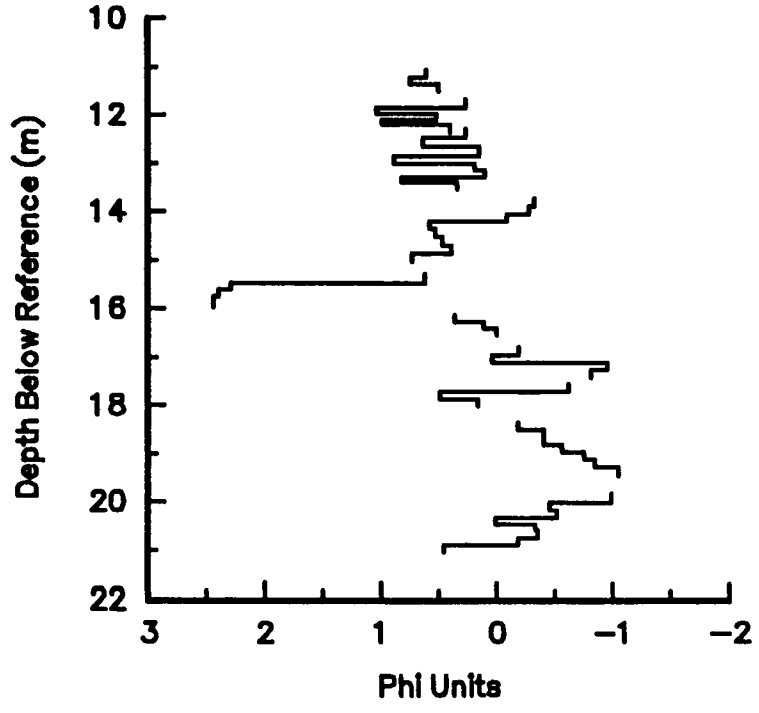

Figure IV.B.14. Mean grain size (in phi units) vs. depth for GEMS well 5-1.

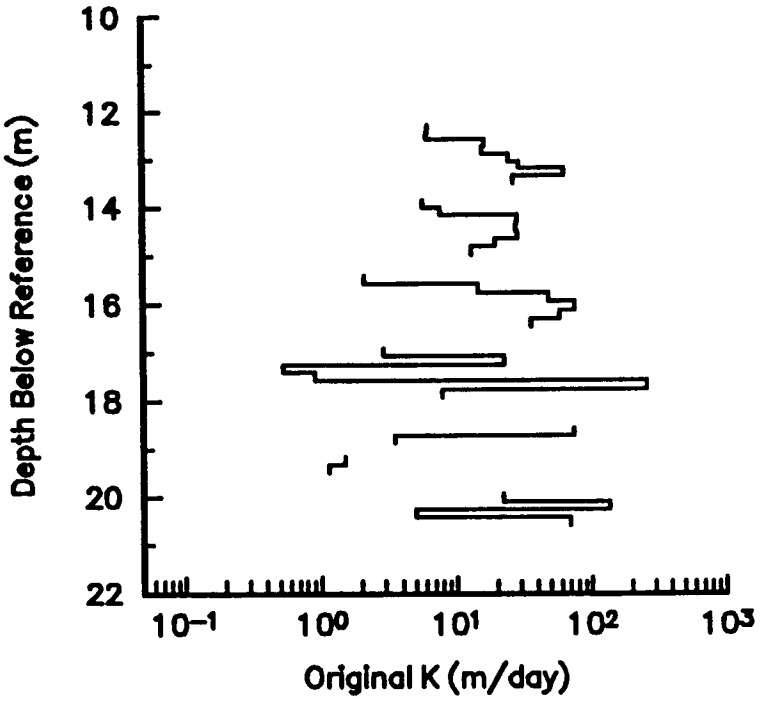

Figure IV.B.15. Original hydraulic conductivity vs. depth for GEMS well 7-1.

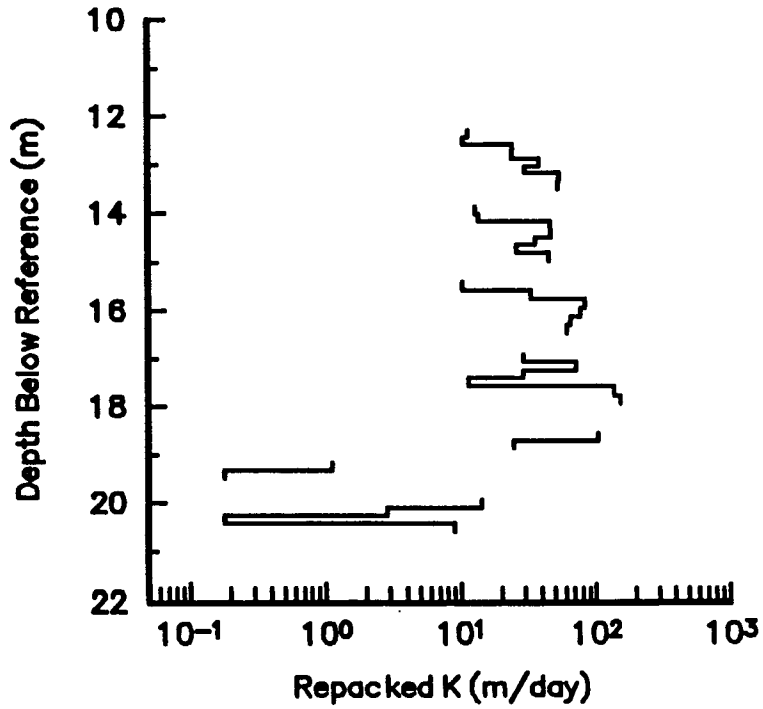

Figure IV.B.16. Repacked hydraulic conductivity vs. depth for GEMS well 7-1.

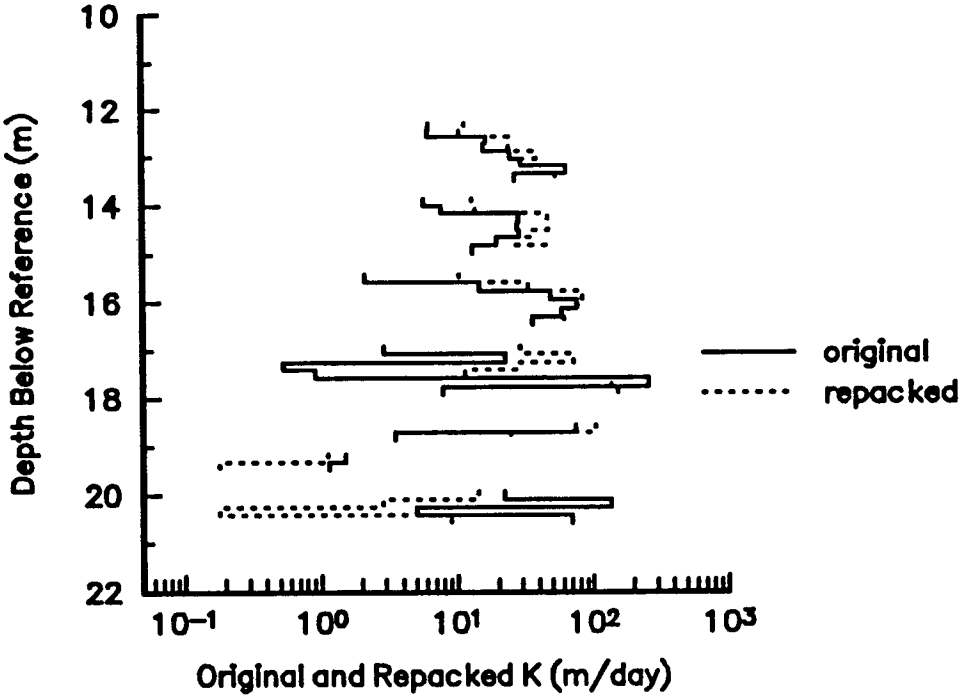

Figure IV.B.17. Original and repacked conductivity vs. depth for GEMS well 7-1.

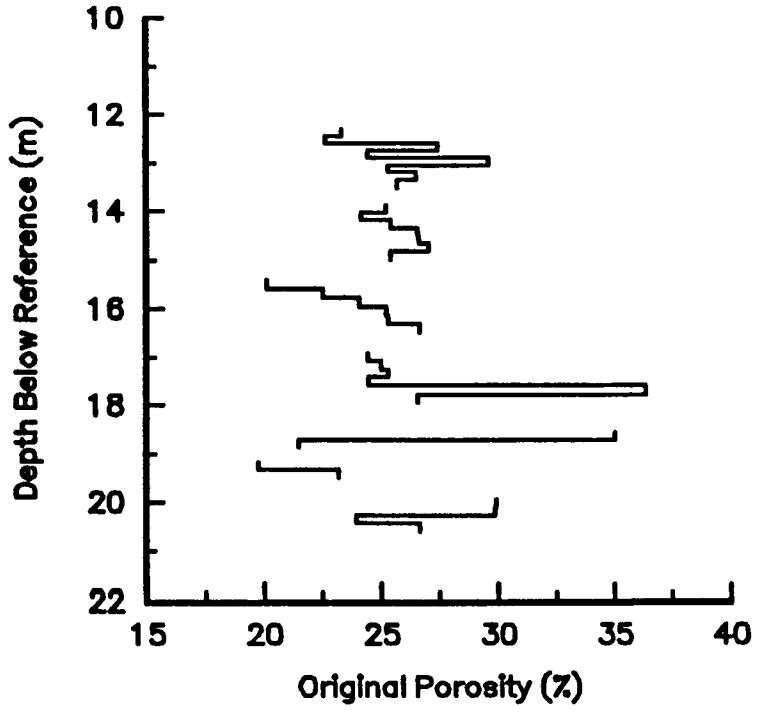

Figure IV.B.18. Original porosity vs. depth for GEMS well 7-1.

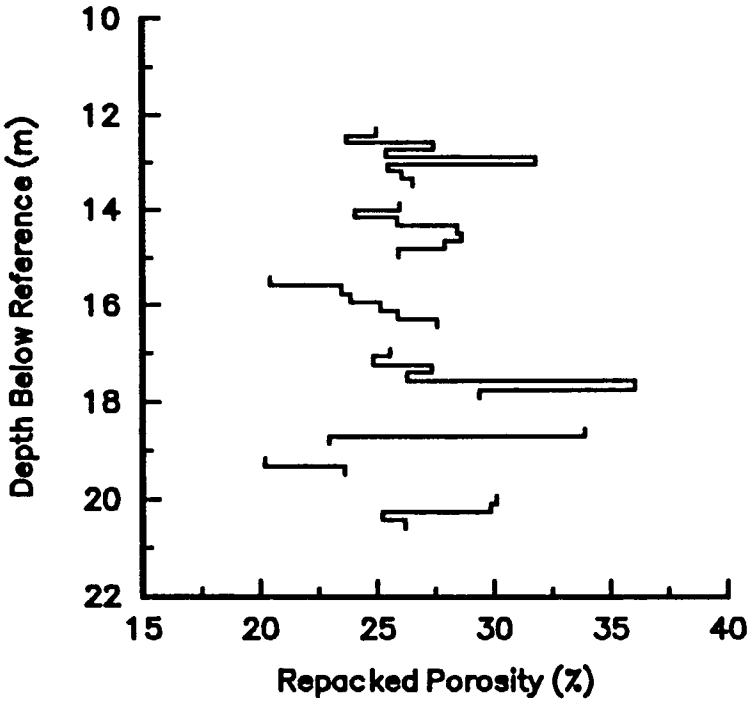

Figure IV.B.19. Repacked porosity vs. depth for GEMS well 7-1.

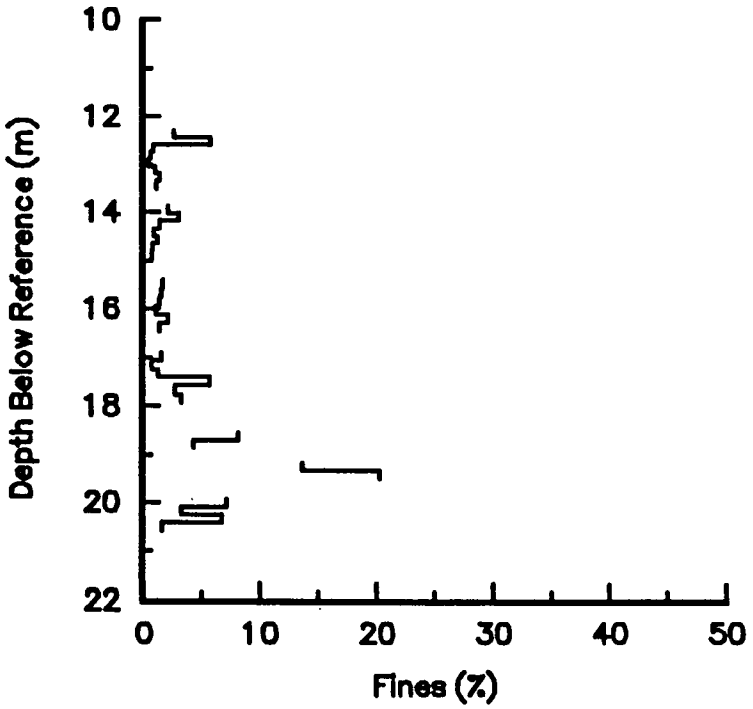

Figure IV.B.20. Percent fines (<.053 mm) vs. depth for GEMS well 7-1.

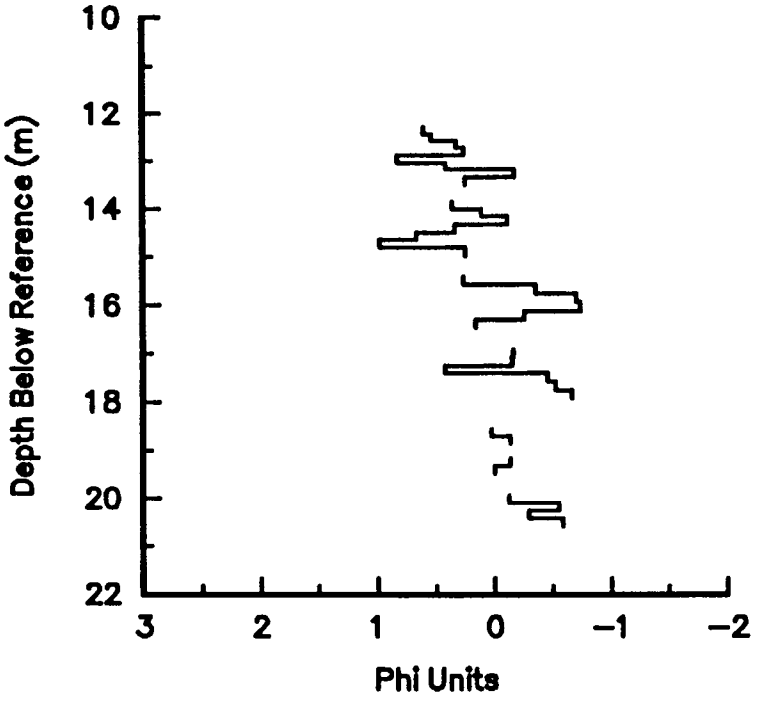

Figure IV.B.21. Mean grain size (in phi units) vs. depth for GEMS well 7-1.

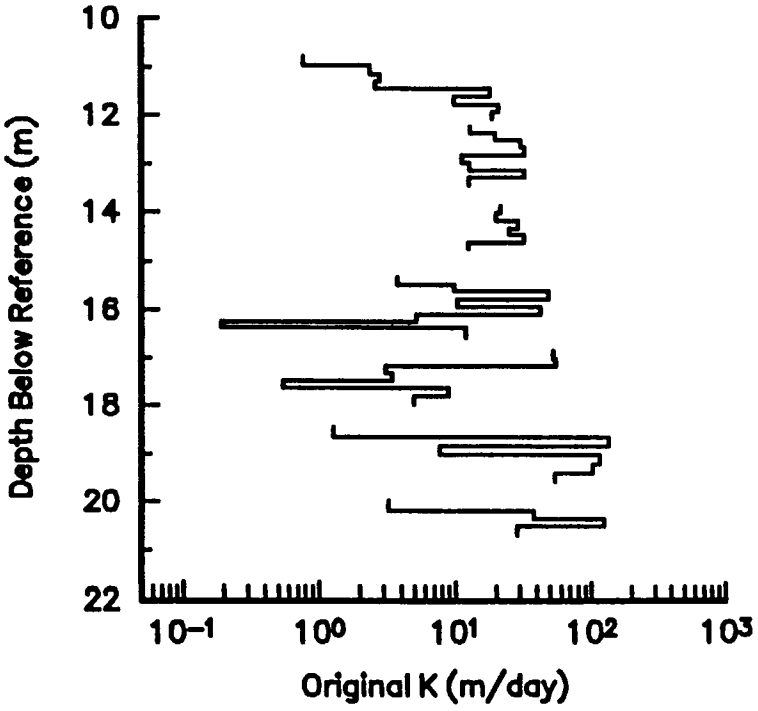

Figure IV.B.22 Original hydraulic conductivity vs. depth for GEMS well 9-1.

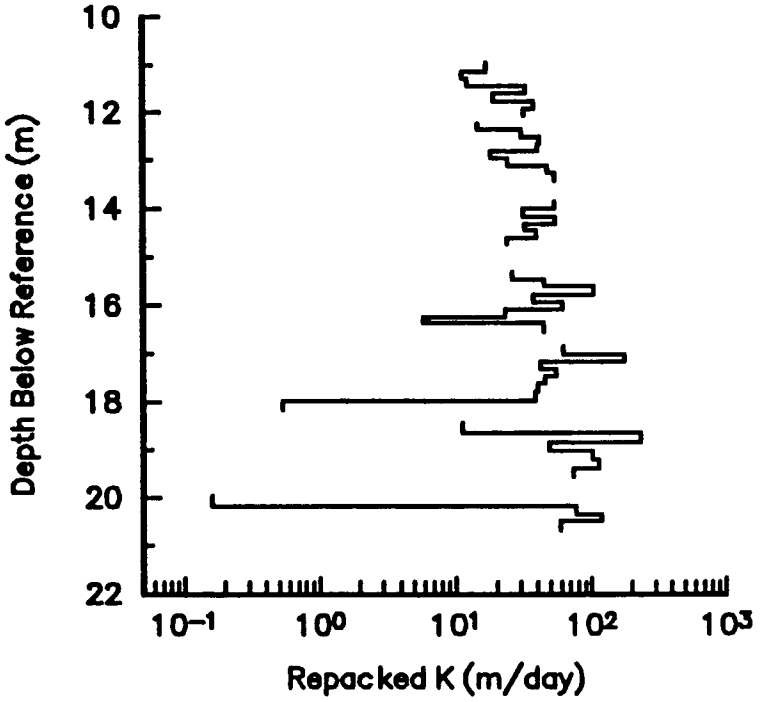

Figure IV.B.23 Repacked hydraulic conductivity vs. depth for GEMS well 9-1.

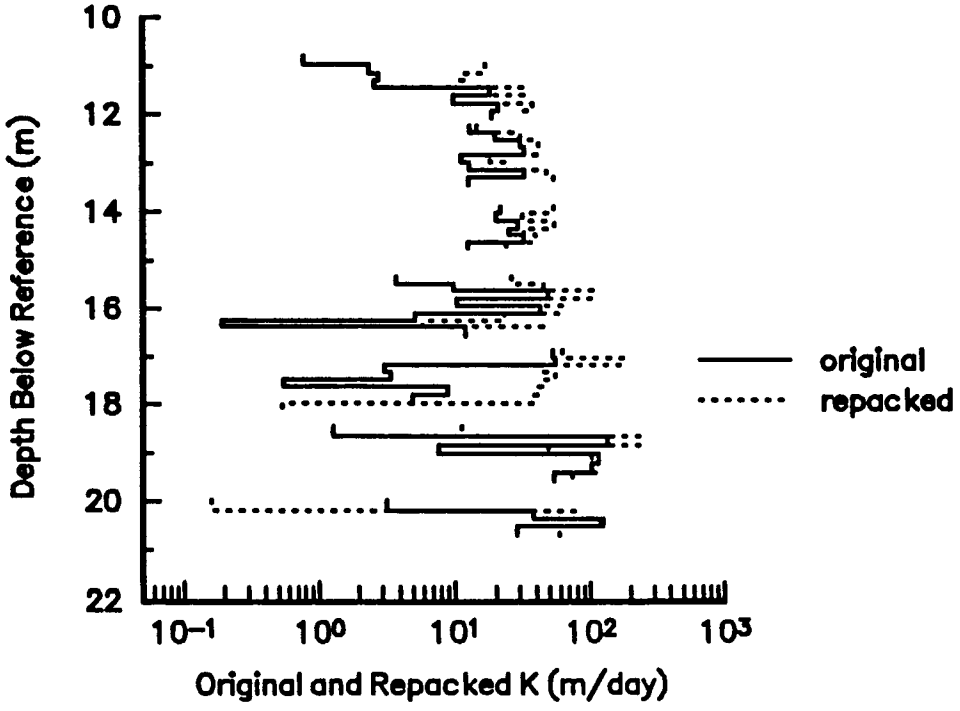

Figure IV.B.24 Original and repacked conductivity vs. depth for GEMS well 9-1.

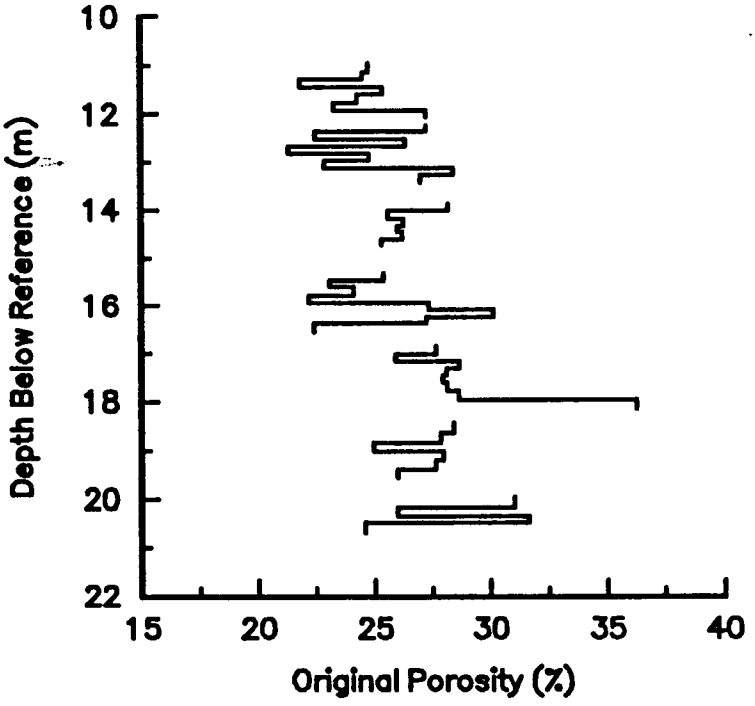

Figure IV.B.25 Original porosity vs. depth for GEMS well 9-1.

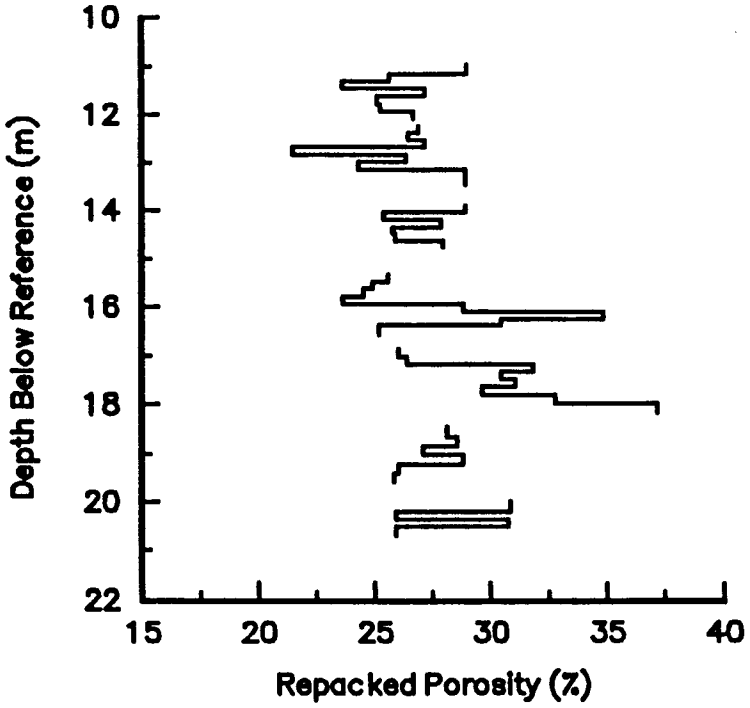

Figure IV.B.26 Repacked porosity vs. depth for GEMS well 9-1.

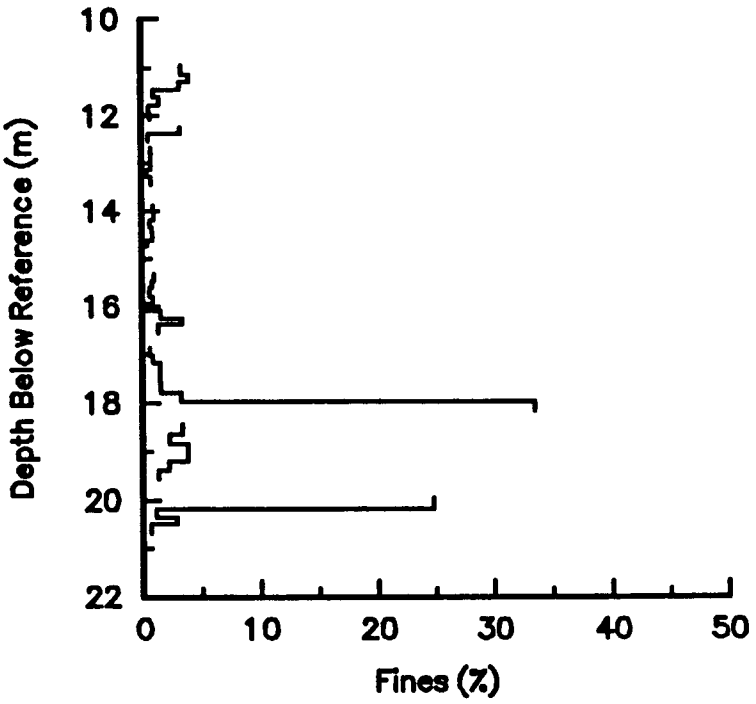

Figure IV.B.27 Percent fines (<.053 mm) vs. depth for GEMS well 9-1.

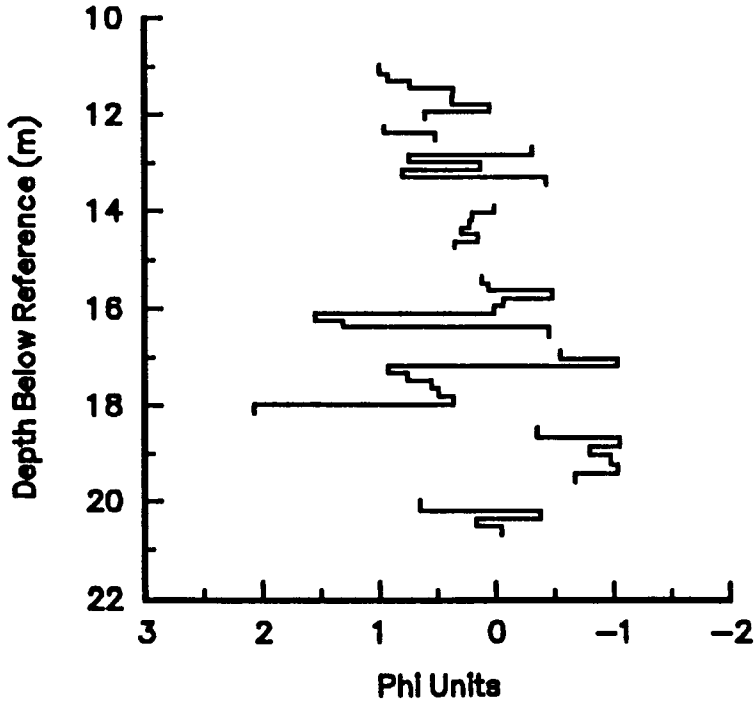

Figure IV.B.28 Mean grain size (in phi units) vs. depth for GEMS well 9-1.

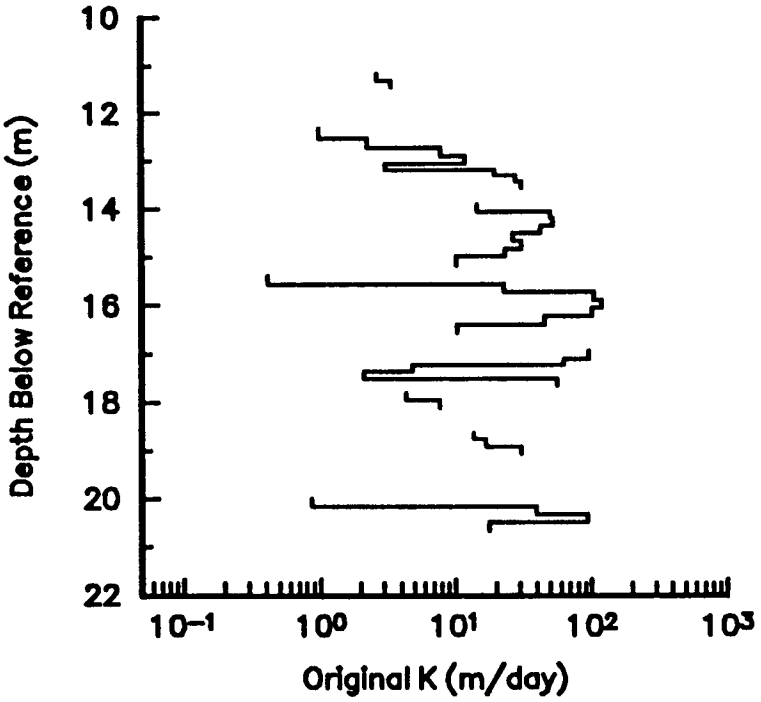

Figure IV.B.29 Original hydraulic conductivity vs. depth for GEMS well 11-1.

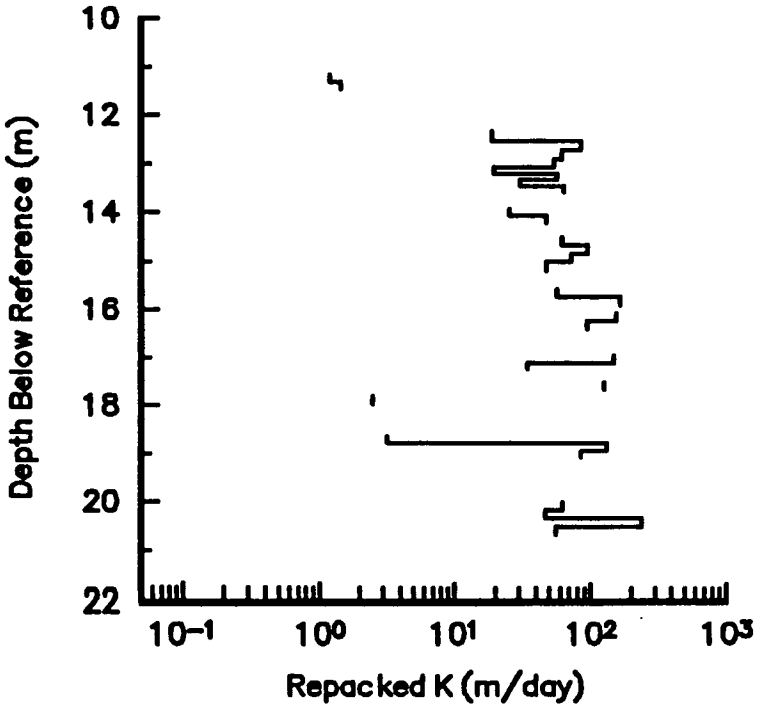

Figure IV.B.30 Repacked hydraulic conductivity vs. depth for GEMS well 11-1.

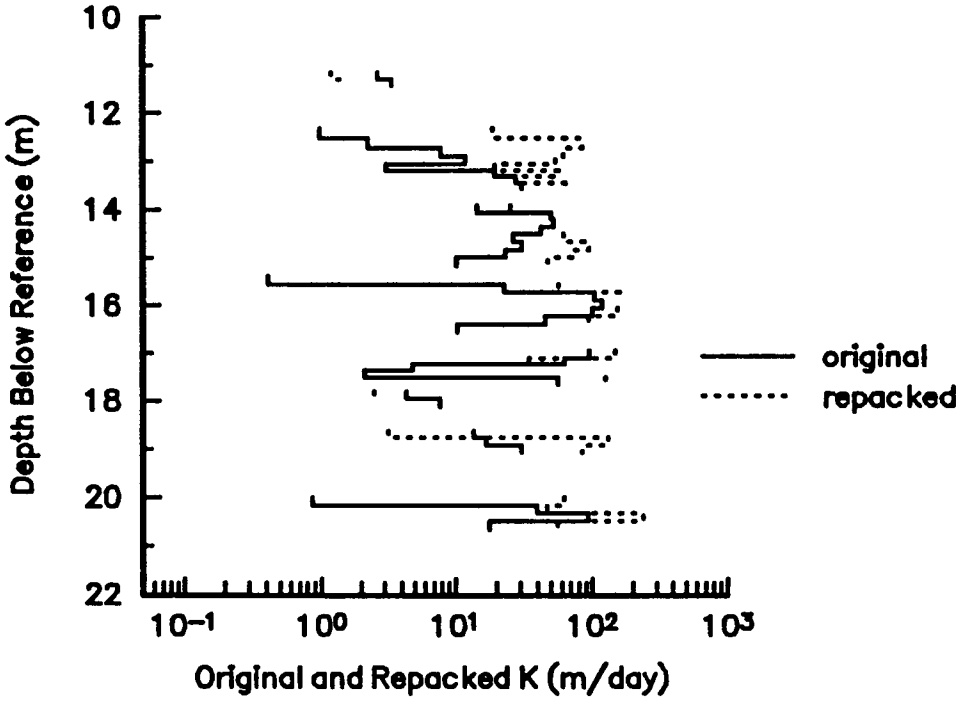

Figure IV.B.31 Original and repacked conductivity vs. depth for GEMS well 11-1.

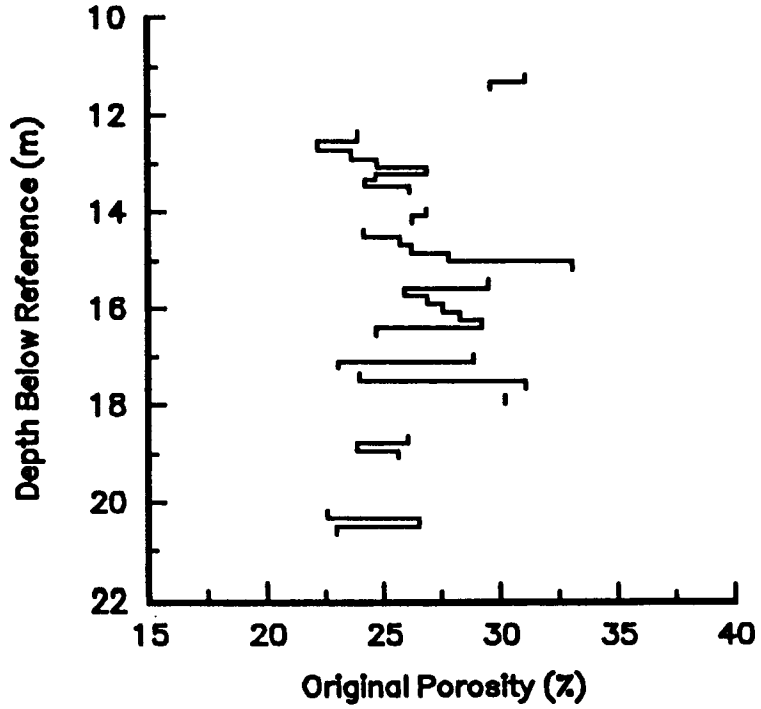

Figure IV.B.32 Original porosity vs. depth for GEMS well 11-1.

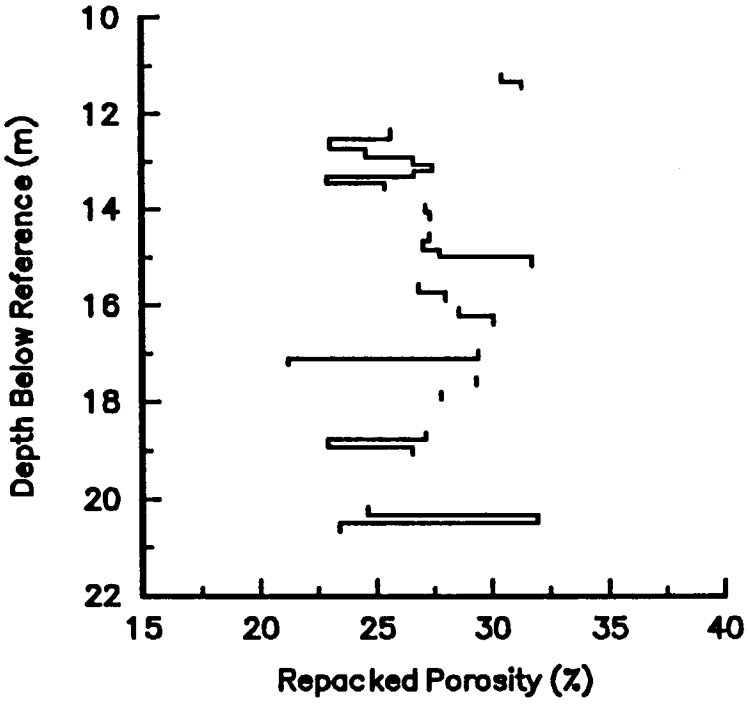

Figure IV.B.33 Repacked porosity vs. depth for GEMS well 11-1.

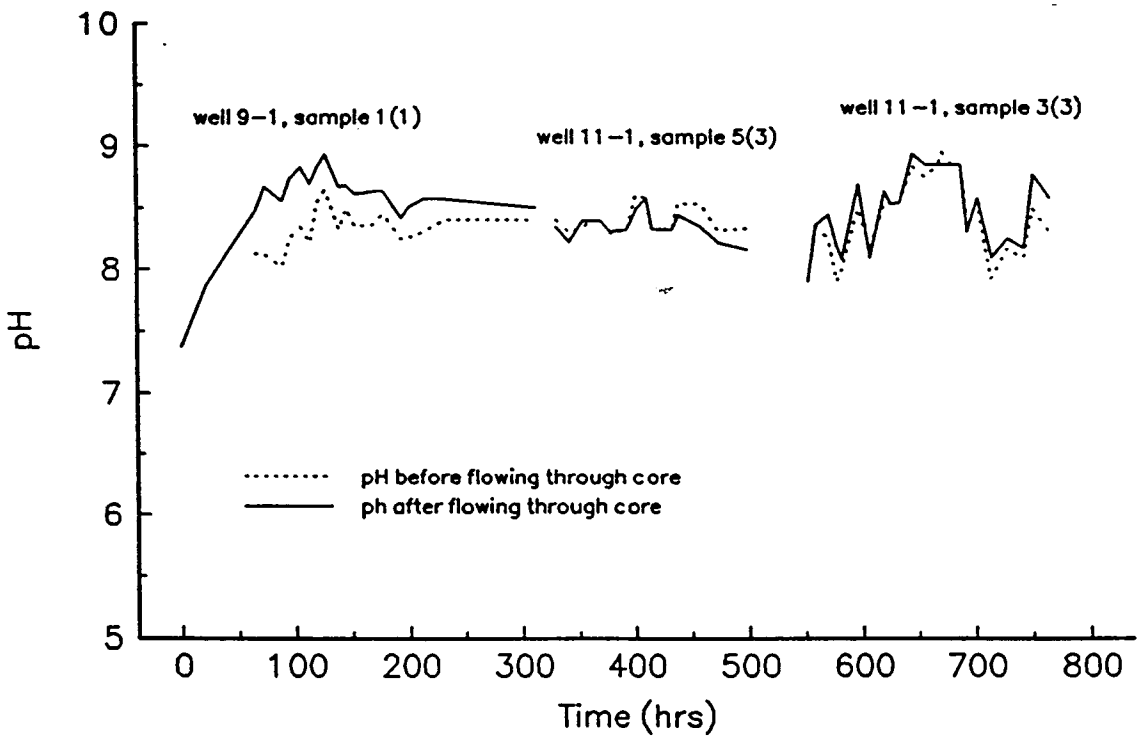

Figure IV.B.34 pH of water vs. time.

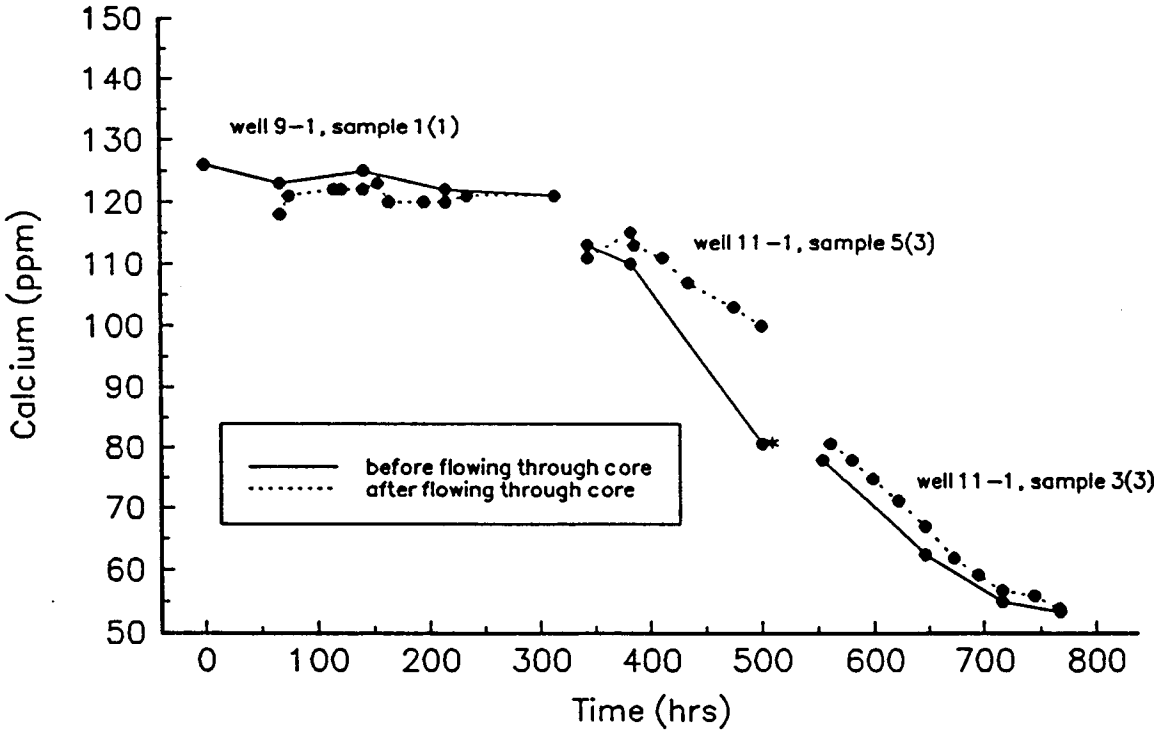

Figure IV.B.35 Calcium content of water vs. time.

V. SUMMARY OF YEAR TWO RESEARCH AND OUTLOOK FOR YEAR THREE

A. SUMMARY OF RESEARCH IN YEAR TWO

The major focus of the second year of this project was on the use of well tests to describe spatial variations in hydraulic conductivity. This research on the viability of well tests in heterogeneous formations had both theoretical and field components.

The theoretical work was directed at developing a better understanding of the kind of information that can be obtained from various types of well tests in heterogeneous units. In the first year of this research, a study of slug tests in layered media was initiated. This study was concluded in the second year of this work. The results of this study helped to 1) define the manner in which layer properties are vertically averaged during a slug test, and 2) delineate conditions under which multilevel slug tests can provide valuable information about vertical variations in hydraulic conductivity within a unit. The best conditions for multilevel slug tests were shown to be units with low frequency vertical variations in hydraulic conductivity in which test intervals considerably shorter than the thickness of the average layer are employed. Even in such conditions, however, well skins of both lower and higher permeability than the undamaged formation can dramatically decrease the effectiveness of the approach. Careful well construction and development procedures were stressed as ways of decreasing the impact of such skins. Assessing the potential of hydraulic tomography, i.e. the utilization of data from multiple well tests in a tomographic inversion procedure, was one of the goals of this project. An initial investigation of hydraulic tomography in a planar steady-state flow field was performed in the second year of this project. The tomographic method is based on the concept that the head drop between any two points on a streamline is given by a line integral of the flux along the streamline multiplied by the hydraulic resistivity (inverse of hydraulic conductivity). Streamline trajectories and flux integrals are computed from a finite difference solution for stream function values based on an estimate of the resistivity distribution. Computing flux integrals along a number of streamlines with known heads at each end results in a system of linear equations that can be solved for an updated set of resistivities. Stream function values and flux integrals are recomputed and the process is repeated until the resistivity estimates converge. Numerical examples indicate that the approach has potential in layered systems of considerable lateral continuity. Further work, however, is clearly needed to fully assess the viability of this approach. As is evident from the well data presented in Table IV.A.1, many of the wells at GEMS are screened for only a portion of the sand and gravel interval. When data from slug tests performed in such wells are

analyzed, the partially penetrating nature of the wells must be considered. One popular approach for the analysis of slug-test data from partially penetrating wells is the method of Nguyen and Pinder. A theoretical evaluation of this method revealed that an error was made in the analytical solution upon which the approach is based. Field and numerical examples demonstrate that the ramifications of this error are of considerable practical significance.

The field component of this study of well tests in heterogeneous formations concentrated on slug tests. A program of multiwell slug tests (slug tests with observation wells) was initiated at GEMS as part of the pulse-test research of this project. The results of this program of field testing and a complementary theoretical analysis demonstrated that the assumption of a fully screened well can introduce a very large amount of error into parameter estimates determined from response data at observation wells. A new analytical model, which allows partial penetration at both the stressed and observation wells, was developed. Application of this model to data from GEMS yielded parameters that were in keeping with the values obtained from the laboratory analysis of cores. As was clearly shown in the report of the first year of this project, slug tests at most of the wells in the alluvial aquifer at GEMS appear to be affected by mechanisms not accounted for in the conventional theory on which the standard methods for slug-test data analysis are based. The existence of these mechanisms are reflected by a concave downward curvature on log head versus arithmetic time plots, a dependence of slug-test responses on the magnitude of the induced slug (H_0), and systematic deviations between plots of the test data and the best-fit conventional models. A general unified model for the analysis of slug-test response data was developed in the second year of this work. This model includes the effects of nonlinearities, inertia, viscosity, and velocity distributions. An iterative numerical solution has been obtained for this model when the assumption of negligible aquifer storage is adopted. This model predicts the general shape and head dependence observed in the field data. Application of this model to field data has proven quite successful for both oscillatory and non-oscillatory situations. Further work, however, is required in order to identify the source of the strong nonlinearity represented by one parameter.

In addition to the research on well tests in heterogeneous formations, a significant amount of the work in the second year of this project was directed at increasing our knowledge of the subsurface at GEMS. This work included continued drilling and sampling activities, and continued laboratory analysis of the cores obtained with the KGS bladder sampler. These characterization efforts, which will continue throughout this project, are directed towards the development of a detailed picture of the subsurface at

GEMS, so that we can better assess the results of the hydraulic tests that are being performed as part of this research.

B. OUTLOOK FOR RESEARCH IN YEAR THREE

The third year of this project will build upon the progress made in the first two years. The major goal of the early part of year three will be to complete the slug-test aspects of this research. The primary tasks will be to finish work on the general unified model for the analysis of slug-test data at GEMS and to bring together all earlier field and theoretical research on slug tests. The objective of this second task will be to develop a series of guidelines for the performance and analysis of slug tests that can be utilized by field practitioners to increase the reliability of parameters estimated from slug-test response data. Following the completion of the slug-test work, the focus of the research will shift to pulse tests. The primary emphasis of the remainder of year three will be on an evaluation of two-dimensional and local three-dimensional pulse tests for providing information concerning the lateral and vertical variations in hydraulic conductivity between wells. A better assessment of this interwell variation should shed light on how these properties might be averaged to form equivalent parameters for mathematical modeling, and thus should lead to more accurate predictions of contaminant movement in the subsurface. As with the first two years of this project, a significant component of the work in year three will be efforts directed at continued characterization of the subsurface at GEMS. The detailed information collected in this characterization effort will be of vital importance in the later portions of this research when high-resolution three-dimensional pulse tests will be performed at GEMS.

VI. REFERENCES

Anderson, M.P., and Woessner, W.W., 1992, Applied Groundwater Modeling, Academic Press, Inc., San Diego, 381 pp.

Bliss, J.C., and Rushton, K.R., 1984, The reliability of packer tests for estimating the hydraulic conductivity of aquifers, Quart. Jour. of Eng. Geol., v. 17, 81-91.

Bohling, G. C. and McElwee, C.D., 1992, SUPRPUMP: An interactive program for well test analysis and design: Ground Water, v. 30, no. 2, 262-268.

Bouwer, H., 1989, The Bouwer and Rice slug test - an update, Ground Water, v. 27, no. 3, 304-309.

Bouwer, H. and Rice, R.C., 1976, A slug test for determining hydraulic conductivity of unconfined aquifers with completely or partially penetrating wells, Water Resour. Res., v. 12, no. 3, 423-428.

Braester, C., and Thunvik, R., 1984, Determination of formation permeability by double-packer tests, J. of Hydrology, v. 72, 375-389.

Brother, M.R., and Christians, G.L., 1993, In situ slug test analysis: A comparison of three popular methods for unconfined aquifers, Proc. of the 7th National Outdoor Action Conf., NGWA Ground Water Management No. 15, 597-607.

Butler, J.J., Jr., 1986, Pumping Tests in Nonuniform Aquifers: A deterministic and stochastic analysis (Ph.D. dissertation), Stanford Univ., Stanford, CA, 220 pp.

Butler, J.J., Jr., Bohling, G.C., Hyder, Z., and McElwee, C.D., 1994, The use of slug tests to describe vertical variations in hydraulic conductivity, J. of Hydrology, v. 156, 137-162.

Butler, J.J., Jr., and Liu, W.Z., 1993, Pumping tests in nonuniform aquifers: The radially asymmetric case, Water Resour. Res., v. 29, no. 2, 259-269.

Butler, J.J., Jr., and McElwee, C.D., 1992, Well-testing methodologies for characterizing heterogeneities in alluvial-aquifer systems: First year report, Kansas Geol. Survey Open-File Rept. 92-53, 152 pp.

Butler, J.J., Jr., McElwee, C.D., Bohling, G.C., and Healey, J.M., 1990, Hydrogeologic characterization of hazardous waste sites, Kansas Water Resources Research Inst. Contribution No. 283, 114 pp.

Butler, J. J., Jr., McElwee, C.D., and Hyder, Z., 1993, Slug tests in unconfined aquifers, Kansas Water Resources Research Inst. Contribution No. 303, 67 pp.

Campbell, M.D., Starrett, M.S., Fowler, J.D., and Klein, J.J., 1990, Slug tests and hydraulic conductivity, Proc. of the Petroleum Hydrocarbons and Organic Chemicals in Ground Water: Prevention, Detection, and Restoration Conf.,

NWWA Ground Water Management No. 4, 85-99.

Carrera, J., and Neuman, S.P., 1986, Estimation of aquifer parameters under transient and steady state conditions: 2. Uniqueness, stability, and solution algorithms, Water Resour. Res., v. 22, no. 2, 211-227.

Chirlin, G. R., 1989, A critique of the Hvorslev method for slug test analysis: The fully penetrating well, Ground Water Monitoring Review, v. 9, no. 2, 130-138.

Churchill, R.V., 1972, Operational Mathematics, McGraw Hill, New York, 481 pp.

Cooper, H. H., Bredehoeft, J.D., and Papadopulos, I.S., 1967, Response of a finite-diameter well to an instantaneous charge of water, Water Resour. Res., v. 3, no. 1, 263-269.

Cordes, C., and Kinzelbach, W., 1992, Continuous groundwater velocity fields and path lines in linear, bilinear, and trilinear finite elements, Water Resour. Res., v. 28, no. 11, 2903-2911.

Dagan, G., 1978, A note on packer, slug, and recovery tests in unconfined aquifers, Water Resour. Res., v. 14, no. 5, 929-934.

Dagan, G., 1986, Statistical theory of groundwater flow and transport: pore to laboratory, laboratory to formation, and formation to regional scale, Water Resour. Res., v. 22, no. 9, 120S-134S.

Demir, Z., and Narasimhan, T.N., 1994, Towards an improved interpretation of Hvorslev tests, ASCE J. of Hydraulics, v. 120, no. 4, 477-494.

Desbarats, A. J., 1991, Spatial averaging of transmissivity, in Proceedings of the 5th Canadian/American Conference on Hydrogeology: Parameter Identification and Estimation for Aquifer and Reservoir Characterization, edited by S. Bachu, 139-154, National Water Well Association, Dublin, Ohio.

Desbarats, A. J., 1992a, Spatial averaging of transmissivity in heterogeneous fields with flow toward a well, Water Resour. Res., 28(3), 757-767.

Desbarats, A. J., 1992b, Spatial averaging of hydraulic conductivity in three-dimensional heterogeneous porous media, Math. Geol., 24(3), 249-267.

Deutsch, C. V., and Journel, A.G., 1992, GSLIB: Geostatistical Software Library and User's Guide, Oxford University Press, New York, 340 pp.

Dougherty, D.E., and Babu, D.K., 1984, Flow to a partially penetrating well in a double-porosity reservoir, Water Resour. Res., v. 20, no. 8, 1116-1122.

Ehlig-Economides, C.A., and Joseph, J.A., 1987, A new test for determination of individual layer properties in a multilayered reservoir, SPE Formation Eval., v. 2, no. 3, 261-283.

Eskinazi, S., 1967, Vector Mechanics of Fluids and Magnetofluids, Academic Press,

New York, pp. 194-206.

Fogler, H. S., and Vaidya, R.N., 1993, Effects of pH on fines migration and permeability reduction, in Manipulation of Groundwater Colloids for Environmental Restoration, J. F. McCarthy and F. J. Wobber (eds.), pp. 123-128.

Freyberg, D.L., 1986, A natural gradient experiment on solute transport in a sand aquifer, 2, Spatial moments and the advection and dispersion of nonreactive tracers, Water Resour. Res., v. 22, no. 13, 2031-2046.

Frind, E. O., and Matanga, G.B., 1985, The dual formulation of flow for contaminant transport modeling, 1, Review of theory and accuracy aspects, Water Resour. Res., v. 21, no. 2, 159-169.

Frind, E. O., and Pinder, G.F., 1973, Galerkin solution of the inverse problem for aquifer transmissivity, Water Resour. Res., v. 9, no. 5, 1397-1410.

Gelhar, L.W., 1986, Stochastic subsurface hydrology from theory to applications, Water Resour. Res., v. 22, no. 9, 135S-145S.

Haberman, R., 1987, Elementary Applied Partial Differential Equations, Prentice-Hall, Inc., Englewood Cliffs, N.J., 547 pp.

Hackett, G., 1987, Drilling and constructing monitoring wells with hollow-stem augers, Part 1: Drilling considerations, Ground Water Monitoring Review, v. 7, no. 4, 51-62.

Hansen, A.G., 1967, Fluid Mechanics, John Wiley and Sons, Inc., New York, pp. 134-137.

Hantush, M.S., 1964, Hydraulics of wells, in: V.T. Chow, ed., Advances in Hydrosciences, Academic Press, New York, v. 1, 281-432.

Harvey, C.F., 1992, Interpreting Parameter Estimates Obtained From Slug Tests in Heterogeneous Aquifers (M.S. thesis), Stanford Univ., Stanford, Ca., 99 pp.

Hayashi, K., Ito, T., and Abe, H., 1987, A new method for the determination of in situ hydraulic properties by pressure pulse tests and application to the Higashi Hachimantai geothermal field, J. Geophys. Res., v. 92, no. B9, 9168-9174.

Hess, K.M., Wolf, S.H., and Celia, M.A., 1992, Large-scale natural gradient tracer test in sand and gravel, Cape Cod, Massachusetts, 3. Hydraulic conductivity variability and calculated macrodispersivities, Water Resour. Res., v. 28, no. 8, 2011-2027.

Hinsby, K., Bjerg, P.L., Andersen, L.J., Skov, B., and Clausen, E.V., 1992, A mini slug test method for determination of a local hydraulic conductivity of an unconfined sandy aquifer, J. of Hydrology, v. 136, 87-106.

Hufschmied, P., 1986, Estimation of three-dimensional anisotropic hydraulic conductivity field by means of single well pumping tests combined with flowmeter measurements, Hydrogeologie, 163-174.

Hvorslev, M.J., 1951, Time lag and soil permeability in ground-water observations, Bull no. 36, Waterways Exper. Sta., Corps of Engrs., U.S. Army, 50 pp.

Hyder, Z., Butler, J.J., Jr., McElwee, C.D., and Liu, W.Z., in press. Slug tests in partially penetrating wells, Water Resour. Res.

Jiang, X., 1991, A Field and Laboratory Study of Scale Dependence of Hydraulic Conductivity (M.S. thesis), Univ. of Ks, Lawrence, Ks, 149 pp.

Kabala, Z.J., Pinder, G.F., and Milly, P.C.D., 1985, Analysis of well-aquifer response to a slug test, Water Resour. Res., v. 21, no.9, pp. 1433-1436.

Karasaki, K., 1986, Well Test Analysis in Fractured Media (Ph.D. dissertation), Univ. of Ca., Berkeley, 239 pp.

Keely, J.F., and Boateng K., 1987, Monitoring well installation, purging and sampling techniques, Part 1: Conceptualizations, Ground Water, v. 25, no. 3, 300-313.

Kipp, K.L., Jr., 1985, Type curve analysis of inertial effects in the response of a well to a slug test, Water Resour. Res., v. 21, no.9, pp. 1397-1408.

Kreyszig, E., 1983, Advanced Engineering Mathematics, John Wiley and Sons, New York, pp. 75-81.

McDonald, M. G., and Harbaugh, A.W., 1984, A modular three-dimensional finite-difference ground-water flow model, USGS Open-File Report 83-875.

McElwee, C. D., 1982, Sensitivity analysis and the ground-water inverse problem, Ground Water, v. 20, no. 6, 723-735.

McElwee, C.D., Butler, J.J., Jr., and Bohling, G.C., 1992, Nonlinear analysis of slug tests in highly-permeable aquifers using a Hvorslev-type approach, EOS, v. 73, no. 43, p. 164.

McElwee, C.D., Butler, J.J., Jr., Bohling, G.C., and Liu, W.Z., in press, Sensitivity analysis of slug tests, II. Observation wells, J. of Hydrology.

McElwee, C.D., Butler, J.J., Jr., and Healey, J.M., 1991, A new sampling system for obtaining relatively undisturbed samples of unconsolidated coarse sand and gravel, Ground Water Monitoring Review, v. 11, no. 3, 182-191.

McLane, G.A., Harrity, D.A., and Thomsen, K.O., 1990, A pneumatic method for conducting rising and falling head tests in highly permeable aquifers, Proc. of 1990 NWWA Outdoor Action Conf.

Melville, J.G., Molz, F.J., Guven, O., and Widdowson, M.A.,1991, Multilevel slug tests with comparisons to tracer data, Ground Water, v. 29, no. 6, 897-907.

Minning, R.C., 1982, Monitoring well design and installation, Proceedings of the Second National Symposium on Aquifer Restoration and Ground Water Monitoring, Columbus, Ohio, 194-197.

Moench, A.F., and Hsieh, P.A., 1985, Analysis of slug test data in a well with finite-thickness skin, In: Memoirs of the 17th Intern. Cong. on the Hydrogeology of Rocks of Low Permeability, v. 17, 17-29.

Moltyaner, G.L., and Killey, R.W.D., 1988, Twin Lake tracer tests: Longitudinal dispersion, Water Resour. Res., v. 24, no. 10, 1613-1627.

Molz, F.J., Guven, O., and Melville, J.G., 1989a, Characterization of the hydrogeologic properties of aquifers: The next step, in: Proc. of the Conf. on New Field Techniques for Quantifying the Physical and Chemical Properties of Heterogeneous Aquifers, National Water Well Association, 407-418.

Molz, F.J., Morin, R.H., Hess, A.E., Melville, J.G., and Guven, O., 1989b, The impeller meter for measuring aquifer permeability variations: Evaluation and comparison with other tests, Water Resour. Res., v. 25, no. 7, 1677-1686.

Morin, R.H., Hess, A.E., and Paillet, F.L., 1988, Determining the distribution of hydraulic conductivity in a fractured limestone aquifer by simultaneous injection and geophysical logging, Ground Water, v. 26, no. 5, 587-595.

National Ground Water Association, 1993, Analysis and design of aquifer tests - including slug tests and fracture flow, 1994 Catalog of Ground Water and Environmental Education, 17-18.

Nelson, R. W., 1960, In-place measurement of permeability in heterogeneous media, 1, Theory of a proposed method, J. Geophys. Res., v. 65, no. 6, 1753-1758.

Nelson, R. W., 1961, In-place measurement of permeability in heterogeneous media, 2, Experimental and computational considerations, J. Geophys. Res., v. 66, no. 8, 2469-2478.

Nelson, R. W., 1968, In-place determination of permeability distribution for heterogeneous porous media through analysis of energy dissipation, Soc. Pet. Eng. J., v. 8, no. 1, 33-42.

Neuman, S. P., 1973, Calibration of distributed parameter groundwater flow models viewed as a multiple-objective decision process under uncertainty, Water Resour. Res., v. 9, no. 4, 1006-1021.

Neuman, S. P., 1980, A statistical approach to the inverse problem of aquifer hydrology, 3, Improved solution method and added perspective, Water Resour. Res., v. 16, no. 2, 331-346.

Nichols, E.M., 1985, Determination of the Hydraulic Parameters of Salt Marsh Peat Using In-Situ Well Tests (M.S. thesis), Mass. Inst. Tech., 109 pp.

Nguyen, V., and Pinder, G.F., 1984, Direct calculation of aquifer parameters in slug test analysis, in: Rosenshein, J., and Bennett, G.D., eds., Groundwater

Hydraulics, AGU Water Resour. Monogr. No. 9, 222-239.

Novakowski, K.S., 1989, Analysis of pulse interference tests, Water Resour. Res., v. 25, no. 11, 2377-2387.

Orient, J.P., Nazar, A., and Rice, R.C., 1987, Vacuum and pressure test methods for estimating hydraulic conductivity, Ground Water Monitoring Review, v. 7, no. 1, 49-50.

Palmer, C.D., and Johnson, R.L., 1989, Determination of physical transport parameters, in: Transport and Fate of Contaminants in the Subsurface, Environmental Protection Agency, EPA/625/4-89/019, 29-40.

Papadopulos, I.S., and Cooper, H.H., Jr., 1967, Drawdown in a well of large diameter, Water Resour. Res., v. 3, no. 1, 241-244.

Perry, C.A. and Hart, R.J., 1985, Installation of observation wells on hazardous waste sites in Kansas using a hollow-stem auger, Ground Water Monitoring Review, v. 5, no. 4, 70-73.

Peterson, J. E., Paulsson, B.N.P., and McEvilly, T.V., 1985, Application of algebraic reconstruction techniques to crosshole seismic data, Geophysics, v. 50, no. 10, 1566-1580.

Pollock, D. W., 1988, Semianalytical computation of path lines for finite-difference models, Ground Water, v. 26, no. 6, 743-750.

Rehfeldt, K.R., Hufschmied, P., Gelhar, L.W., and Schaefer, M.E., 1989, Measuring hydraulic conductivity with the borehole flowmeter, Rept. EN-6511, Electric Power Res. Inst., Palo Alto, Ca.

Rushton, K.R., and Chan, Y.K., 1977, Numerical pumping test analysis in unconfined aquifers, J. Irrigation and Drainage Div., v. 103, no. IR1, 1-12.

Scott, D. M., 1992, Evaluation of flow net analysis for aquifer identification, Ground Water, v. 30, no. 5, 755-764.

Settari, A., and Aziz, K., 1974, A computer model for two-phase coning simulation, Soc. of Pet. Eng. J., v. 14, no. 3, 221-236.

Stone, D.B. and Clarke, G.K.C., in press, Estimation of subglacial hydraulic properties from induced changes in basal water pressure: a theoretical framework for borehole response tests, J. of Glaciology.

Streltsova, T.D., 1988, Well Testing in Heterogeneous Formations, John Wiley and Sons, Inc., New York, 413 pp.

Taylor, K., and Molz, F., 1990, Determination of hydraulic conductivity and porosity logs in wells with a disturbed annulus, J. of Contaminant Hydrology, v. 5, 317-332.

Taylor, K., Hess, J., Mazzella, A., and Hayworth, J., 1990, Comparisons of three methods

to determine the vertical stratification of pore fluids, Ground Water Monitoring Review, v. 10, no. 1, 91-95.

Van der Kamp, G., 1976, Determining aquifer transmissivity by means of well response tests: The underdamped case, Water Resour. Res., v. 12, no. 1, 71-77.

van Dyke, N.V.R., Rhodes, J.R., Richardson, D.W., and McTigue, W.H., 1993, Evaluating confined aquifer properties using the pneumatic displacement method and the repeated pressure pulse technique, in Proc. of the Seventh National Outdoor Action Conf., Ground Water Management Series No. 15, 405-419.

Vennard, J.K., and Street, R.L., 1975, Elementary Fluid Mechanics, Wiley and Sons, New York, 740 pp.

Wang, H. F., and Anderson, M.P., 1982, Introduction to Groundwater Modeling: Finite Difference and Finite Element Methods, W. H. Freeman and Company, New York, 237 pp.

Widdowson, M.A., Molz, F.J., and Melville, J.G., 1990, An analysis technique for multilevel and partially penetrating slug test data, Ground Water, v. 28, no. 6, 937-945.

Yeh, W. W-G., 1986, Review of parameter identification procedures in groundwater hydrology: The inverse problem, Water Resour. Res., v. 22, no. 2, 95-108.

Yu, Y.H., and Lloyd, J.W., 1992, A multi-layered radial flow model interpretation of drill stem test data, J. of Hydrology, v. 136, 73-86.

Zapico, M.M., 1987, Aquifer Evaluation Procedures - Core Acquisition and an Assessment of Slug Tests (M.S. thesis), University of Waterloo.

Zapico, M., Vales, S., and Cherry, J., 1987, A wireline piston core barrel for sampling cohesionless sand and gravel below the water table, Ground Water Monitoring Review, v. 7, no. 3, 74-82.

VII. APPENDIX A - NGUYEN AND PINDER DERIVATION

In this appendix, a brief overview of the mathematical derivation of the solution discussed in section II.C is presented. The equation numbering will be the same as that given in Appendix A of Nguyen and Pinder (Nguyen and Pinder, 1984). The only difference between the equations given here and those of Nguyen and Pinder will be the notation used for derivatives and constants, and the neglecting of their pumping-rate term (Q).

Equations (II.C.1)-(II.C.8) in section II.C constitute the mathematical model of interest here. Nguyen and Pinder attempt to find a solution to this model by employing classical integral transform techniques (Churchill, 1972). Using initial conditions (II.C.2) and (II.C.7), Nguyen and Pinder apply the Laplace transform to equations (II.C.1) and (II.C.3)-(II.C.6) to produce the following set of equations in Laplace space:

$$\frac{\partial^2 \bar{s}}{\partial r^2} + \frac{1}{r}\frac{\partial \bar{s}}{\partial r} + \frac{\partial^2 \bar{s}}{\partial z^2} = \left(\frac{S_s}{K}\right) p\bar{s} \tag{A1}$$

$$\frac{\partial \bar{s}(r,0)}{\partial z} = \frac{\partial \bar{s}(r,b)}{\partial z} = 0 \tag{A2}$$

$$\bar{s}(\infty,z) = 0 \tag{A3}$$

$$\frac{1}{(z_2 - z_1)} \int_{z_1}^{z_2} \bar{s}(r_s,z)dz = \bar{H} \tag{A4}$$

$$2\pi r_s K \int_{z_1}^{z_2} \frac{\partial \bar{s}(r_s,z)}{\partial r} dz = \pi r_c^2 (p\bar{H} - H_0) \tag{A5}$$

where

$\bar{s}$, $\bar{H}$ = the Laplace transform of s and H(t), respectively;

p = the Laplace transform variable.

Using the no-flow boundary condition given in (A2), Nguyen and Pinder then apply a finite Fourier cosine transform in the z direction to equations (A1) and (A3) to produce the following equations in Fourier-Laplace space:

$$\frac{\partial^2 \bar{s}_t}{\partial r^2} + \frac{1}{r}\frac{\partial \bar{s}_t}{\partial r} - \left(\frac{S_s}{K}p + \left(\frac{\pi n}{b}\right)^2\right)\bar{s}_t = 0 \qquad \text{(A6)}$$

$$\bar{s}_t(\infty) = 0 \qquad \text{(A7)}$$

where

$\bar{s}_t$ = the Fourier-Laplace transform of s;

n = the Fourier-transform variable.

Note that Nguyen and Pinder do not apply a Fourier transform to the well-bore flow condition given by equation (A5) because this condition is undefined in Fourier-Laplace space, i.e. the application of a finite Fourier cosine transform to (A5) will not produce an expression in terms of $\bar{s}_t$.

The Fourier-Laplace solution to (A6) is quite straightforward, as (A6) is simply a form of the modified Bessel equation (Haberman, 1987). The solution can be written as

$$\bar{s}_t(r) = A_{1n} I_0(\alpha_n r) + A_{2n} K_0(\alpha_n r) \qquad \text{(A8)}$$

where

$$\alpha_n^2 = \frac{S_s}{K}p + \left(\frac{\pi n}{b}\right)^2, \quad n=0,1,2,...$$

A_{1n}, A_{2n} = constants;

I_0 = modified Bessel function of the first kind of order 0;

K_0 = modified Bessel function of the second kind of order 0.

Note that the equation constants are a function of n and p.

The standard procedure for the evaluation of the constants in an equation such as (A8) is to employ the boundary conditions. Application of (A7), the boundary condition at an infinite radial distance from the well, to (A8) results in constant A_{1n} being equal to 0 for all n. Thus, (A8) is reduced to

$$\bar{s}_t(r) = A_{2n}K_0(\alpha_n r) \tag{A9}$$

At this point, Nguyen and Pinder face a problem because the boundary condition at $r=r_s$ is undefined in Fourier-Laplace space. Rather than redefining the wellbore boundary condition into a form that yields an expression in terms of $\bar{s}_t$, Nguyen and Pinder incorrectly attempt to circumvent this problem by applying an inverse finite Fourier cosine transform to (A9) prior to evaluation of the constant. The expression that Nguyen and Pinder give for the inverse finite Fourier cosine transform is

$$\bar{s}(r,z) = \frac{A_{2n}}{b}[K_0(\alpha_0 r) + 2\sum_{n=1}^{\infty} K_0(\alpha_n r)\cos(\frac{n\pi z}{b})] \tag{A10}$$

Note that the constant A_{2n}, which is a function of n, has been taken out of the infinite series summation. Although moving A_{2n} out of the infinite series summation greatly simplifies the problem and allows the constant to be readily evaluated, this manipulation is mathematically incorrect and introduces further error into the proposed solution. Thus, even though the remaining manipulations outlined by Nguyen and Pinder in their Appendix A are performed without error, the errors described above make all remaining expressions developed in the derivation, including the expressions for parameter estimation, incorrect and, therefore, of little practical value.

In summary, the derivation of Nguyen and Pinder has two interrelated problems. First, the boundary condition at the well screen is undefined in the transform space in which the authors propose a solution to their mathematical model. Second, an attempt to circumvent this problem through an application of an inverse Fourier transform is in error because a constant coefficient in Fourier-Laplace space is assumed to be independent of n. The theoretical and practical ramifications of these two problems are discussed in section II.C.